Neuroanatomical variation in Parkinson's disease motor subtypes

Neuroanatomical Variation In Parkinson's Disease Motor Subtypes

by

Jackson Tyler Boonstra

Cover art: Generative AI tools
Cover design: Jackson Tyler Boonstra
Layout: Douwe Oppewal
Production: Ipskamp Printing

ISBN: 978-94-6469-420-8

Financial support for production was received from Maastricht University

NEUROANATOMICAL VARIATION IN PARKINSON'S DISEASE MOTOR SUBTYPES

DISSERTATION

To obtain the degree of Doctor at Maastricht University,
on the authority of the Rector Magnificus,
Prof. dr. Pamela Habibović
in accordance with the decision of the Board of Deans,
to be defended in public
on Monday June 26th 2023, at 16:00 hours

by

Jackson Tyler Boonstra

Promoters
Prof. dr. Yasin Temel
Dr. Ali Jahanshahi

Co-promoter
Dr. Alard Roebroeck

Assessment Committee
Prof. dr. D.E.J. Linden (chair)
Dr. L. Ackermans
Prof. dr. B.U. Forstmann (University of Amsterdam)
Prof. dr. A.F.G. Leentjens
Dr. F. Schaper (Harvard Medical School, Boston)

Dedicated to my late grandfathers

Drs. Bert (Engelbertus) Boonstra,
Middle School Principal and Director of Transportation at
the American School of The Hague

&

Richard 'Dick' Hills Jackson,
Wharfinger and retired Lieutenant Commander of
the United States Navy

Contents

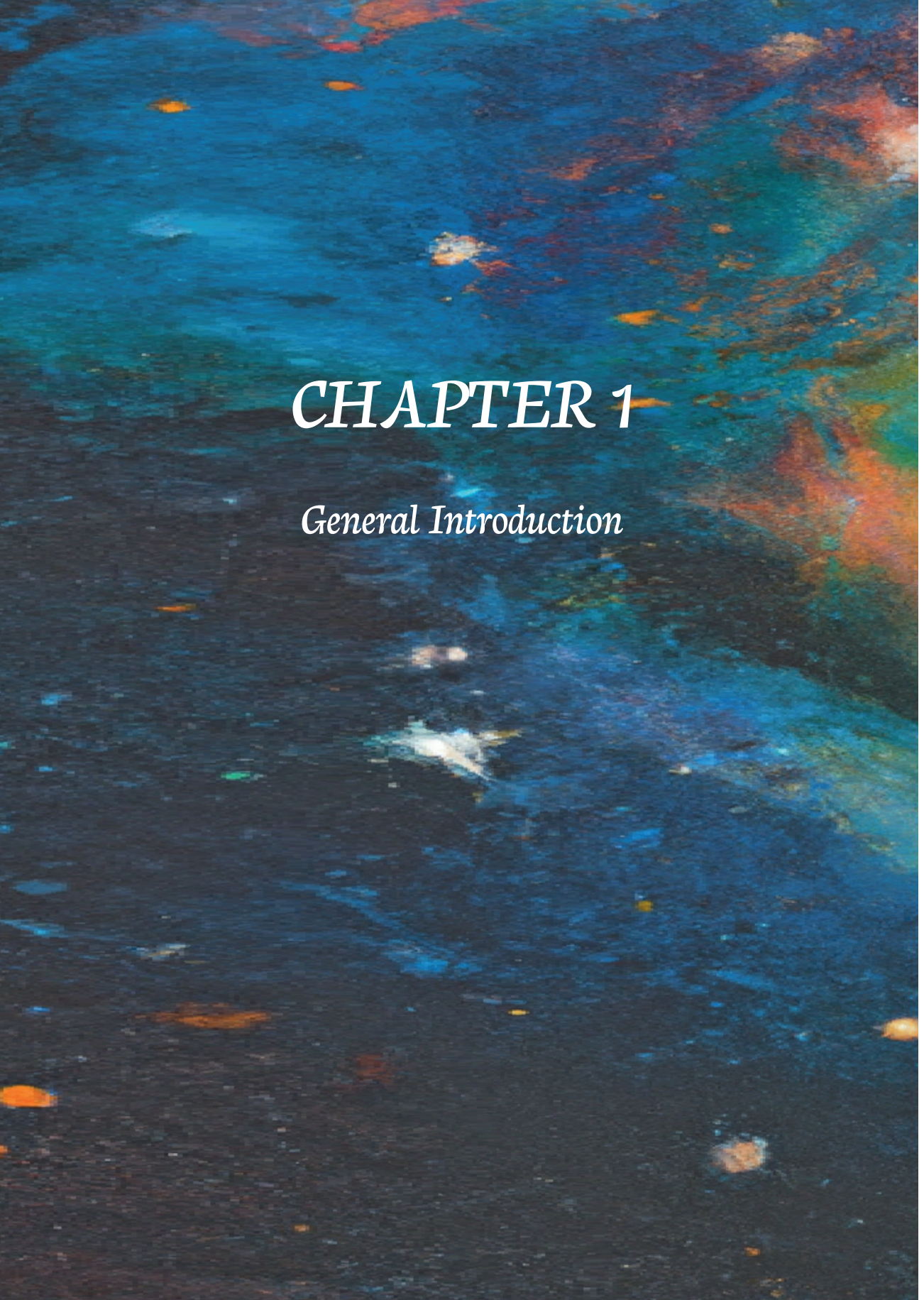

CHAPTER 1

General Introduction

Parkinson's Disease

Parkinson's disease (PD) is a progressive neurodegenerative disorder principally characterized by the loss of dopamine-producing neurons in the substantia nigra, a region of the midbrain at the heart of human motor circuitry.[1,2] The main clinical symptoms of PD are motor symptoms such as tremors, bradykinesia (slowness of movement), rigidity, postural instability, falls and dizziness, freezing (-of gait), muscle cramps, and dystonia (involuntary muscle contractions that cause slow repetitive movements or abnormal postures).[3,4] Furthermore, non-motor symptoms, such as depression, anxiety, sleep disturbances, cognitive and memory impairments, hallucinations, pain, fatigue, low blood pressure, restless legs, bladder and incontinence problems, excessive sweating, swallowing and eating impairments, speech and communication issues, eye sight deterioration, and low dental health are also commonly present and greatly impact patients' quality of life.[5,6] An estimated 50–80% of those with PD also eventually develop dementia.[7]

As the prevalence of PD increases with age, it is estimated that approximately 1% of individuals over the age of 60 years are affected.[8] Moreover, as the global population continues to age, the number of individuals with Parkinson's disease is expected to rise.[9] From 1990 to 2015, the number of individuals with Parkinson's disease doubled from 3 to 6+ million, a number that is projected to double again to over 12 million by the year 2040.[10] Currently, there are more than 10 million people worldwide are living with PD.[11] The estimated PD-associated economic burden in the United States is $51 billion every year, and is projected to surpass $79 billion by 2037, a figure that was previously, and may still be, underestimated.[12]

The diagnosis of PD can be a complex and challenging process, typically involving a combination of several different diagnostic tools and tests.[13] These methods including reviewing ones medical history, performing physical and neurological examinations, undergoing medical imaging such as MRI or CT, dopamine testing, and genetic testing.[14-17] The process can be time-consuming and may require multiple visits to a specialist, but it is important to receive a correct and accurate diagnosis in order to receive the best possible treatment.[18]

The exact cause of PD is not yet known[2], but research shows a combination of genetic and environmental factors are believed to play important roles.[19] Several gene mutations have been identified that increase an individual's risk of developing PD[20,21]; these mutations affect proteins involved in the regulation of dopamine production and degradation, as well as the maintenance of cellular structures (e.g., mitochondria). Interestingly, there are currently human trials to test blocking genetic interactions (e.g., LRRK2 inhibitors) to protect neurons and slow or halt disease progression.[22,23] However, genetic mutations

are only found in a small percentage of PD cases, and most cases are considered *sporadic*, meaning they occur in individuals without a family history of the disease.[24] Environmental factors have also been associated with an increased risk of PD, include exposure to toxins such as pesticides, herbicides (e.g., paraquat), farming chemicals, heavy metals, solvents and polychlorinated biphenyls (PCBs), industrial detergents, trichloroethylene (a solvent), lead, and even Agent Orange during the Vietnam War.[25-27]

There are potential protective factors that may reduce the risk of developing PD, including caffeine intake, anti-inflammatory drugs, cigarette smoking (perhaps due to protective nicotine factors), statins used to lower cholesterol, high vitamin D levels, and exercise in life.[28-30] It has been further proposed that an interaction between genetic and environmental factors may exacerbate disease progression.[31] Some theories suggest certain genetic variations alter an individual's susceptibility to environmental toxins and lead to an increased risk of PD development.[32,33] Others propose genetic variations influences an individual's ability to clear toxic agents from the body[34] and increase the accumulation of toxins that ultimately contributing to disease development.

Despite ongoing research, there is currently no cure for PD. However, there are a variety of treatment options available including prescription medication, neurosurgery, and rehabilitation aimed to manage symptoms and improve quality of life.[35] Pharmacological intervention is one of the most common forms of treatment for PD, typically involving the use of medications such as levodopa that converts into dopamine and can help alleviate tremors and other motor symptoms.[36] In addition to levodopa, other medications, such as anticholinergics and dopamine agonists, can also be used for additional benefits. Physical rehabilitation involving exercises to improve balance and coordination and strategies to help manage falls can also help improve mobility, gait, and overall physical function.[37] Additionally, neurosurgery is another treatment option, although it is only considered in more severe cases or when other treatments have not been effective. Neurosurgical procedures include deep brain stimulation (DBS) involving the implantation of electrodes into the brain to regulate electrical activity to alleviate symptoms[38], or pallidotomy, that is, the removal of small portions of the brain in specific areas involved in PD circuitopathy.[39] There is no one-size-fits-all approach to treating PD, and the best treatment plan will always depend on the individual patient and the progression of their symptoms.

Parkinson's Disease Motor Subtypes

PD can be categorized into motor subtypes, clinically determined with the Movement Disorder Society Unified Parkinson's Disease Rating Scale (MDS-UPDRS), an assessment of motor and non-motor PD symptoms.[40] The ratio of the mean tremor score to the

mean score of their postural instability and gait difficulty (PIGD) score can be used to differentiate tremor-dominance (TD) patients (ratio ≥ 1.5), from PIGD patients (ratio ≤ 1), and from intermediate or 'mixed-type' patients (ratios > 1.0 and < 1.5). Those patients diagnosed with PIGD have been called akinetic-rigid (AR) with both subtypes often denoted as non-tremor dominant (nTD).[41]

Heterogeneous motor symptom presentation between PD subtypes suggest correspondingly diverse neuropathophysiologies. Research shows both TD and nTD PD patients differing in various neuroanatomical and neurofunctional domains as well as in non-motor symptoms and quality of life.[42] Patients with nTD have shown accelerated motor, functional, and cognitive decline compared to TD, resulting in TD to be considered the less severe subtype. The full extent of PD pathology is poorly understood and even less is known about pathological differences between PD motor subtypes. Given the complexity of divergent PD symptoms and treatment regimes, interdisciplinary approaches are needed for the identification, management, and treatment of this debilitating disorder. Moreover, how pathophysiological alterations between PD motor subtypes fit into contemporary mechanistic circuitry theories of PD symptoms genesis has yet to be fully elucidated upon.

Neurological Imaging

Magnetic resonance imaging (MRI) is a non-invasive medical imaging technique used for the diagnoses of a wide range of medical conditions. Utilizing strong magnetic fields and radio waves to generate high-resolution images of the body's internal structures, MRI has the ability to provide detailed images of the human brain. In the context of PD, MRI is used to help diagnose and monitor the progression of the disease, as it can measure and monitor changes in the anatomy and function of specific regions associated with certain symptoms and pathologies.[43] MRI can also assess brain damage, evaluate the efficacy of treatments, and provide further insights into the neural changes associated with the underlying mechanisms of PD.

Tractography is an MRI technique that measures the diffusion of water molecules in the brain and can help reveal the streamline orientation and integrity of white matter fibers. In PD, these streamlines of white matter in the brain are often used to study specific neural connections and networks that may be affected by the disease. For example, connectivity indices derived from diffusion images have shown lower structural connectivity in nTD in key neuronal motor areas compared to TD.[44] Diffusion imaging may be able to detect subtle changes in the brain that other non-invasive imaging techniques cannot and be utilized to locate potential new biomarkers, allowing for earlier and more accurate diagnoses and further monitoring of treatment.

Another imaging technique, histology, is the study of the microscopic anatomy of cells and tissues. While PD can be diagnosed by a medical professional during a patient's lifetime with various clinical tests, there is no one definitive test. A diagnosis postmortem through histological analysis is considered the gold standard.[45] The hallmark of PD is the degeneration of dopamine-producing neurons in the substantia nigra.[46] This degeneration leads to a reduction of dopamine levels in the basal ganglia motor circuitry and largely underlies motor disturbances. Histological examinations also reveal the presence of abnormal protein aggregates called Lewy bodies in affected neurons that are highly associated with the loss of dopaminergic neurons.[46] These protein aggregates are toxic as the clumps of alpha-synuclein are passed from one neuron to another causing the disease to spread throughout the brain. Despite extensive research towards PD pathology, histological variations between motor subtypes are less explored.

MRI and histology are both valuable tools in the diagnosis and understanding of PD. While MRI offers non-invasive means of observing brain structure and function, histology provides direct evidence of underlying neuropathological changes. When combined, these imaging methodologies provide complementary information towards PD and help to create more comprehensive images of the disease.[47,48] Differentiating motor-subtypes through these multimodal imaging regimes is imperative to increases the ability to monitor *in vivo* disease progression and identify at risk populations, possibly even at an asymptomatic phase of PD.[49]

Aims and research questions from the thesis

One of the overall aims of this thesis is to fill gaps between pathology and neurocircuitry. Here, we consolidate studies characterizing pathological variances between TD and nTD subtypes of PD with contemporary mechanistic circuitry theories of PD symptom genesis. Translational neuroscience works in this regard to understand the underlying mechanisms of PD and develop new and more effective therapeutic strategies. Four research questions have thus been formulated and addressed as aims in this thesis.

(1) What does previous literature tell us about the differences between Parkinson's disease (PD) motor subtypes?
(2) What can MR imaging tell us about PD motor subtypes?
(3) What can histological analyses tell us about PD motor subtypes?
(4) How can multimodal imaging regimes integrate and work together to create a better understanding of PD circuitopathies?

Outline of the thesis

The review in **Chapter 2** addresses research aim (1) by giving a detailed overview of studies showing diverse neuroimaging alterations between TD PD patients and those with nTD motor subtypes. It shows various neuroimaging regimes display variability between TD and nTD PD patients and persistently support the notion that the subtype of TD is the more '*benign*' subtype as TD shows less negative alternations compared to nTD, while nTD show symptoms that are more aggressive, revealed by earlier and more rapid physical decline.

In **Chapter 3,** we work towards research aim (2) by highlighting a dedicated container designed for scanning postmortem brains in an ultra-high field MRI machine. Several considerations made to optimize the container to be easy to use within MR facilities and engender high quality images with a low number of artefacts are discussed. Proof that the container has the necessary qualifications needed for postmortem imaging including ease of transportation, vacuum sealing capabilities, and compatibility with previously designed sequences and procedures are demonstrated.

Chapter 4 addresses aim (2) by investigating diffusion MRI on twelve post-mortem hemispheres (eight parkinsonian (four TD, four nTD) and four healthy controls) scanned with a bespoke 9.4 Tesla human brain radiofrequency coil. Diffusion tensor analysis was performed for local scalar diffusion metrics and constrained spherical deconvolution tractography was performed for global connectivity matrixes. Multiple regional diffusion metrics and interconnections within basal ganglia circuitry are analysed and discussed.

Chapter 5 address aim (1) and (4) with pathological literature. It reviews an array of pathological examination techniques and show significant differences between TD and nTD PD subtypes. The reviewed pathological studies are consistent with neuroimaging data and support contemporary mechanistic circuitry theories of PD motor symptom genesis.

Chapter 6 addresses aims (3 & 4) via pathological examinations on the same postmortem material scanned in **Chapter 4**. Various histological and immunohistochemical stainings were performed, quantified, and examined across subtypes and against healthy controls. Results are compared against MR imaging data and discussed in view of their multimodal imaging qualities.

Chapter 7 summarizes and discusses all main findings to further address aim (4). Strengths and limitations towards multimodal imaging modalities are discussed and future investigatory works are proposed. We hope that this research presented in full helps to create a more holistic understanding of Parkinsonian neurodegeneration, improves clinical outcomes for patients undergoing treatment, and supports the imperative challenge to one day rid humanity of this disease.

References

1. Braak, H., K. Del Tredici, U. Rub, et al., *Staging of brain pathology related to sporadic Parkinson's disease.* Neurobiol Aging, 2003. **24**(2): p. 197-211.
2. Kalia, L.V. and A.E. Lang, *Parkinson's disease.* Lancet, 2015. **386**(9996): p. 896-912.
3. Jankovic, J., *Parkinson's disease: clinical features and diagnosis.* J Neurol Neurosurg Psychiatry, 2008. **79**(4): p. 368-76.
4. Moustafa, A.A., S. Chakravarthy, J.R. Phillips, et al., *Motor symptoms in Parkinson's disease: A unified framework.* Neurosci Biobehav Rev, 2016. **68**: p. 727-740.
5. Chaudhuri, K.R., D.G. Healy, A.H. Schapira, and E. National Institute for Clinical, *Non-motor symptoms of Parkinson's disease: diagnosis and management.* Lancet Neurol, 2006. **5**(3): p. 235-45.
6. Rana, A.Q., U.S. Ahmed, Z.M. Chaudry, and S. Vasan, *Parkinson's disease: a review of non-motor symptoms.* Expert Rev Neurother, 2015. **15**(5): p. 549-62.
7. Aarsland, D. and M.W. Kurz, *The epidemiology of dementia associated with Parkinson's disease.* Brain Pathol, 2010. **20**(3): p. 633-9.
8. Pringsheim, T., N. Jette, A. Frolkis, and T.D. Steeves, *The prevalence of Parkinson's disease: a systematic review and meta-analysis.* Mov Disord, 2014. **29**(13): p. 1583-90.
9. Lang, A.E. and A.M. Lozano, *Parkinson's disease. First of two parts.* N Engl J Med, 1998. **339**(15): p. 1044-53.
10. Dorsey, E.R., T. Sherer, M.S. Okun, and B.R. Bloem, *The Emerging Evidence of the Parkinson Pandemic.* J Parkinsons Dis, 2018. **8**(s1): p. S3-S8.
11. Prasad, E.M. and S.Y. Hung, *Current Therapies in Clinical Trials of Parkinson's Disease: A 2021 Update.* Pharmaceuticals (Basel), 2021. **14**(8).
12. Yang, W., J.L. Hamilton, C. Kopil, et al., *Current and projected future economic burden of Parkinson's disease in the U.S.* NPJ Parkinsons Dis, 2020. **6**: p. 15.
13. Postuma, R.B., D. Berg, M. Stern, et al., *MDS clinical diagnostic criteria for Parkinson's disease.* Mov Disord, 2015. **30**(12): p. 1591-601.
14. Stiasny-Kolster, K., F. Sixel-Doring, C. Trenkwalder, et al., *Diagnostic value of the REM sleep behavior disorder screening questionnaire in Parkinson's disease.* Sleep Med, 2015. **16**(1): p. 186-9.
15. Yang, K., W.X. Xiong, F.T. Liu, et al., *Objective and quantitative assessment of motor function in Parkinson's disease-from the perspective of practical applications.* Ann Transl Med, 2016. **4**(5): p. 90.
16. Baranauskas, M., R. Jurkonis, A. Lukosevicius, et al., *Diagnostic Ability of Radiofrequency Ultrasound in Parkinson's Disease Compared to Conventional Transcranial Sonography and Magnetic Resonance Imaging.* Diagnostics (Basel), 2020. **10**(10).
17. Chakraborty, S., S. Aich, and H.C. Kim, *Detection of Parkinson's Disease from 3T T1 Weighted MRI Scans Using 3D Convolutional Neural Network.* Diagnostics (Basel), 2020. **10**(6).
18. Frohlich, H., N. Bontridder, D. Petrovska-Delacreta, et al., *Leveraging the Potential of Digital Technology for Better Individualized Treatment of Parkinson's Disease.* Front Neurol, 2022. **13**: p. 788427.
19. Olanow, C.W. and W.G. Tatton, *Etiology and pathogenesis of Parkinson's disease.* Annu Rev Neurosci, 1999. **22**: p. 123-44.
20. Elsayed, I., A. Martinez-Carrasco, M. Cornejo-Olivas, and S. Bandres-Ciga, *Mapping the Diverse and Inclusive Future of Parkinson's Disease Genetics and Its Widespread Impact.* Genes (Basel), 2021. **12**(11).
21. Grover, S., A.A. Kumar Sreelatha, L. Pihlstrom, et al., *Genome-wide Association and Meta-analysis of Age at Onset in Parkinson Disease: Evidence From the COURAGE-PD Consortium.* Neurology, 2022. **99**(7): p. e698-e710.
22. Wojewska, D.N. and A. Kortholt, *LRRK2 Targeting Strategies as Potential Treatment of Parkinson's Disease.* Biomolecules, 2021. **11**(8).
23. Thakur, G., V. Kumar, K.W. Lee, and C. Won, *Structural Insights and Development of LRRK2 Inhibitors for Parkinson's Disease in the Last Decade.* Genes (Basel), 2022. **13**(8).
24. Chai, C. and K.L. Lim, *Genetic insights into sporadic Parkinson's disease pathogenesis.* Curr Genomics, 2013. **14**(8): p. 486-501.

25. De Miranda, B.R., S.M. Goldman, G.W. Miller, J.T. Greenamyre, and E.R. Dorsey, *Preventing Parkinson's Disease: An Environmental Agenda.* J Parkinsons Dis, 2022. **12**(1): p. 45-68.
26. Goldman, S.M., *Environmental toxins and Parkinson's disease.* Annu Rev Pharmacol Toxicol, 2014. **54**: p. 141-64.
27. Ball, N., W.P. Teo, S. Chandra, and J. Chapman, *Parkinson's Disease and the Environment.* Front Neurol, 2019. **10**: p. 218.
28. Belvisi, D., R. Pellicciari, G. Fabbrini, et al., *Modifiable risk and protective factors in disease development, progression and clinical subtypes of Parkinson's disease: What do prospective studies suggest?* Neurobiol Dis, 2020. **134**: p. 104671.
29. Mentis, A.A., E. Dardiotis, V. Efthymiou, and G.P. Chrousos, *Non-genetic risk and protective factors and biomarkers for neurological disorders: a meta-umbrella systematic review of umbrella reviews.* BMC Med, 2021. **19**(1): p. 6.
30. Ma, C., S. Molsberry, Y. Li, et al., *Dietary nicotine intake and risk of Parkinson disease: a prospective study.* Am J Clin Nutr, 2020. **112**(4): p. 1080-1087.
31. Pang, S.Y., P.W. Ho, H.F. Liu, et al., *The interplay of aging, genetics and environmental factors in the pathogenesis of Parkinson's disease.* Transl Neurodegener, 2019. **8**: p. 23.
32. Logroscino, G., *The role of early life environmental risk factors in Parkinson disease: what is the evidence?* Environ Health Perspect, 2005. **113**(9): p. 1234-8.
33. Schaffner, S.L. and M.S. Kobor, *DNA methylation as a mediator of genetic and environmental influences on Parkinson's disease susceptibility: Impacts of alpha-Synuclein, physical activity, and pesticide exposure on the epigenome.* Front Genet, 2022. **13**: p. 971298.
34. Erekat, N.S., *Autophagy and Its Association with Genetic Mutations in Parkinson Disease.* Med Sci Monit, 2022. **28**: p. e938519.
35. Gouda, N.A., A. Elkamhawy, and J. Cho, *Emerging Therapeutic Strategies for Parkinson's Disease and Future Prospects: A 2021 Update.* Biomedicines, 2022. **10**(2).
36. Fahn, S., D. Oakes, I. Shoulson, et al., *Levodopa and the progression of Parkinson's disease.* N Engl J Med, 2004. **351**(24): p. 2498-508.
37. Bouca-Machado, R., A. Rosario, D. Caldeira, et al., *Physical Activity, Exercise, and Physiotherapy in Parkinson's Disease: Defining the Concepts.* Mov Disord Clin Pract, 2020. **7**(1): p. 7-15.
38. Temel, Y. and V. Visser-Vandewalle, *Targets for deep brain stimulation in Parkinson's disease.* Expert Opin Ther Targets, 2006. **10**(3): p. 355-62.
39. Nikkhah, G., G.A. Carvalho, and M. Pinsker, *Functional neurosurgery in Parkinson's disease: a long journey from destruction over modulation towards restoration.* Acta Neurochir Suppl, 2013. **117**: p. 5-11.
40. Goetz, C.G., S. Fahn, P. Martinez-Martin, et al., *Movement Disorder Society-sponsored revision of the Unified Parkinson's Disease Rating Scale (MDS-UPDRS): Process, format, and clinimetric testing plan.* Mov Disord, 2007. **22**(1): p. 41-7.
41. Ren, J., P. Hua, Y. Li, et al., *Comparison of Three Motor Subtype Classifications in de novo Parkinson's Disease Patients.* Front Neurol, 2020. **11**: p. 601225.
42. Boonstra, J.T., S. Michielse, Y. Temel, G. Hoogland, and A. Jahanshahi, *Neuroimaging Detectable Differences between Parkinson's Disease Motor Subtypes: A Systematic Review.* Mov Disord Clin Pract, 2021. **8**(2): p. 175-192.
43. Heim, B., F. Krismer, R. De Marzi, and K. Seppi, *Magnetic resonance imaging for the diagnosis of Parkinson's disease.* J Neural Transm (Vienna), 2017. **124**(8): p. 915-964.
44. Barbagallo, G., M.E. Caligiuri, G. Arabia, et al., *Structural connectivity differences in motor network between tremor-dominant and nontremor Parkinson's disease.* Hum Brain Mapp, 2017. **38**(9): p. 4716-4729.
45. Geut, H., D.H. Hepp, E. Foncke, et al., *Neuropathological correlates of parkinsonian disorders in a large Dutch autopsy series.* Acta Neuropathol Commun, 2020. **8**(1): p. 39.
46. Antony, P.M., N.J. Diederich, R. Kruger, and R. Balling, *The hallmarks of Parkinson's disease.* FEBS J, 2013. **280**(23): p. 5981-93.

47. He, N., K. Ghassaban, P. Huang, et al., *Imaging iron and neuromelanin simultaneously using a single 3D gradient echo magnetization transfer sequence: Combining neuromelanin, iron and the nigrosome-1 sign as complementary imaging biomarkers in early stage Parkinson's disease.* Neuroimage, 2021. **230**: p. 117810.
48. Jonkman, L.E., B. Kenkhuis, J.J.G. Geurts, and W.D.J. van de Berg, *Post-Mortem MRI and Histopathology in Neurologic Disease: A Translational Approach.* Neurosci Bull, 2019. **35**(2): p. 229-243.
49. Gatto, R.G. and Y.C. Wu, *Editorial: Innovative Imaging Techniques in Preclinical Models of Neurodegenerative Diseases.* Front Neurosci, 2021. **15**: p. 801037.

CHAPTER 2

Neuroimaging Detectable Differences between Parkinson's Disease Motor Subtypes: A Systematic Review

Boonstra, J. T., Michielse, S., Temel, Y., Hoogland, G. & Jahanshahi, A.

Neuroimaging detectable differences between Parkinson's disease motor subtypes: a systematic review. Mov. Disord. Clin. Pr. 8, 175–192 (2021).

Abstract

Background: The neuroanatomical substrates of Parkinson's disease (PD) with tremor-dominance (TD) and those with non-tremor dominance (nTD), postural instability and gait difficulty (PIGD), and akinetic-rigid (AR) are not fully differentiated. A better understanding of symptom specific pathoanatomical markers of PD subtypes may result in earlier diagnosis and more tailored treatment. Here, we aim to give an overview of the neuroimaging literature that compared PD motor subtypes.

Methods: A systematic literature review on neuroimaging studies of PD subtypes was conducted according to the Preferred Reporting Items for Systematic Reviews and Meta-Analyses (PRISMA) guidelines. Search terms submitted to the PubMed database included: "Parkinson's disease", "MRI" and "motor subtypes" (TD, nTD, PIGD, AR). The results are first discussed from macro to micro level of organization (i.e., (1) structural; (2) functional; and (3) molecular) and then by applied imaging methodology.

Findings: Several neuroimaging methods including diffusion imaging and positron emission tomography (PET) distinguish specific PD motor subtypes well, although findings are mixed. Furthermore, our review demonstrates that nTD-PD patients have more severe neuroalterations compared to TD-PD patients. More specifically, nTD-PD patients have deficits within striato-thalamo-cortical (STC) circuitry and other thalamocortical projections related to cognitive and sensorimotor function, while TD-PD patients tend to have greater cerebello-thalamo-cortical (CTC) circuitry dysfunction.

Conclusions: Based on the literature, STC and CTC circuitry deficits seem to be the key features of PD and the subtypes. Future research should make greater use of multimodal neuroimaging and techniques that have higher sensitivity in delineating subcortical structures involved in motor diseases.

Introduction

Parkinson's disease (PD) is a progressive and complex neurodegenerative disorder. Patients with PD show highly heterogeneous clinical characteristics developing tremors and/or kinesia paradoxa, an umbrella term for non-tremor motor symptoms including absence of movement (akinesia), decreased amplitude of movement (hypokinesia), and slowness in movement execution (bradykinesia).[1]

PD motor subtypes, including tremor-dominant (TD) and non-tremor dominant (nTD) (often characterized by postural instability & gait difficulty (PIGD) and akinetic-rigid (AR)), suggest different pathophysiologies.[2-5] These motor subtypes are mainly determined by the Movement Disorder Society Unified Parkinson's Disease Rating Scale (MDS-UPDRS), a comprehensive 50-question assessment of both motor and non-motor symptoms associated with PD.[6] Similarly, the original UPDRS is also utilized in PD research and can be used for the same purpose. The ratio of the mean tremor scores (eight items from Part III) to the mean of the PIGD scores (five items from Part III) is used to delineate TD patients (ratio ≥ 1.5), from PIGD patients (ratio ≤ 1), and from intermediate or 'mixed-type' patients (ratios >1.0 and < 1.5).[7] Additionally, subscores of TD and AR can be derived by averaging symptom specific questions from Part III.[8] These classifications help to clinically distinguish PD subtypes and allow for steady investigations of symptom specific alterations.

On a pathological level, PD is characterized by progressive degeneration of intertwined subcortical dopaminergic nigrostriatal systems,[9, 10] Lewy body aggregations, and depletion of dopamine in the striatum[11-13] all of which can be identified via postmortem histology. Compared to TD, AR patients have shown more severe cell loss in the substantia nigra (SN) and such cell loss was shown to negatively correlate with AR symptom severity.[14] nTD patients have shown more severe cell loss in the ventrolateral part of the substantia nigra pars compacta (SNc) that projects to the dorsal putamen, causing inhibition of the glutamatergic thalamo-cortical (*direct*) pathway and reduced cortical activation, while in contrast, TD patients show more severe neuronal loss in the medial, rather than in the lateral SNc that projects to the lateral putamen, caudate nucleus, ventromedial thalamus, and rubral areas (*indirect pathway*) leading to hyperactivity of thalamo-motor projections.[14] In this light, nTD is thought to be due more to abnormal basal ganglia (BG) output while TD evolves additional downstream compensatory mechanisms.[5] Previous studies using diverse neuroimaging methodologies have been utilized to understand PD circuitopathies. However, the full extent of the neuroanatomical and neurofunctional differences between the PD motor subtypes TD and nTD that can be seen with neuroimaging are poorly understood.[10, 15-17] Further differentiating motor-subtypes of PD through neuroimaging will increase the ability to monitor progression and identify at risk populations, possibly

even at an asymptomatic phase of PD,[18-20] and work to improve localization and targeting for non-invasive and invasive neuromodulation therapies.[21, 22] Here, previous research that used neuroimaging techniques to characterize structural and functional variances between TD and nTD subtypes of PD are consolidated. First, an overview of imaging studies related to the neuroanatomical, functional, and neurochemical basis of TD and nTD PD is given. These are followed by descriptions of limitations that occur within each imaging methodology when applied to PD. Lastly, potential hypotheses are addressed that may be tested by neuroimaging PD motor subtypes, their clinical implications, and how this may increase insight into neurobiological underpinnings.

Methods

Literature Selection

This review was conducted according to the Preferred Reporting Items for Systematic Reviews and Meta-Analyses (PRISMA) guidelines. We evaluated human neuroimaging studies on PD subtypes TD, nTD, PIGD, and AR published in international English written peer reviewed journals up to May 2020. A PubMed search based on various dictions of Parkinson's disease (PD) (MeSH), neuroimaging technique (MRI) (MeSH), and PD subtypes (TD (MeSH), nTD, PIGD, AR) were applied (see Supplementary Material **File S1**). This resulted in 546 publications that were independently reviewed by two assessors. Full text of the articles were reviewed and additional articles were found via reference sections. Seventy-five articles were included in the final analysis.

Inclusion Criteria

1. Study analyzed human data and was published in English.
2. Study reported the proportion of PD patients with TD-PD and nTD-PD.
3. Comparative neuroimaging analysis had been carried out directly concerning TD-PD versus nTD-PD.

Data Extraction

Relevant data obtained and collected using a data extraction spreadsheet and grouped per neuroimaging modality included:

- Primary author and year of publication
- Imaging method
- MRI strength and vendor
- Number of participants in PD subtypes
- Key findings

Results

Structural Imaging

Structural Imaging Techniques

MR-based techniques allow for visualization of the microstructural anatomy of brain tissue. One processing method on high-resolution 3DT1 sequences is called voxel based morphometry (VBM) that can compare local concentrations of gray matter between groups of subjects.[23] Other techniques include diffusion-weighted imaging (DWI), a method to measure the diffusion of water molecules within the brain, and diffusion tensor imaging (DTI), a paradigm that analyses the three-dimensional shape of such diffusion and allows for visualization of fiber tracts. Additional quantitative structural MR-based techniques include neuromelanin sensitive MRI (NM-MRI) used to detect a product of dopamine metabolism called neuromelanin, age-related white matter changes (ARWMC) which are hyperintense lesions observed on T2-weighted MR images, and leukoaraiosis or white matter hyperintensities (WMH), an abnormal change in white matter near lateral ventricles.[24]

Cortical and Subcortical Volumes

Gray Matter

Measurements of gray matter (GM) can potentially reveal more about neural functions that underpin particular symptomologies (Table **1**). In reference **25**, researchers found that TD had less GM atrophy in frontal, parietal, occipital, and temporal lobes, as well as in the caudate nucleus and the cerebellar culmen, and later found TD had larger GM volumes (GMV) in the amygdala and globus pallidus (GP) compared to PIGD but with no cerebellar differences.[26] In 2017, one group found lower GMV in the frontal cortex of TD compared to PIGD, but this difference did not hold true when nuisance covariates of disease severity, disease duration, and medication were controlled for.[27] Another study showed TD to have significantly larger GMV along the lateral border of the right thalamus compared to nTD.[28] The GM degeneration in frontal regions could be the underlying cause or consequence of the greater cognitive decline that is commonly seen within PIGD[29] while cognitive decline itself may also feed into gait difficulties, as fall risk was previously found to be related to the motor-cognitive interdependence of executive function.[30] The amygdala GMV changes could also underlie numerous affective (non-motor) symptoms in nTD, including depression, apathy, and anxiety.[31] Similarly, as loss of smell is a prodromal sign of PD,[1] TD having larger olfactory bulb volumes compared to nTD[32] could point towards differing symptoms between subtypes.

Table 1. Differences with structural MRI between PD motor subtypes

Study	MRI Strength	PD	TD	nTD	PIGD	AR	Mixed	HC	Findings
Gray Matter									
(Al-Bachari et al., 2017 [27]	3T Philips		21		24		6		TD trended to have lower GMV in the frontal cortex compared to PIGD. TD had lower WML volume compared to PIGD.
(Altinayar et al., 2014) [32]	1.5T Siemens		27	14				19	TD had larger olfactory bulb volumes than nTD.
(Benninger et al., 2009) [28]	3T Philips		14	10					TD had lower GMV in the mainly right posterior part of the cerebellar quadrangular lobe. TD had larger GMV along the lateral border of the right thalamus compared to nTD.
(Piccinin et al., 2017) [33]	3T Philips		44			19			TD had decreased GMV in the left lobule VIIIa compared to AR.
(Rosenberg-Katz et al., 2013) [25]	3T GE		29		30				TD had higher GMV in frontal, parietal, occipital, temporal lobes, right caudate nucleus, amygdala, and the bilateral cerebellar culmen and left declive compared to PIGD.
(Rosenberg-Katz et al., 2016) [26]	3T GE		30		30			28	TD had larger GMV in amygdala and globus pallidus compared to PIGD.
Cortical Thickness									
(Danti et al., 2015) [40]	1.5T Siemens		22		14			18	MCI-TD showed no significant cortical thinning compared to MCI-PIGD.
(Herb et al., 2016) [38]	3T Philips		45		74	58			TD had greater cortical thickness than PIGD in the dorsolateral frontal lobes, anterior temporal lobes, and cuneus, and precuneus. PIGD had reduced cortical thickness compared to AR in multiple areas. No cortical distinctions were shown between TD and AR.
(Karunanayaka et al., 2016) [39]	3T Siemens		15			17		24	No differences in cortical thickness were seen between AR, TD, and controls in the DMN.
(Linder et al., 2009) [43]	1.5T Philips		23		35		8	30	TD showed no difference in MRI parameters compared to PIGD.
(Nyberg et al., 2015) [41]	3T GE		12		9			20	TD had no significant subcortical volume differences compared to PIGD.

(Prodoehl et al., 2013) [44]	3T GE		10	10			20	TD did not differ in cortical or subcortical GMV or WMV compared to nTD.
(Tessa et al., 2008) [45]	1.5T Siemens		13		11	3	16	TD did not differ in total brain GMV or WMV compared to AR or healthy controls.
(Vervoort et al., 2016a) [69]	3T Philips		16	39			19	No volumetric differences in caudate, putamen and pallidum were shown between TD and PIGD. No shape alterations in right caudate and the bilateral putamen and pallidum were seen between TD and PIGD.
White Matter								
(Bohnen et al., 2011a) [48]	3T Philips		25	36		10		TD had lower WMH compared to PIGD.
(Fang et al., 2020) [56]	3T Siemens	21		23			20	PIGD patients showed significantly higher white matter lesion load in the caudate and lateral and third ventricle when compared to non-PIGD.
(Herman et al., 2013) [54]	3T GE		42	62		4		TD did not differ in mean number of voxels with WMHs compared to PIGD.
(Lee et al., 2009) [55]	1.5 GE		75	54				TD were independently associated with lower leukoaraiosis grade compared to PIGD.
(Moccia et al., 2016) [49]	1.5T Philips		27, 35, 36	18, 20, 22		18, 8, 4		TD had lower ARWMC compared to PIGD at baseline and at 2 and 4 years follow up.
(Shen et al., 2019) [52]	1.5T Philips		40	136				TD/non-PIGD patients had lower white matter hyperintensity scores compared to PIGD.
(Wan et al., 2019) [50]	3T GE	38		89				PIGD showed more severe deep WMH in the frontal and occipital lobes when compared to non-PIGD.
Iron-sensitive								
(He et a., 2017) [2]	3T GE		19		24		48	TD had significantly higher DN susceptibility values than AR.
(Jin et al., 2012) [59]	3T GE		25		48	14	50	TD and AR had correlations between serum ceruloplasmin levels and nigral bilateral average phase values. No differences in the bilateral average phase values between TD, AR, and Mixed in the bilateral substantia nigra, globus pallidus, putamen, the head of caudate, and the red nucleus.

(Schneider et al., 2016) [60]	3T Siemens	21		19		20	PIGD had lower SWI intensity values in putamen and globus pallidus compared to nPIGD.
(Xiang et al., 2017) [61]	3T Philips		9	14		20	PIGD had more severe signal attenuation in the medial part of the substantia nigra pars compacta compared to TD.
Other Structural Metrics							
(Chiu et al., 2018) [92]	1.5T, 3T GE		48	22	64		PIGD was associated with a higher prevalence of cerebral microbleeds when compared to TD and AR.

Note. Rosenberg-Katz et al., 2013 & 2016 report upon the same study sample. In Moccia et al., 2016, multiple numbers reflect baseline cohort and follow up cohorts at 2 and 4 years, respectively. AR = akinetic-rigid. ARWMC = age-related white matter changes. DMN = default mode network. DN = dentate nucleus. GE = General Electric. GMV = gray matter volumes. HC = healthy controls. MCI = mild cognitive impairment. Mixed = mixed-type/intermediate/indeterminate subtype. nPIGD = non postural instability and gait difficulty. nTD = non tremor-dominant. PD = Parkinson's disease. PIGD = postural instability and gait difficulty. SWI = susceptibility weighted imaging. T = Tesla. TD = tremor-dominant. WMH = white matter hyperintensity. WML = white matter lesions.WMV = white matter volumes..

Interestingly, TD had lower GMV in the posterior part of the right quadrangular lobe and in the declive of the cerebellum[28] while a separate study showed TD had decreased GM in the cerebellular left lobule VIIIa compared to AR.[33] Cerebellar atrophy could explain deficits within cerebello-thalamo-cortical (CTC) circuitry known to be deficient in TD patients[34] as the cerebellum has shown to perceive tremor as a voluntary motor behavior and modulate tremor amplitude.[35] The smaller pallidal, putamen, and caudate volumes in nTD are in line with the model of degenerating neurons in the cortico-basal ganglia-thalamo-cortical loop that seem to be related to hypokinesia.[36] Furthermore, increased thalamic and GP volumes found in TD suggest this regional enlargement indicates that TD are initially protected from a damaged basal ganglia-thalamocortical circuitry and could potentially explain why the TD subtype does not experience PIGD symptoms associated with BG degeneration.[26] These results are further supported by a recent lesion study showing PIGD patients have higher novel deep gray nuclear lesion load in the caudate compared to non-PIGD and healthy controls (HC).[56] GM analysis appears to support current PD circuitry models that underlie motor subtype differentiation of neuronal loss in key relay nuclei and stands as a valuable tool in the diagnostics and evaluation of PD subtypes.

Cortical Thickness

An important neuroanatomical aspect of PD is the thickness of gray matter in the cortex, as cortical thinning has shown to be primarily responsible for the reduction of cortical GMV.[37] One study found reduced cortical thickness in PIGD patients compared to AR patients in areas including the bilateral frontal lobes, superior parietal cortices, and posterior cortical regions.[38] The study reported PIGD to have reduced cortical thickness compared to TD in areas including the dorsolateral frontal lobes, anterior temporal lobes, and cuneus/precuneus, although no distinctions were seen when TD were compared to AR individuals or between PIGD and AR as the most pronounced cortical differences were between TD and PIGD patients localized to the left frontal region.

In contrast, a study using a smaller sample found that cortical thickness was similar between AR, TD, and healthy controls in specific brain regions part of the default mode network (DMN) such as the posterior cingulate cortex (PCC), the precuneus, the bilateral IPC, the medial prefrontal cortex (PFC), the anterior cingulate cortex (ACC), and the medial/lateral temporal lobe,[39] while another study of PD patients with mild cognitive impairment (MCI) also showed similar cortical thinning amongst MCI-TD compared to MCI-PIGD.[40] Another study showed that TD mean subcortical volumes were larger than PIGD in the putamen, caudate nucleus, GP, amygdala, and nucleus accumbens (NAc), and although these differences did not reach statistical significance, shape analysis resulting from local outward surface deviations revealed a significant difference in the right NAc shape between the two PD subtypes, mainly driven by the TD subtype, and the magnitude

of the shape deviation was significantly correlated with MDS-UPDRS TD and PIGD ratios suggesting that this NAc metric may hold as a neuroimaging biomarker for PD subtype.[41]

While cortical thinning has shown to be a significant characteristic of advancing PD severity, progression, and dementia-risk stratification,[42] cortical volume disparities between PD motor subtypes are less clear. While many studies investigating cortical volumes show no difference between PD subtypes,[40, 41, 43-45] these results could be due to dissimilarities in disease duration, amyloid deposition, and acetylcholine denervation, all of which differentially affect neuronal degeneration.[46, 47] Furthermore, several of the studies that did not find differences between PD subtypes used 1.5 T MRI.[40, 43, 45] Subcortical volumes that require higher resolution MRI to image may prove to be more efficacious in volumetrically distinguishing TD from PIGD patients. Nevertheless, alterations in cortical thickness in PD may still be due to divergent etiologies as results show more cortical changes in PIGD when differences were found.[38]

White Matter

White matter (WM) provides connections between cortical and subcortical GM regions. WM alterations are thought to interfere significantly with postural control due to greater degeneration of complex bilaterally distributed visual, somatosensory, and vestibular systems shown via higher WM signal hyperintensity burden in PIGD compared to TD.[48] Age-related white matter changes (ARWMC) have been shown to be lower in TD patients compared to PIGD, and a follow up 2 and 4 years later showed that total ARWMC scores remained lower in TD compared to PIGD patients.[49] Similarly, studies show that PIGD have reduced white matter integrity compared to non-PIGD, and that non-PIGD patients have lower white matter hyperintensity scores (WMHs) when compared to PIGD.[50-53] Conversely, a different study showed that the mean number of voxels with WMHs did not differ between TD and PIGD, even when patients with low and high burdens of WMHs were compared.[54]

When TD patients were compared to PIGD, PIGD patients were associated with additional degradations of white matter such as higher leukoaraiosis grade.[53, 55] More recently, when compared to non-PIGD and HC, PIGD patients showed a significantly higher white matter lesion (WML) load.[56] In reference **27**, researchers also showed PIGD to have higher WML volume compared to TD while reference **57** showed PIGD exhibited more WM degradation relative to TD.

Such white matter alterations are important within PD patients, as a single unit increase in ARWMC score at baseline was associated with a 2.7 times increased likelihood of developing PIGD during a 4-year observation, showing WM changes may help in defining progression into a specific PD motor subtype at an early stage.[49] Additionally, significant

clinical correlations between WMHs and ratings of posture, as well as borderline correlations of freezing with WM changes further support the view that nTD have worse WM integrity in corticocortical tracts.[48, 53]

Iron-Sensitive Sequences

Regional iron depositions in deep brain nuclei can be evaluated using phase shifts (radians) derived from filtered MR phase images. Parkinson's symptoms have previously shown to result as a consequence of dopaminergic neurodegeneration, as higher levels of iron measured using substantia nigra (SN) radians have shown to be positively correlated with UPDRS-III scores as well as bradykinesia-rigidity subscores, but not with tremor subscores[58] although TD patients have shown to have higher bilateral dentate nucleus (DN) magnetic susceptibility values compared to AR patients.[2]

Nigral bilateral average phase values and serum ceruloplasmin levels have shown to correlate significantly with each other in both TD and AR.[59] One study showed PIGD to have lower susceptibility weighted imaging (SWI) intensity values (containing both magnitude and phase information) in all regions compared to non-PIGD, particularly in the globus pallidus and with a similar trend in other basal ganglia nuclei.[60] Another study applied NM-MRI and found that the PIGD subtype had more severe signal attenuation in the medial part of the SNc compared to TD, and that the SNc ipsilateral to the most clinically affected side was the strongest in discriminating the two PD subtypes.[61] These findings suggest that iron load is involved in the development of bradykinesia and rigidity symptoms such that susceptibility values and NM-MRI relating to relative iron concentrations could be used to differentiate PD motor subtypes.

Structural Imaging Limitations

The major limitations of structural imaging study designs to investigate PD involve inconsistent subtype classification and patient selection bias.[25, 38, 41, 53] Moreover, many lack longitudinal study strategies[33, 39, 45, 48, 49, 53, 54] and have relatively small sample sizes as summarized in Tables **1** and **2**.[33, 39, 40, 45, 55] As MR technology (e.g., ultra-high field) and imaging techniques advance (e.g., quantitative susceptibility mapping (QSM) that quantifies the magnetic susceptibility value of brain tissue and provides contrast between iron-rich gray matter nuclei and surrounding tissues), MRI could be used to examine more subtle and subcortical structural changes that occur in PD that cannot be detected with low-field strengths and current approaches.[2, 58]

Table 2. Differences with diffusion MRI (dMRI) between PD motor subtypes

Study	MRI Strength	PD	TD	nTD	PIGD	AR	Mixed	HC	Findings
Fractional Anisotropy									
(Gu et al., 2014) [66]	3T GE	12			12				PIGD had reduced FA in bilateral SLF, bilateral anterior corona radiate, and the left genu of the corpus callosum compared to nPIGD. PIGD had increased RD in the left SLF. No significant differences were seen in AD between subtypes.
(Lenfeldt et al., 2016) [65]	1.5T Philips		40		64		18		TD had higher FA in the EEC and the anterior PFC compared to PIGD.
(Wen et al., 2018) [57]	3T Siemens		52		13			61	TD showed increased FA, RD, and AD in multiple projection, association, and commissural tracts compared to PIGD.
Mean Diffusivity									
(Lenfeldt et al., 2013) [67]	1.5T Philips	36							TD had higher MD in thalamus compared to PIGD.
(Luo et al., 2017) [68]	3T GE		30	30				26	TD had increased MD and axial diffusivity (AD) along multiple white matter tracts mainly in the cerebello-thalamo-cortical (CTC) pathway.
(Nagae et al., 2016) [64]	3T GE		12		9			20	Compared to TD, PIGD had increased MD in the left and right SN and bilateral GP that correlated with disease stage and motor severity.
(Surova et al., 2016) [70]	3T Siemens		50		47			44	PIGD had increased MD in the putamen compared to TD.
(Tessa et al., 2008) [45]	1.5T Siemens		13			11	3	16	TD did not differ in GMV, WMV, or histogram-derived MD metrics compared to AR.
(Vervoort et al., 2016a) [69]	3T Philips		16		33			18	No differences were shown in FA or MD at the whole-brain level between patient groups. TD had increased MD in tracts connecting the right M1 and right inferior parietal lobule compared to PIGD. No volumetric differences in caudate, putamen and pallidum between TD and PIGD were seen. No shape alterations in right caudate and the bilateral putamen and pallidum between TD and PIGD were detected.

Other Diffusion Metrics					
(Barbagallo et al., 2017a) [62]	3T GE	35	28	30	TD had higher tract integrity in the globus pallidus–substantia nigra, putamen–precentral cortex, and caudate nucleus–supplementary motor area tracts compared to nTD; TD had higher connectivity values in the thalamus–precentral cortex tract compared to nTD; nTD had structural connectivity alterations of cortico–basal ganglia pathways while TD did not.
(Tan et al., 2019) [51]	3T Siemens	21	19	20	PIGD had reduced white matter integrity in the superior longitudinal fasciculus, inferior longitudinal fasciculus, inferior fronto-occipital fasciculus, anterior thalamic radiation, genu of the corpus callosum, and body of the corpus callosum compared to TD.

Notes: AD = axial diffusivity. AR = akinetic-rigid. ECC = external capsule. FA = fractional anisotropy. GE = General Electric. GMV = gray matter volumes. GP = globus pallidus. HC = healthy controls. M1 = primary motor cortex. MD = mean diffusivity. Mixed = mixed-type/intermediate/indeterminate subtype. nTD = non-tremor-dominant. PD = Parkinson's disease. PFC = prefrontal cortex. PIGD = postural instability and gait difficulty. RD = radial diffusivity. SLF = superior longitudinal fasciculus. SN = substantia nigra. T = Tesla. TD = tremor-dominant. WMV = white matter volumes

Diffusion Imaging

It has been suggested that microstructural integrity degradations of the BG visible via MR diffusion data play a fundamental role in the underlying neural correlates of TD-PD symptomologies.[8] Correspondingly, connectivity indices derived from diffusion images have shown lower structural connectivity in nTD in key neuronal motor areas such as the globus pallidus–substantia nigra tract, globus pallidus–thalamus tract, putamen–precentral cortex tract, thalamus–precentral cortex tract, and the caudate nucleus–supplementary motor area tract compared to TD.[62]

Fractional Anisotropy

Fractional anisotropy (FA), or the extent that the diffusion of water molecules is restricted or unrestricted in specific directions, is used to denote the *integrity* of white matter within the brain by providing information about myelination, fiber organization, and the number of axons in a single measure.[63] While an increase in FA could indicate increased myelin, increased axonal density/caliber, or decreased fiber mixture[63] in general decreased FA along with increases in mean diffusivity (MD) in the SN have pointed towards an ability to distinguish PD patients from healthy controls.[64]

TD patients have shown to have increased FA compared to PIGD patients in multiple projection, association, and commissural tracts, while motor severity was correlated with FA within the corpus callosum of TD patients and even stronger in multiple association tracts within PIGD patients.[57, 64] In ,[64] PIGD displayed lower FA in the left substantia nigra compared to TD. These studies are in line with others that show TD patients have increased FA compared to PIGD in the external capsule (ECC), anterior PFC, and lateral to the horn of the anterior ventricle[65] and that PIGD patients have significantly decreased FA in the bilateral superior longitudinal fasciculi (SLF), bilateral anterior corona radiate, and in the left genu (front) of the corpus callosum when compared to non-PIGD.[66] These diffusion studies exemplify that the decreased FA found in PIGD are in line with models demonstrating PIGD to have more motor impairments and worse prognosis due to microstructural white matter abnormalities in the cortico-basal ganglia-thalamocortical tract.

Mean Diffusivity

Alongside FA, mean diffusivity (MD) is a diffusion measurement that denotes the average diffusion within a voxel and is used to measure the mobility of water molecules. TD patients have shown increased MD in the thalamus and middle and superior cerebellar peduncle when compared to PIGD[67, 68] as well as increased MD in the tracts connecting the right inferior parietal lobule (IPL) with the right premotor cortex and primary motor cortex[67, 69] and in major white matter tracts including the fornix, longitudinal fasciculi, and corpus callosum.[68] While one article showed that TD did not differ in histogram-derived

MD metrics compared to AR[45] and another showed no significant group difference in MD between PIGD and TD,[57] one showed TD patients had a 7% decrease in MD within the putamen compared to PIGD patients.[70]

These results suggest that while diffusion data shows TD to have deficits in connecting fibers in motor cortical areas, PIGD patients show impaired WM tracts involved in both cognitive and motor control which could partially account for the more severe postural and gait impairments[29, 64] as well as PIGD related incidences of freezing of gait (FOG)[71] and non-motor PD symptoms like depression.[72] Because diffusion parameters can correlate with worse motor and cognitive function in PD[69] and TD patients seem to have increases in MD compared to the PIGD in certain areas, such WM alterations may underlie the greater impact on motor and non-motor function seen in PIGD.[71, 72]

Diffusion Imaging Limitations

Since diffusion parameters are sensitive to various microscopic alterations in the brain such as crossing-fiber mixture, demyelination, and axonal density/caliber, the degree to which the variability in diffusion measurements indicate alternations in PD must be interpreted with caution. Additional limitations across diffusion studies include differences in MRI field strength, sequences used, age of the cohorts, time of disease onset, and sample sizes.[8, 65, 69, 70] Longitudinal studies are additionally needed to understand the progression of diffusion alterations in PD on white matter microstructure.[57, 70, 73, 74] Overall, high-quality diffusion stands as a useful method in differentiating structural aberrations between PD subtypes and serves as an important complement in histological studies that investigate fiber organization and the microstructure of circuitopathies.

Functional Imaging

Functional Imaging Techniques

A pivotal brain-imaging technique is functional magnetic resonance imaging (fMRI) which indirectly measures brain activity via changes associated with cerebral blood flow called a blood-oxygen level dependent (BOLD) response (Table **3**). Outcome measurements of fMRI include functional connectivity (FC) where temporal synchronizations of activity between ROIs reflect communication and correlation during a task, and resting state fMRI (rs-fMRI) used to calculate interactions between regions while the brain is in a resting state. Furthermore, arterial spin labelling (ASL) is a technique that measures cerebral blood perfusion and allows for the measurement of cerebral blood flow (CBF). Lastly, magnetic resonance spectroscopy (MRS), a non-invasive technique that quantifies in vivo patterns of neurometabolic alterations, analyzes specific molecules and evaluates metabolites and products of metabolism.[75]

Table 3. Differences with functional MRI (fMRI) between PD motor subtypes

Study	Field Strength	TD	nTD	PIGD	AR	Mixed	HC	Findings
Functional Activity and Connectivity								
(Chen et al., 2015) [76]	3T Siemens	12		19			22	TD had higher ALFF values in the lobule VIII of the right cerebellum and the bilateral putamen and lower ALFF values in the bilateral temporal gyrus and the left superior parietal lobule compared with PIGD.
(DiMarzio et al., 2020) [83]	1.5T, 3T GE	11		7	5			AR showed more activation in primary motor cortex (M1) compared to TD.
(Helmich et al., 2011) [34]	3T Siemens	21	23				36	TD had enhanced GPi-MC and putamen-MC coupling compared to nTD, mainly in the MAH.
(Hou et al., 2018) [88]	3T GE	21		19			35	TD had higher FC between the BG and calcarine region (occipital lobe) compared to PIGD.
(Hu et al., 2017) [15]	3T Siemens	25			25		26	TD showed significantly decreased global FCD in the left inferior frontal gyrus, right middle frontal gyrus and right superior frontal gyrus, and increased global FCD in the cerebellum anterior lobe compared to AR.
(Hu et al., 2019) [89]	3T Siemens	16		23			28	TD showed increase ReHo values in the right para-hippocampal gyrus compared to PIGD.
(Jiang et al., 2016) [78]	3T Siemens	15		13			17	TD exhibited lower ReHo in the left precuneus, left S1, left cuneus and left superior occipital gyrus and higher ReHo values in the right lingual gyrus, right parahippocampal gyrus, and cerebellum
(Karunanayaka et al., 2016) [39]	3T Siemens	15			17		24	AR had lower activation in the left IPC and left PCC compared to TD and controls.
(Lewis et al., 2011) [79]	3T Siemens	9			8		14	TD had decreased activation in all STC and CTC circuits expect for the ipsilateral STC compared to AR. TD had decreased activity in the lentiform nucleus of the BG compared to AR. TD had higher activity in cerebellular and thalamic regions compared to AR.
(Liu et al., 2013) [80]	3T GE	10			8		18	TD had decreased positive correlations of the left and right DN with the bilateral CPL compared to AR.
(Ma et al., 2017) [81]	3T Siemens	12		19		14	22	TD had higher FCS values in the cerebellum, mainly in the left hemisphere and tonsils compared to PIGD.

(Mohl et al., 2017) [82]	3T GE	14		12		21	PIGD ON had increased activation in the right superior temporal gyrus compared to TD ON.
(Prodoehl et al., 2013) [44]	3T GE	10	10			20	TD had higher activation in the bilateral DLPFC, contralateral pre-SMA, ipsilateral IPL, ipsilateral precuneus, contralateral lingual gyrus, contralateral caudate, contralateral (GPi, GPe), and ipsilateral thalamus compared to nTD. nTD did not show increased activity in any area compared to TD.
(Shen et al., 2020) [87]	3T Siemens	16		23		28	TD showed increased FC between the left putamen and right cerebellum lobule VI and cerebellum crus I compared to PIGD.
(Vervoort et al., 2016b) [71]	3T Philips	16		33		18	PIGD had decreased FC in the striatum (e.g. between the left caudate and bilateral ventral and dorsal putamen) and lower FC between the left caudate and right pallidum and between the left caudate and left PMC and right STL. No increases of FC were found in PIGD compared to TD.
(Zeng et al., 2019) [86]	3T GE	43		36		31	TD showed to have greater connectivity between the bilateral Vim and the bilateral cerebellum compared to PIGD.
(Zhang et al., 2014) [17]	1.5T Siemens	15			10	20	The ability to distinguish TD from nTD using network nodal efficiency (i.e., local and global efficiencies) was heavily influenced by the cerebellum.
Resting-State fMRI							
(Baudrexel et al., 2011) [85]	3T Siemens	16	15			44	No direct statistical difference in STN FC or left STN-M1 hand area FC between TD and nTD.
(Hu et al., 2015) [90]	3T Siemens	21			29	26	TD had decreased VHMC in the posterior lobe of the cerebellum compared to AR.
(Jiang et al., 2016) [78]	3T Siemens	12		13		17	TD had lower ReHo values in the left precuneus, left S1, left cuneus and left superior occipital gyrus, and higher ReHo values in the right lingual gyrus, right parahippocampal gyrus, and cerebellar areas compared to PIGD.
(Wang et al., 2016) [84]	3T Siemens	12		19		22	PIGD had greater STN FC with the left middle occipital lobe, left superior parietal lobe, and right middle frontal lobe. TD had greater FC between the bilateral STN and left cerebellar anterior lobe and right middle cingulate gyrus.

Cerebral Blood Flow						
(Al-Bachari et al., 2017) [27]	3T Philips	21		24	6	TD did not differ in whole brain CBF compared to PIGD. TD had more hypoperfusion in temporo–parieto–frontal networks compared to PIGD, while PIGD showed hypoperfusion in a predominantly posterior pattern as well as hyperperfusion in the BG
Other Functional Metrics						
(Barbagallo et al., 2017b) [93]	3T GE	14	12 (rET)		10	TD showed reductions of NAA/Cr and Cho/Cr in the thalami compared to rET and HC. The combination of thalamic NAA/Cr and Cho/Cr ratios showed a 100% accuracy in distinguishing TD from rET and HC. No differences were seen regarding Glu/Cr ratios.

Note. ALFF = amplitude of low-frequency fluctuation. AR = akinetic-rigid. BG = basal ganglia. CBF = cerebral blood flow. Cho = glycerophosphocholine with phosphocholine. CPL = cerebellar posterior lobe. Cr = creatine with phosphocreatine. CTC = cerebello-thalamo-cortical circuit. DLPFC = dorsolateral prefrontal cortex. DN = dentate nucleus. FC = functional connectivity. FCD = Functional connectivity density. FCS = functional connectivity strength. GE = General Electric. Glu = glutamate with glutamine. GPe = external globus pallidus. GPi = internal globus pallidus. HC = healthy controls. IPC = inferior parietal cortex. IPL = inferior parietal lobule. M1= primary motor cortex. MAH = most affected hemisphere. MC = motor cortex. Mixed = mixed-type/intermediate/indeterminate subtype. NAA = N-acetyl-aspartate with N-acetyl-aspartyl-glutamate. nTD = non-tremor-dominant. ON = on Levodopa medication. PCC = posterior cingulate cortex. PIGD = postural instability and gait difficulty. PMC = premotor cortex. rET = essential tremor with resting tremor. ReHo = regional homogeneity. S1 = right postcentral gyrus. SMA = supplementary motor cortex. STC = striato-thalamo-cortical. STL = superior temporal lobe. STN = subthalamic nucleus. T = Tesla. TD = tremor-dominant. VHMC = voxel-mirrored homotopic connectivity.

fMRI

Functional Activity and Connectivity

Many studies have shown task-based functional alterations between TD patients and nTD within the cerebellum, the putamen, the temporal cortex, and the parietal cortex.[34, 39, 44, 74, 76-82] Other areas have also shown to have functional differences between motor subtypes including TD having enhanced GPi–motor cortex (MC) and putamen–MC coupling compared to nTD, mainly in the most-affected hemispheres (MAH),[34] PIGD having lower FC (i.e., more disrupted hubs) in the cerebellum, mainly in the left hemisphere and tonsils compared to TD,[81] and nTD showing reduced BOLD activity in the PFC and GP compared to TD.[44]

Compared to TD, nTD have also shown reduced activation in bilateral dorsolateral PFC, contralateral pre-supplementary motor area, ipsilateral IPL, ipsilateral precuneus, contralateral caudate, contralateral GPi and GPe, and the ipsilateral thalamus during a gripping task, while no areas in nTD showed increased activity compared to TD, showing that even in the earliest stages of PD nTD show greater deficits in frontal cortical areas compared to TD.[44] Furthermore, when compared to TD, AR have shown to have increased activation during sequential finger tapping tasks in cortical and subcortical ROI related to PD such as the lentiform nucleus of the basal ganglia, as AR showed increased activity in contralateral CTC circuits while TD showed significant differences in the contralateral striato-thalamo-cortical circuit (STC) and CTC pathways including the cerebellar vermis, contralateral cerebellar hemisphere, and ipsilateral thalamus.[79] Likewise, a recent study with patient›s deep brain stimulation (DBS) cycling ON and OFF showed AR have increased activation in the supplementary motor area (SMA) and primary motor cortex (M1) compared to TD.[83]

Resting-State fMRI

Using rs-fMRI, PIGD have shown less subthalamic nucleus (STN) FC within the left anterior and posterior lobes of the cerebellum, less FC between the bilateral STN and left cerebellar anterior lobe and right middle cingulate gyrus, but greater FC between the STN and the left middle occipital lobe, left superior parietal lobe, and right middle frontal lobe compared to TD.[84] Conversely,[85] found no significant differences in STN FC between TD and nTD.

In reference **17**, the ability to functionally distinguish TD and nTD was influenced by the cerebellum, while in **15** TD showed increased global functional connectivity density (FCD) in the cerebellum anterior lobe relative to AR. In **86**, TD showed to have greater connectivity between the bilateral ventral intermediate nucleus (Vim) and the bilateral cerebellum compared to PIGD while reference **87** showed TD to have increased FC between the left putamen and right cerebellum lobule VI and cerebellum crus I compared to PIGD.

TD has also shown to have higher FC between the BG and calcarine region (occipital lobe) compared to PIGD.[88] In a later study, PD patients with FOG showed decreased FC between the left caudate and the right superior temporal lobe (STL) and left cerebellum, between the right caudate and bilateral dorsal putamen, left GP, and bilateral STL, and increased FC between the right precuneus and the left dorsal putamen compared to those without FOG.[74]

Using amplitude of low frequency fluctuations (ALFF) which detect the regional intensity of spontaneous fluctuations in BOLD signals,[76] found TD to have increased ALFF in the putamen and the posterior lobes of cerebellum compared to PIGD, and decreased ALFF in the temporal gyri and left superior parietal lobule. In another study using low frequency rs-fMRI, TD had decreased correlation of the left and right DN with the bilateral posterior lobe of cerebellum compared to AR.[80]

TD have also shown more regional homogeneity (ReHo) alterations, a resting-state analysis that examines synchronizations of temporal changes in BOLD signal, in the cerebellum, right para-hippocampal gyrus, and CTC loops while PIGD showed increased ReHo values in areas involved in the STC loop including in the frontal, parietal, occipital, temporal, and limbic lobes, basal ganglia, and thalamus.[78, 89] Lastly, compared to AR, TD have shown lower voxel-mirrored homotopic connectivity (VMHC) values, which denote synchrony in patterns of spontaneous rs-fMRI activity, in the posterior lobe of the cerebellum.[90]

These results show that fMRI and rs-fMRI are valuable imaging techniques to better understand functional differences in PD subtypes and further underline the importance of cerebellular and basal nuclei activity as well as the STC and CTC tracts in functional PD imaging, with[86] recently denoting the cerebellar-receiving nucleus of the thalamus, the Vim, as a "key nodal point" in both PD subtypes. It seems that the dysfunction of the STC seen in bradykinesia and rigidity and the primary dysfunction of the CTC in TD are the key functional deficits between PD subtypes.[79] These results are in line with structural findings and support network models of PD subtypes.

Cerebral Blood Flow

Cerebral blood flow (CBF) is the movement of blood in arteries and veins within the brain and is an important marker of PD as it maintains proper brain function by supplying the brain with oxygen and energy substrates that remove waste products of metabolism.[91] A recent study using ASL showed TD to have more hypoperfusion in the temporo–parieto–frontal network while PIGD showed hypoperfusion in a predominantly posterior pattern as well as hyperperfusion in the BG, although these differences were removed when levodopa medication, and disease severity and duration were controlled for.[27] Comparatively, in a recent structural study PIGD were associated with an increased prevalence of thalamic and

WM cerebral microbleeds (ie, small chronic brain hemorrhages caused by abnormalities of small brain vessels) when compared to TD and AR.[92] These results suggest that CBF and other cerebral blood parameters could be valuable imaging techniques to differentiate between PD subtypes.

Other Functional Metrics

One study that used proton MR spectroscopy (^{1}H-MRS) reported TD patients had reduced N-acetyl-aspartate (NAA)/creatine (Cr) and glycerophosphocholine (Cho)/Cr ratios in the ipsi- and contralateral thalami compared to patients with essential and resting tremor (rET) and to healthy controls.[93] Although rET is not a PD subtype, NAA/Cr and Cho/Cr ratios were 100% accurate at differentiating TD from rET and controls[93] showing that TD PD can be differentiated from those with postural and kinetic tremors using MRS which could help with diagnostics during the early stages of these diseases. Therefore, MRS might have the potential to accurately classify PD subtypes.

Limitations of fMRI

Dissimilar and low resolution MR, variations in cohort disease stage, and small sample sizes limit the generalization of functional imaging findings across PD subtypes. Furthermore, artifacts in the BOLD signal from head motion originating from tremor symptoms are significant limiting factors across PD fMRI studies. Nevertheless, functional MRI, and especially rs-fMRI, hold legitimate potential for better characterizations of PD subtypes and have translational applications for clinical and psychotherapeutic PD domains.

Molecular Imaging

Molecular Imaging Techniques

Little is known about the differences in metabolism and disrupted molecular processing within identical brain regions between PD subtypes.[34, 94] Functional nuclear medicine tomographic imaging techniques are used to investigate such alterations on a molecular level such as positron emission tomography (PET) that uses positron emitting radioisotopes (Table **4**), and single photon emission computed tomography (SPECT) that can differentiate between isotopes with different energy levels (Table **5**).

Table 4. Differences with positron emission tomography (PET) imaging between PD motor subtypes

Study	Company	TD	nTD	PIGD	nPIGD	AR	Mixed	HC	Radiotracer	Findings
Dopaminergic										
(Eggers et al., 2014) [94]	Siemens	32				32			[^{18}F]F-DOPA	AR had reduced dopaminergic uptake in the caudate and anterior putamen compared to TD patients.
(Lee et al., 2019) [100]	X	221		75			29		I-^{123} FP-CIT	Specific binding ratios of the caudate and putamen were significantly lower in the PIGD group than the TD group.
(Song et al., 2014) [95]	GE	21	22					18	^{18}F-FP-CIT	TD did not differ in DAT uptake in the striatum compared to nTD at the same early stage of disease
Non-dopaminergic										
(Ahrweiller et al., 2019) [102]	GEMS			10	46				^{18}F-FDG	PIGD showed increased metabolism in the dorsal midbrain/pons and right motor cerebellum compared to non-PIGD.
(Antonini et al., 1998) [101]	GE	8	8					10	^{18}F-FDG	PDRP expression did not differ between TD and nTD.
(Eggers et al., 2014) [94]	Siemens	32				32			^{18}F-FDG	Global FDG-metabolism did not differ between AR and TD. AR showed lower glucose metabolism in the striatal areas compared to TD.
(Loane et al., 2013) [104]	Siemens	12				12		12	^{11}C-DASB	TD had lower serotonin transporter uptake in the caudate and putamen compared to AR. TD trended to have lower binding values in the raphe nuclei compared to AR.
(Zhang et al., 2016) [103]	Siemens	15		15				17	^{18}F-FDG	Compared to TD patients, PIGD had more metabolic decreases in caudate and inferior parietal lobule (IPL, BA 40).

Note. [^{18}F]F-DOPA = ^{18}F-radiolabeled nonproteinogenic amino acid 3,4-dihydroxy-6-[F]fluoro-l-phenylalanine. ^{18}F-FDG = 2-deoxy-2-[F]fluoro-D-glucose. ^{18}F-FP-CIT = Fluorinated N-3-fluoropropyl-2β-carbomethoxy-3β-(4-iodophenyl) nortropane. AR = akinetic-rigid. BA = Brodmann area. DAT = dopamine transporter. GE = General Electric. GEMS = GE Signa scanner. HC = healthy controls. I-^{123} FP-CIT = Ioflupane (FPCIT); [I-12] N-ω-fluoropropyl-2β-carbomethoxy- 3β-(4-iodophenyl) nortropane. IPL = inferior parietal lobule. Mixed = mixed-type/intermediate/indeterminate subtype. . nPIGD = non postural instability and gait difficulty. nTD = non-tremor-dominant. PDRP = Parkinson's disease -related pattern *'characterized by relative hyper-metabolism of the lentiform nucleus and the thalamus associated with metabolic decreases in the primary and association motor cortices'* (Antonini et al., 1998) [101]. PIGD = postural instability and gait difficulty. TD = tremor-dominant. X = Images were taken from the Parkinson's Progression Markers Initiative (PPMI) database and presumably come from various company's machines.

Table 5. Differences with single-photon emission computerized tomography (SPECT) imaging between PD motor subtypes

Study	Company	TD	nTD	PIGD	AR	Mixed	HC	Radiotracer	Findings
Dopaminergic									
(Barbagallo et al., 2017b) [93]	GE	14	12 (rET)				10	[^{123}I]FP-CIT	DAT was abnormal in TD but normal in rET patients.
(Barbagallo et al., 2017a) [62]	GE	35	28				30	[^{123}I]FP-CIT	nTD had lower uptakes values in the less affected side caudate nucleus compared to TD
(Eggers et al., 2011) [97]	GE	23			23			[^{123}I]FP-CIT	TD and AR matched for age, disease duration, and disease severity did not differ in dopaminergic uptake in the caudate and the putamen.
(Eggers et al., 2012) [98]	GE	14			13			[^{123}I]FP-CIT	AR showed reduced dopaminergic uptake in the contralateral caudate and the ipsi- and contralateral putamen over time, while TD did not show differences in the same period.
(Helmich et al., 2011) [34]	Siemens	21	23				36	[^{123}I]FP-CIT	TD had enhanced GPi-MC and putamen-MC coupling compared to nTD in the most-affected hemisphere. TD had lower pallidal DAT binding in the most-affected hemisphere and higher pallidal DAT binding in the least-affected hemisphere compared to nTD. TD trended to have higher overall DAT binding compared to nTD.
(Isaias et al., 2007) [110]	GE	10			10			[^{123}I]FP-CIT	TD had lower ipsilateral striatum and caudate nucleus uptake compared to AR. TD did not differ in putamen mean uptake values, asymmetry index, or putamen caudate index values compared to AR.
(Kaasinen et al., 2014) [111]	GE	157	74				230	[^{123}I]FP-CIT	TD had higher mean caudate nucleus uptake and left caudate nucleus uptake compared to nTD.
(Mo et al., 2010) [109]	GE	39		75		14	48	[^{123}I]FP-CIT	TD had higher presynaptic putamen uptake ratios compared to PIGD even when controlling for disease severity. TD also had higher presynaptic caudate uptake ratios compared to PIGD but not after disease severity was controlled for.
(Moccia et al., 2014) [105]	GE	27			24			[^{123}I]FP-CIT	TD had higher DAT availability in the affected and unaffected putamen but no differences in the caudate.
(Qamhawi et al., 2015) [99]	GE	37			106	202	185	[^{123}I]FP-CIT	TD had less severe striatal dopaminergic deficits compared to nTD.
(Ramani et al., 2017) [112]	GE	7			17	18		[^{123}I]FP-CIT	TD did not differ in baseline uptake ratios compared to AR and Mixed.

(Rossi et al., 2010) [106]	GE	24		38			[^{123}I]FP-CIT	TD had higher average uptake compared to AR. TD had higher FP-CIT uptake in the putamen contralateral to the most clinically affected side compared to AR, but no differences were seen in bilateral caudate and ipsilateral putaminal uptakes, or in asymmetry indices and caudate or putamen ratios.
(Schillaci et al., 2011) [107]	GE	20		20	7		[^{123}I]FP-CIT	TD had higher uptake in the caudate contralateral to the side affected compared to AR and Mixed, while no differences were seen between AR and Mixed. TD had higher uptake in the contralateral putamen compared to AR, but not compared to Mixed, nor when AR was compared to Mixed. TD had higher uptake in the ipsilateral caudate compared to AR and Mixed, while no difference were seen when AR was compared to Mixed. TD had higher uptake in the ipsilateral putamen compared to AR. No differences were seen between TD and Mixed, or between AR and Mixed in ipsilateral putamen uptake.
(Spiegel et al., 2007) [108]	Siemens	22		26	19		[^{123}I]FP-CIT	TD had higher uptake in the ipsilateral and contralateral putamen compared to AR and Mixed. AR and Mixed did not differ in their binding ratios in the contra- or ipsilateral putamen. TD had higher uptake in the ipsilateral and contralateral caudate nucleus compared to AR and Mixed. AR and Mixed did not differ in their binding ratios in the contra- or ipsilateral caudate nucleus or contra- or ipsilateral putamen.
Non-dopaminergic								
(Caretti et al., 2008) [113]	Strichmann	8,6	12,11			13	[^{123}I]β-CIT	TD had 19% lower SNS thalamic binding ratios compared to nTD at baseline. TD did not differ in whole striatum, putamen, and caudate nucleus average SNS binding ratios compared to nTD at baseline nor at follow up. There were no differences in thalamic binding ratios between nTD and TD at follow-up.
(Mito et al., 2006) [114]	Toshiba	10	19			17	Iofetamine (^{123}I)	TD did not differ in patterns of regional cerebral blood flow (rCBF) when directly compared to PIGD. .
(Qamhawi et al., 2015) [99]	GE	37		106	202	185	[^{123}I]FP-CIT	TD had lower raphe serotonin transporter availability compared to nTD.

Note. In Caretti et al., (2008) multiple numbers reflect baseline cohort and 17 month follow up cohorts. [^{123}I]FP-CIT = N-(3-Fluoropropyl)-2β-carbomethoxy-3β-(4-[I]iodophenyl)nortropane. [^{123}I]β-CIT = Iodine-123-β-carbomethoxy-3 β-(4-iodophenyltropane). AR = akinetic-rigid. DAT = dopamine transporter. GE = General Electric. GPi = internal globus pallidus. HC = healthy controls. Iofetamine (^{123}I) = N-isopropyl-(123I)-p-iodoamphetamine. MC = motor cortex. Mixed = mixed-type/intermediate/indeterminate subtype. nTD = non-tremor-dominant. PIGD = postural instability and gait difficulty. rCBF = regional cerebral blood flow. rET = resting essential tremor. SNS = specific to non-specific. TD = tremor-dominant.

PET Imaging

Dopaminergic PET Imaging

The clinical expression of PD can be partially explained by dopamine transporter (DAT) loss localized in presynaptic nigrostriatal nerve terminals. Most PET studies used ^{18}F-FP-CIT (N-3–fluoropropyl-2-b-carboxymethoxy-3-b-(4-iodophenyl) nortropane) as a radioligand for dopamine receptors and re-uptake sites due to its fast kinetics, relatively long half-life, and low radiation exposure as compared to other radioligands. The main ROI is the striatum with subregions defined as the caudate and putamen (both split into anterior and posterior parts). Compared with a HC group, PD patients overall show a reduced striatal ^{18}F-FP-CIT binding in the caudate and putamen.[95, 96]

Although reference **97** showed no significant differences in dopaminergic uptake between TD and AR, two later studies of theirs showed TD had increased dopaminergic uptake in the caudate and anterior putamen compared to AR patients[94, 98] and a separate study showed TD to have less severe striatal dopaminergic defects compared to AR.[99] Further comparisons between TD and PIGD show increased dopamine uptake in TD in the caudate, putamen, and IPL (Brodmann area [BA] 40),[100] and although one study showed no differences in FP-CIT uptake in the striatum between the TD and nTD[95] another reported TD to have enhanced GPi–MC and putamen–MC coupling compared to nTD in the MAH.[34]

Non-Dopaminergic PET Imaging

Early work using ^{18}F-fluorodeoxyglucose (FDG) PET imaging showed that PD patients had increased metabolic activity in the motor association cortices, pons, and thalamus.[101] In another study of PD patients who underwent subthalamic nucleus deep brain stimulation and subsequent PET scans using FDG, PIGD showed increased metabolism in the dorsal midbrain/pons and right motor cerebellum compared to non-PIGD.[102] Separate studies show increased glucose uptake in the ventral striatum in TD compared to AR,[94] PIGD having metabolic decreases in the caudate and inferior parietal lobule (Brodmann area (BA) 40) compared to TD,[103] and TD having lower raphe serotonin transporter availability.[99] Another study investigated the vesicular monoamine transporter type 2 (VMAT2) binding with [^{11}C]dihydrotetrabenazine as a tracer and showed a significant covariate effect of VMAT2 when comparing TD with AR.[53] Furthermore, using ^{11}C-labeled 3-amino-4-[2-[(di(methyl)amino) methyl]phenyl]sulfanylbenzonitrile (^{11}C-DASB) to investigate serotonin transporter uptake, one study showed lower uptake in the caudate and putamen in the TD compared to the AR, and TD trended to have lower raphe nucleus ^{11}C-DASB values compared to AR.[104] In addition to these findings, the study also reported reductions of ^{11}C-DASB uptake in the thalamus and in BA 4 and 10 in TD compared to AR with a voxel-based analysis.

PET Limitations

Motor impairments in PD cannot be fully explained by PET findings, as complex comorbid deficits and the degeneration of other neuronal systems occur simultaneously.[48, 53] Some studies focus on local glucose metabolism while others look at whole brain analysis, making multimodal imaging techniques necessary to consolidate PD specific degenerations found via PET imaging. As summarized in Table **4**, there seems to be an increase in dopamine uptake in the TD group compared to the nTD group.

SPECT Imaging

Dopaminergic SPECT Imaging

SPECT studies in PD make use of ^{123}I-FP-CIT for tracing dopamine uptake in the striatum. Based on available literature it can be noted that TD compared to nTD show higher uptake in the putamen contralateral to the MAH.[62, 97, 105-108] TD compared to nTD show higher uptake on the ipsilateral side,[62, 97, 107] and TD show higher uptakes when the means of the right and left uptake ratios of the putamen were compared between groups as well.[99, 109] Differences in the striatum support previous neuropathological models for PD motor subtypes in vivo, where AR have reduced dopaminergic projections to the dorsal putamen and TD have reduced projections in the lateral putamen and caudate nucleus.[97] Contrary to these findings, several SPECT studies found no difference between motor subtypes in the anterior or posterior putamen.[110-112] Interestingly, there seems to be a differential pattern of progression in the FP-CIT binding in the ipsi- and contralateral putamen, since nTD had decreased binding over time, while TD showed no differences.[98] One study reported PIGD to have lower striatal presynaptic ratios as PIGD were seen to be more affected by the disease than TD.[109]

While the putamen region is the most examined region in PD SPECT studies, few studies report on other dopaminergic regions. When TD was compared against AR, higher uptake was found in the ipsilateral and contralateral caudate nucleus,[97, 107, 108] and in mean caudate uptake,[111] while two studies found no difference in contralateral or ipsilateral caudate binding ratios.[105, 112] Contrary to the findings of higher ipsilateral FP-CIT uptake in the caudate nucleus, one study found lower ipsilateral striatum and caudate nucleus uptake in TD compared to AR[110] and another showed PD subtypes with the same severity of disease show no difference in caudate uptake ratios.[109]

Non-Dopaminergic SPECT Imaging

One study that used [^{123}I]β-CIT binding to measure serotonin reported a 19% higher binding ratio in the thalamus in nTD compared to TD but no differences in binding ratios within the striatum, putamen, or caudate nucleus.[113] When raphe nuclei serotonin transporter availability was investigated using ^{123}I-iodoamphetamine, TD showed significantly lower uptake compared to AR.[99] Lastly, when the mean brain CBF, deemed regional CBF (rCBF)

was examined with SPECT, one study found TD had no significant decreases in rCBF compared to PIGD in any region.[114]

SPECT Limitations

The asymmetric findings, as summarized in Table **5**, are of important note as bilateral and interhemispheric differences in PD are a fundamental aspect of the disease. As these findings are mixed, whereas TD show less FP-CIT uptake in some neuronal areas and more in others compared to nTD, SPECT should be used in combination with other techniques to distinguish PD subtype etiology.

Discussion

As variable presentations of motor symptoms suggest divergent pathophysiological, anatomical, and neurochemical mechanisms during the course of PD progression[62, 93, 114] neuroimaging is a valuable tool towards identifying neuronal alterations and predicting symptom manifestation. To our knowledge, the current paper is the first to review studies of diverse neuroimaging alterations between TD-PD patients and those with nTD motor subtypes. Neuroimaging has shown variability between TD and nTD PD patients and persistently supports the notion that the subtype of TD is the more "benign" subtype as TD shows less negative alternations compared to nTD.

Importantly, while nTD have shown symptoms that are more aggressive compared to TD, revealed by earlier and more rapid physical decline,[16, 29] circuitry theories of how PD tremor is generated have only been minimally investigated within different nTD PD subtypes. The literature reviewed here shows that nTD patients have deficits within striato-thalamo-cortical (STC) circuitry and other thalamocortical projections related to cognitive and sensorimotor function, while TD patients show greater cerebello-thalamo-cortical (CTC) circuitry dysfunction. Comparatively, structural connectivity analysis show nTD have alterations of cortico–basal ganglia pathways while TD do not.[62] This is in line with the "*dimmer-switch model*" of PD resting tremor, that suggests pathological activity in the STC from dopaminergic denervation of the GP triggers tremor-related responses in the CTC via the motor cortex where both circuits converge; the BG acts as a light switch triggering tremors on and off, while the CTC modulates the tremors intensity similar to a light dimmer.[34] The results further support studies showing depletion of nigrostriatal dopamine and subsequent BG dysfunction alone is insufficient to characterize TD pathology fully[5, 115, 116] as other neuronal systems such as the cerebellum play ample roles in the production of tremors.[34, 117] Activity in the BG and cerebellum has shown to be highly

associated and structurally connected via the thalamus and pontine nucleus.[117] When targeted surgically with DBS, the Vim has shown to produce relief of tremor[21] and activity in the Vim that receives projections from the cerebellum, as well as from the GPi, has shown to synchronize with, mediate, and be directly related to tremor activity.[118-121] These finding are consistent with reports that the GP and putamen in TD patients have increased connectivity with the Vim–motor cortex–cerebellum circuit via the motor cortex[34] and further support results showing that a combination of STC and CTC circuitry might be behind the generation of tremors in PD.[17]

Complementary neuroimaging techniques are required to isolate neural mechanisms underlying PD motor symptomologies that can be used as non-invasive biomarkers in assessing PD trajectories and responses to treatment. Altogether, there remains an urgent need for more complete consolidation of macro/microstructural, functional, perfusion, chemical, and metabolic data from dissimilar PD cohorts to aid in refining antemortem diagnoses and improve epidemiological and clinical-therapeutic trial designs.

References

1. Poewe, W., et al., Parkinson disease. Nat Rev Dis Primers, 2017. 3: p. 17013.
2. He, N., et al., Dentate nucleus iron deposition is a potential biomarker for tremor-dominant Parkinson's disease. NMR Biomed, 2017. 30(4).
3. Rajput, A.H., et al., Course in Parkinson disease subtypes: A 39-year clinicopathologic study. Neurology, 2009. 73(3): p. 206-12.
4. van Rooden, S.M., et al., The identification of Parkinson's disease subtypes using cluster analysis: a systematic review. Mov Disord, 2010. 25(8): p. 969-78.
5. Zaidel, A., et al., Akineto-rigid vs. tremor syndromes in Parkinsonism. Curr Opin Neurol, 2009. 22(4): p. 387-93.
6. Goetz, C.G., et al., Movement Disorder Society-sponsored revision of the Unified Parkinson's Disease Rating Scale (MDS-UPDRS): Process, format, and clinimetric testing plan. Mov Disord, 2007. 22(1): p. 41-7.
7. Jankovic, J., et al., Variable expression of Parkinson's disease: A base-line analysis of the DATATOP cohort. 1990(October).
8. Zhan, W., et al., Regional alterations of brain microstructure in Parkinson's disease using diffusion tensor imaging. Mov Disord, 2012. 27(1): p. 90-7.
9. Hacker, C.D., et al., Resting state functional connectivity of the striatum in Parkinson's disease. Brain, 2012. 135(Pt 12): p. 3699-711.
10. Jellinger, K.A., The pathomechanisms underlying Parkinson's disease. Expert Rev Neurother, 2014. 14(2): p. 199-215.
11. Kordower, J.H., et al., Disease duration and the integrity of the nigrostriatal system in Parkinson's disease. Brain, 2013. 136(Pt 8): p. 2419-31.
12. Mazzoni, P., B. Shabbott, and J.C. Cortes, Motor control abnormalities in Parkinson's disease. Cold Spring Harb Perspect Med, 2012. 2(6): p. a009282.
13. Obeso, J.A., et al., The basal ganglia in Parkinson's disease: current concepts and unexplained observations. Ann Neurol, 2008. 64 Suppl 2(SUPPL. 2): p. S30-46.
14. Jellinger, K. Post mortem studies in Parkinson's disease - Is it possible to detect brain areas for specific symptoms. in Journal of Neural Transmission, Supplement. 1999.
15. Hu, X., et al., Altered Functional Connectivity Density in Subtypes of Parkinson's Disease. Front Hum Neurosci, 2017. 11(September): p. 458.
16. Thenganatt, M.A. and J. Jankovic, Parkinson disease subtypes. JAMA Neurol, 2014. 71(4): p. 499-504.
17. Zhang, D., et al., Distinguishing patients with Parkinson's disease subtypes from normal controls based on functional network regional efficiencies. PLoS One, 2014. 9(12): p. e115131.
18. Delenclos, M., et al., Biomarkers in Parkinson's disease: Advances and strategies. Parkinsonism Relat Disord, 2016. 22 Suppl 1(Suppl 1): p. S106-10.
19. Jankovic, J., Parkinson's disease: clinical features and diagnosis. J Neurol Neurosurg Psychiatry, 2008. 79(4): p. 368-76.
20. Wu, Y., W. Le, and J. Jankovic, Preclinical biomarkers of Parkinson disease. Arch Neurol, 2011. 68(1): p. 22-30.
21. Machado, A., et al., Deep brain stimulation for Parkinson's disease: surgical technique and perioperative management. Mov Disord, 2006. 21 Suppl 14: p. S247-58.
22. Mehanna, R. and E.C. Lai, Deep brain stimulation in Parkinson's disease. Transl Neurodegener, 2013. 2(1): p. 22.
23. Ashburner, J. and K.J. Friston, Voxel-based morphometry--the methods. Neuroimage, 2000. 11(6 Pt 1): p. 805-21.
24. Heim, B., et al., Magnetic resonance imaging for the diagnosis of Parkinson's disease. J Neural Transm (Vienna), 2017. 124(8): p. 915-964.
25. Rosenberg-Katz, K., et al., Gray matter atrophy distinguishes between Parkinson disease motor subtypes. Neurology, 2013. 80(16): p. 1476-84.

26. Rosenberg-Katz, K., et al., Subcortical Volumes Differ in Parkinson's Disease Motor Subtypes: New Insights into the Pathophysiology of Disparate Symptoms. Front Hum Neurosci, 2016. 10(July): p. 356.
27. Al-Bachari, S., et al., Structural and physiological neurovascular changes in idiopathic Parkinson's disease and its clinical phenotypes. J Cereb Blood Flow Metab, 2017. 37(10): p. 3409-3421.
28. Benninger, D.H., et al., Morphological differences in Parkinson's disease with and without rest tremor. J Neurol, 2009. 256(2): p. 256-63.
29. Burn, D.J., et al., Motor subtype and cognitive decline in Parkinson's disease, Parkinson's disease with dementia, and dementia with Lewy bodies. J Neurol Neurosurg Psychiatry, 2006. 77(5): p. 585-9.
30. Mirelman, A., et al., Executive function and falls in older adults: new findings from a five-year prospective study link fall risk to cognition. PLoS One, 2012. 7(6): p. e40297.
31. Marras, C. and K.R. Chaudhuri, Nonmotor features of Parkinson's disease subtypes. Mov Disord, 2016. 31(8): p. 1095-102.
32. Altinayar, S., et al., Olfactory disfunction and its relation olfactor bulbus volume in Parkinson's disease. European Review for Medical and Pharmacological Sciences, 2014. 18(23): p. 3659-3664.
33. Piccinin, C.C., et al., Differential Pattern of Cerebellar Atrophy in Tremor-Predominant and Akinetic/Rigidity-Predominant Parkinson's Disease. Cerebellum, 2017. 16(3): p. 623-628.
34. Helmich, R.C., et al., Pallidal dysfunction drives a cerebellothalamic circuit into Parkinson tremor. Ann Neurol, 2011. 69(2): p. 269-81.
35. Duval, C., et al., A brain network model explaining tremor in Parkinson's disease. Neurobiol Dis, 2016. 85: p. 49-59.
36. Lanciego, J.L., N. Luquin, and J.A. Obeso, Functional neuroanatomy of the basal ganglia. Cold Spring Harb Perspect Med, 2012. 2(12): p. a009621.
37. Storsve, A.B., et al., Differential longitudinal changes in cortical thickness, surface area and volume across the adult life span: regions of accelerating and decelerating change. J Neurosci, 2014. 34(25): p. 8488-98.
38. Herb, J.N., et al., Cortical Implications of Advancing Age and Disease Duration in Parkinson's Disease Patients with Postural Instability and Gait Dysfunction. J Parkinsons Dis, 2016. 6(2): p. 441-51.
39. Karunanayaka, P.R., et al., Default mode network differences between rigidity- and tremor-predominant Parkinson's disease. Cortex, 2016. 81: p. 239-50.
40. Danti, S., et al., Cortical thickness in de novo patients with Parkinson disease and mild cognitive impairment with consideration of clinical phenotype and motor laterality. Eur J Neurol, 2015. 22(12): p. 1564-72.
41. Nyberg, E.M., et al., Morphologic changes in the mesolimbic pathway in Parkinson's disease motor subtypes. Parkinsonism Relat Disord, 2015. 21(5): p. 536-40.
42. Compta, Y., et al., Combined dementia-risk biomarkers in Parkinson's disease: a prospective longitudinal study. Parkinsonism Relat Disord, 2013. 19(8): p. 717-24.
43. Linder, J., et al., Degenerative changes were common in brain magnetic resonance imaging in patients with newly diagnosed Parkinson's disease in a population-based cohort. J Neurol, 2009. 256(10): p. 1671-80.
44. Prodoehl, J., et al., Differences in brain activation between tremor- and nontremor-dominant Parkinson disease. JAMA Neurol, 2013. 70(1): p. 100-6.
45. Tessa, C., et al., A whole-brain analysis in de novo Parkinson disease. AJNR Am J Neuroradiol, 2008. 29(4): p. 674-80.
46. Braak, H. and E. Braak, Frequency of stages of Alzheimer-related lesions in different age categories. Neurobiol Aging, 1997. 18(4): p. 351-7.
47. Sowell, E.R., et al., Sex differences in cortical thickness mapped in 176 healthy individuals between 7 and 87 years of age. Cereb Cortex, 2007. 17(7): p. 1550-60.
48. Bohnen, N.I., et al., Leucoaraiosis, nigrostriatal denervation and motor symptoms in Parkinson's disease. Brain, 2011. 134(Pt 8): p. 2358-65.
49. Moccia, M., et al., White matter changes and the development of motor phenotypes in de novo Parkinson's Disease. J Neurol Sci, 2016. 367: p. 215-9.
50. Wan, Y., et al., Exploring the association between Cerebral small-vessel diseases and motor symptoms in Parkinson's disease. Brain Behav, 2019. 9(4): p. e01219.

51. Tan, S.Y.Z., et al., Periventricular White Matter Abnormalities on Diffusion Tensor Imaging of Postural Instability Gait Disorder Parkinsonism. AJNR Am J Neuroradiol, 2019. 40(4): p. 609-613.
52. Shen, Y., et al., Association of homocysteine, folate, and white matter hyperintensities in Parkinson's patients with different motor phenotypes. Neurol Sci, 2019. 40(9): p. 1855-1863.
53. Bohnen, N.I. and R.L. Albin, White matter lesions in Parkinson disease. Nat Rev Neurol, 2011. 7(4): p. 229-36.
54. Herman, T., et al., White matter hyperintensities in Parkinson's disease: do they explain the disparity between the postural instability gait difficulty and tremor dominant subtypes? PLoS One, 2013. 8(1): p. e55193.
55. Lee, S.J., et al., The severity of leukoaraiosis correlates with the clinical phenotype of Parkinson's disease. Arch Gerontol Geriatr, 2009. 49(2): p. 255-259.
56. Fang, E., et al., Differentiating Parkinson's disease motor subtypes using automated volume-based morphometry incorporating white matter and deep gray nuclear lesion load. J Magn Reson Imaging, 2020. 51(3): p. 748-756.
57. Wen, M.C., et al., Differential White Matter Regional Alterations in Motor Subtypes of Early Drug-Naive Parkinson's Disease Patients. Neurorehabil Neural Repair, 2018. 32(2): p. 129-141.
58. Martin-Bastida, A., et al., Motor associations of iron accumulation in deep grey matter nuclei in Parkinson's disease: a cross-sectional study of iron-related magnetic resonance imaging susceptibility. Eur J Neurol, 2017. 24(2): p. 357-365.
59. Jin, L., et al., Nigral iron deposition occurs across motor phenotypes of Parkinson's disease. Eur J Neurol, 2012. 19(7): p. 969-76.
60. Schneider, E., et al., Susceptibility-weighted MRI of extrapyramidal brain structures in Parkinsonian disorders. Medicine (Baltimore), 2016. 95(26): p. e3730.
61. Xiang, Y., et al., Subtypes evaluation of motor dysfunction in Parkinson's disease using neuromelanin-sensitive magnetic resonance imaging. Neurosci Lett, 2017. 638: p. 145-150.
62. Barbagallo, G., et al., Structural connectivity differences in motor network between tremor-dominant and nontremor Parkinson's disease. Hum Brain Mapp, 2017a. 38(9): p. 4716-4729.
63. Mori, S. and J. Zhang, Principles of diffusion tensor imaging and its applications to basic neuroscience research. Neuron, 2006. 51(5): p. 527-39.
64. Nagae, L.M., et al., Microstructural Changes within the Basal Ganglia Differ between Parkinson Disease Subtypes. Front Neuroanat, 2016. 10: p. 17.
65. Lenfeldt, N., et al., Frontal white matter injuries predestine gait difficulties in Parkinson's disease. Acta Neurol Scand, 2016. 134(3): p. 210-8.
66. Gu, Q., et al., Greater loss of white matter integrity in postural instability and gait difficulty subtype of Parkinson's disease. Can J Neurol Sci, 2014. 41(6): p. 763-8.
67. Lenfeldt, N., et al., Diffusion tensor imaging and correlations to Parkinson rating scales. J Neurol, 2013. 260(11): p. 2823-30.
68. Luo, C., et al., White matter microstructure damage in tremor-dominant Parkinson's disease patients. Neuroradiology, 2017. 59(7): p. 691-698.
69. Vervoort, G., et al., Structural Brain Alterations in Motor Subtypes of Parkinson's Disease: Evidence from Probabilistic Tractography and Shape Analysis. PLoS One, 2016a. 11(6): p. e0157743.
70. Surova, Y., et al., Alterations of Diffusion Kurtosis and Neurite Density Measures in Deep Grey Matter and White Matter in Parkinson's Disease. PLoS One, 2016. 11(6): p. e0157755.
71. Vervoort, G., et al., Functional connectivity alterations in the motor and fronto-parietal network relate to behavioral heterogeneity in Parkinson's disease. Parkinsonism Relat Disord, 2016b. 24: p. 48-55.
72. Petrovic, I.N., et al., White matter lesions and depression in patients with Parkinson's disease. J Neurol Sci, 2012. 322(1-2): p. 132-6.
73. Scholz, J., V. Tomassini, and H. Johansen-Berg, Individual Differences in White Matter Microstructure in the Healthy Brain, in Diffusion MRI. 2014. p. 301-316.
74. Vervoort, G., et al., Dual-task-related neural connectivity changes in patients with Parkinson' disease. Neuroscience, 2016. 317: p. 36-46.

75. Tedeschi, G., et al., Reproducibility of proton MR spectroscopic imaging findings. AJNR Am J Neuroradiol, 1996. 17(10): p. 1871-9.
76. Chen, H.M., et al., Different patterns of spontaneous brain activity between tremor-dominant and postural instability/gait difficulty subtypes of Parkinson's disease: a resting-state fMRI study. CNS Neurosci Ther, 2015. 21(10): p. 855-66.
77. Alhourani, A., et al., Network effects of deep brain stimulation. J Neurophysiol, 2015. 114(4): p. 2105-17.
78. Jiang, S., et al., Regional homogeneity alterations differentiate between tremor dominant and postural instability gait difficulty subtypes of Parkinson's disease. J Neural Transm (Vienna), 2016. 123(3): p. 219-29.
79. Lewis, M.M., et al., Differential involvement of striato- and cerebello-thalamo-cortical pathways in tremor- and akinetic/rigid-predominant Parkinson's disease. Neuroscience, 2011. 177: p. 230-9.
80. Liu, H., et al., Altered resting-state functional connectivity of the dentate nucleus in Parkinson's disease. Psychiatry Res, 2013. 211(1): p. 64-71.
81. Ma, L.Y., et al., Disrupted Brain Network Hubs in Subtype-Specific Parkinson's Disease. Eur Neurol, 2017. 78(3-4): p. 200-209.
82. Mohl, B., et al., Levodopa response differs in Parkinson's motor subtypes: A task-based effective connectivity study. J Comp Neurol, 2017. 525(9): p. 2192-2201.
83. DiMarzio, M., et al., Use of Functional Magnetic Resonance Imaging to Assess How Motor Phenotypes of Parkinson's Disease Respond to Deep Brain Stimulation. Neuromodulation, 2020.
84. Wang, Z., et al., Resting-state functional connectivity of subthalamic nucleus in different Parkinson's disease phenotypes. J Neurol Sci, 2016. 371: p. 137-147.
85. Baudrexel, S., et al., Resting state fMRI reveals increased subthalamic nucleus-motor cortex connectivity in Parkinson's disease. Neuroimage, 2011. 55(4): p. 1728-38.
86. Zeng, Q., et al., The Ventral Intermediate Nucleus Differently Modulates Subtype-Related Networks in Parkinson's Disease. Front Neurosci, 2019. 13: p. 202.
87. Shen, B., et al., Altered putamen and cerebellum connectivity among different subtypes of Parkinson's disease. CNS Neurosci Ther, 2020. 26(2): p. 207-214.
88. Hou, Y., et al., Patterns of striatal and cerebellar functional connectivity in early-stage drug-naive patients with Parkinson's disease subtypes. Neuroradiology, 2018. 60(12): p. 1323-1333.
89. Hu, J., et al., Regional homogeneity analysis of major Parkinson's disease subtypes based on functional magnetic resonance imaging. Neurosci Lett, 2019. 706: p. 81-87.
90. Hu, X., et al., Decreased interhemispheric functional connectivity in subtypes of Parkinson's disease. J Neurol, 2015. 262(3): p. 760-7.
91. Fantini, S., et al., Cerebral blood flow and autoregulation: current measurement techniques and prospects for noninvasive optical methods. Neurophotonics, 2016. 3(3): p. 031411.
92. Chiu, W.T., et al., Cerebral Microbleeds are Associated with Postural Instability and Gait Disturbance Subtype in People with Parkinson's Disease. Eur Neurol, 2018. 80(5-6): p. 335-340.
93. Barbagallo, G., et al., Thalamic neurometabolic alterations in tremulous Parkinson's disease: A preliminary proton MR spectroscopy study. Parkinsonism Relat Disord, 2017b. 43: p. 78-84.
94. Eggers, C., et al., Parkinson's disease subtypes show a specific link between dopaminergic and glucose metabolism in the striatum. PLoS One, 2014. 9(5): p. e96629.
95. Song, I.U., et al., An FP-CIT PET comparison of the difference in dopaminergic neuronal loss in subtypes of early Parkinson's disease. Acta Radiol, 2014. 55(3): p. 366-71.
96. Wang, J., et al., 18F-FP-CIT PET imaging and SPM analysis of dopamine transporters in Parkinson's disease in various Hoehn & Yahr stages. J Neurol, 2007. 254(2): p. 185-90.
97. Eggers, C., et al., Akinetic-rigid and tremor-dominant Parkinson's disease patients show different patterns of FP-CIT single photon emission computed tomography. Mov Disord, 2011. 26(3): p. 416-23.
98. Eggers, C., et al., Parkinson subtypes progress differently in clinical course and imaging pattern. PLoS One, 2012. 7(10): p. e46813.
99. Qamhawi, Z., et al., Clinical correlates of raphe serotonergic dysfunction in early Parkinson's disease. Brain, 2015. 138(Pt 10): p. 2964-73.

100. Lee, J.W., et al., Alteration of Tremor Dominant and Postural Instability Gait Difficulty Subtypes During the Progression of Parkinson's Disease: Analysis of the PPMI Cohort. Front Neurol, 2019. 10: p. 471.
101. Antonini, A., et al., The metabolic anatomy of tremor in Parkinson's disease. Neurology, 1998. 51(3): p. 803-10.
102. Ahrweiller, K., et al., Postural instability and gait disorders after subthalamic nucleus deep brain stimulation in Parkinson's disease: a PET study. J Neurol, 2019. 266(11): p. 2764-2771.
103. Zhang, L., et al., The Neural Basis of Postural Instability Gait Disorder Subtype of Parkinson's Disease: A PET and fMRI Study. CNS Neurosci Ther, 2016. 22(5): p. 360-7.
104. Loane, C., et al., Serotonergic loss in motor circuitries correlates with severity of action-postural tremor in PD. Neurology, 2013. 80(20): p. 1850-5.
105. Moccia, M., et al., Dopamine transporter availability in motor subtypes of de novo drug-naive Parkinson's disease. J Neurol, 2014. 261(11): p. 2112-8.
106. Rossi, C., et al., Differences in nigro-striatal impairment in clinical variants of early Parkinson's disease: evidence from a FP-CIT SPECT study. Eur J Neurol, 2010. 17(4): p. 626-30.
107. Schillaci, O., et al., Different patterns of nigrostriatal degeneration in tremor type versus the akinetic-rigid and mixed types of Parkinson's disease at the early stages: molecular imaging with 123I-FP-CIT SPECT. Int J Mol Med, 2011. 28(5): p. 881-6.
108. Spiegel, J., et al., Striatal FP-CIT uptake differs in the subtypes of early Parkinson's disease. J Neural Transm (Vienna), 2007. 114(3): p. 331-5.
109. Mo, S.J., et al., Pre- and postsynaptic dopamine SPECT in the early phase of idiopathic parkinsonism: a population-based study. Eur J Nucl Med Mol Imaging, 2010. 37(11): p. 2154-64.
110. Isaias, I.U., et al., [123I]FP-CIT striatal binding in early Parkinson's disease patients with tremor vs. akinetic-rigid onset. Neuroreport, 2007. 18(14): p. 1499-502.
111. Kaasinen, V., et al., Differences in striatal dopamine transporter density between tremor dominant and non-tremor Parkinson's disease. Eur J Nucl Med Mol Imaging, 2014. 41(10): p. 1931-7.
112. Ramani, L., et al., Relationship between [(123) I]-FP-CIT SPECT and clinical progression in Parkinson's disease. Acta Neurol Scand, 2017. 135(4): p. 400-406.
113. Caretti, V., et al., Loss of thalamic serotonin transporters in early drug-naive Parkinson's disease patients is associated with tremor: an [(123)I]beta-CIT SPECT study. J Neural Transm (Vienna), 2008. 115(5): p. 721-9.
114. Mito, Y., et al., Brain SPECT analysis by 3D-SSP and clinical features of Parkinson's disease. Hokkaido Igaku Zasshi, 2006. 81(1): p. 15-23.
115. Fishman, P.S., Paradoxical aspects of parkinsonian tremor. Mov Disord, 2008. 23(2): p. 168-73.
116. Helmich, R.C., et al., Cerebral causes and consequences of parkinsonian resting tremor: a tale of two circuits? Brain, 2012. 135(Pt 11): p. 3206-26.
117. Wu, T., et al., Effective connectivity of brain networks during self-initiated movement in Parkinson's disease. Neuroimage, 2011. 55(1): p. 204-15.
118. Du, G., et al., Properties of oscillatory neuronal activity in the basal ganglia and thalamus in patients with Parkinson's disease. Transl Neurodegener, 2018. 7: p. 17.
119. Hurtado, J.M., et al., Dynamics of tremor-related oscillations in the human globus pallidus: a single case study. Proc Natl Acad Sci U S A, 1999. 96(4): p. 1674-9.
120. Lenz, F.A., et al., Single unit analysis of the human ventral thalamic nuclear group. Tremor-related activity in functionally identified cells. Brain, 1994. 117 (Pt 3): p. 531-43.
121. Pedrosa, D.J., et al., A functional micro-electrode mapping of ventral thalamus in essential tremor. Brain, 2018. 141(9): p. 2644-2654.

CHAPTER 3

Dedicated container for postmortem human brain ultra-high field magnetic resonance imaging

Boonstra JT, Michielse S, Roebroeck A, Temel Y, Jahanshahi A.

Dedicated container for postmortem human brain ultra-high field magnetic resonance imaging. NeuroImage. 2021;235:118010.

Abstract

Background: The emerging field of ultra-high field MRI (UHF-MRI, 7 Tesla and higher) provides the opportunity to image human brains at a higher resolution and with higher signal-to-noise ratios compared to the more widely available 1.5 and 3T scanners. Scanning post-mortem tissue additionally allows for greatly increased scan times and fewer movement issues leading to improvements in image quality. However, typical postmortem neuroimaging routines involve placing the tissue within plastic bags that leave room for susceptibility artifacts from tissue-air interfaces, inadequate submersion, and leakage issues. To address these challenges in postmortem imaging, a custom-built nonferromagnetic container was developed that allows whole brain hemispheres to be scanned at sub-millimeter resolution within typical head-coils.

Method: The custom-built polymethylmethacrylaat container consists of a cylinder with a hemispheric side and a lid with valves on the adjacent side. This shape fits within common MR head-coils and allows whole hemispheres to be submerged and vacuum sealed within it. Two hemisphere samples were scanned on a Siemens 9.4T Magnetom MRI scanner. High resolution T2* weighted data was obtained with a custom 3D gradient echo (GRE) sequence and diffusion-weighted imaging (DWI) scans were obtained with a 3D kT-dSTEAM sequence along 48 directions.

Results: The custom-built container proved to submerge and contain tissue samples effectively and showed no interferences with MR scanning acquisition. The 3D GRE sequence provided high resolution isotropic T2* weighted data at 250μm which showed a clear visualization of grey and white matter structures. DWI scans allowed for dense reconstruction of structural white matter connections via tractography.

Conclusion: Using this custom-built container worked towards achieving high quality MR images of postmortem brain material. This procedure can have advantages over traditional schemes including utilization of a standardized protocol and the reduced likelihood of leakage. This methodology could be adjusted and used to improve typical postmortem imaging routines.

Introduction

Postmortem magnetic resonance imaging (MRI) of human brain tissue improves the understanding of clinical MRI and provides insight into pathological data found via histological assessments of tissue.[1,2] Human brain postmortem imaging has proven to be valuable due to the ability to scan for long periods (hours/days), compared to *in vivo* where patients are typically scanned for about one hour.[3,4] Longer scan times can lead to higher quality images through improved spatial resolution and greater signal-to-noise ratios (SNR) [5-7]. Typically, ultra high field MRI (UHF-MRI, 7 Tesla and higher) examinations take place on preclinical or animal MRI systems to utilize high field strengths and increased gradient performance, but are often limited to small tissue samples restricting the size of brain regions examined [8]. Employing UHF-MRI systems to generate high resolution images of large human brain samples is an important step in investigating neuronal architecture which can then be translated to *in vivo* paradigms.

In preparation for scanning postmortem tissue, several aspects need to be addressed to obtain optimal data quality. The standard method of preserving large neuronal tissue is to contain it in fixatives such as formaldehyde that cross-links tissue proteins. This method, along with lowering of temperature, is an important factor in altering various MRI properties within tissue (*e.g.* T1 and T2 relaxation times) when compared to *in vivo* and *in situ* MRI.[9] Because of these altered tissue properties scanning procedures must compensate with higher field and gradient strengths, close-fitting RF coils, optimized MR pulse sequences, and/or longer scan times to achieve high-resolution images.[3] Developing hardware for *ex vivo* imaging is imperative for optimal and more applicative postmortem imaging. Likewise, such hardware should aid in combating some of the main *ex vivo* MRI challenges including minimizing magnetic susceptibility gradients at tissue borders and removal of air bubbles from tissue that interfere with the MR signal.

The quality of *in vivo* brain scans are limited due to a few factors that can be alleviated in post mortem acquisitions: the limited acquisition time, physiological noise from heartbeat and breathing, peripheral nerve stimulation, and specific arbsorbtion rate limits. B0 inhomogeneity caused by air cavities within the ear canals and sinuses are also a significant factor limiting the quality of in vivo scans. In order to obtain high quality images, a relatively homogeneous magnetic environment must be created over the entire sample, including at its borders. To achieve this for postmortem acquisitions, before scanning brains are typically submerged in a proton-free fluid such as Fluorinert™ or Fomblin®. Fluorinert, a perfluoropolyether fluorocarbon, avoids off-resonance distortions at tissue borders due to the fluids' magnetic susceptibility matched to that of brain tissue [3]. Fluorinert has shown to pose no risk to tissues histochemical properties even after a one-week immersion period.[10] Although less optimal, submersion in phosphate-buffered

saline (PBS), or formalin is sometimes performed. Prior to scanning, it is important to remove air bubbles from the surface, ventricles, sulci, and fissures, as trapped air bubbles will cause imaging artifacts. This can be done by gently agitating and rotating the tissue while having it completely submerged in liquid. Additional removal of air bubbles can be performed via a vibrating plate and/or placing the container inside a vacuum chamber. After scanning, Fluorinert™ can be stored and recycled for use during the next scanning session.

Within an MRI scanner, radio frequency receive coils made for certain areas of the body (e.g. head, chest, and knee coils) are used to measure the MR signal. Some studies have used custom-built receive coils specifically designed to image large postmortem samples at high resolution [8,11,12] although these methods are currently too financially and technically complex to become widespread common practice. Another study used a jug filled with formalin inside a head-coil to examine whole postmortem brains, but there was a large distance between the coils and the sample that limited the uniformity of the SNR profile, restricting image quality.[13] Although several studies have simply submerged large tissue samples in sealed plastic bags within MR head-coils with good results [9,14-16] this leaves room for susceptibility effects caused by air–tissue interfaces while the possibility of leaks poses considerable risk to the tissue sample and the MRI scanner.

Lastly, MRI scanners are made by different vendors (e.g. General Electric, Siemens, Philips) and the head coils used may be made by diverse manufacturers, the same vendors, or third parties, which may not allow for the accommodation of all types of containers. Therfore, here we describe the manufacturing and use of a dedicated container for whole human brain postmortem imaging. The standard sized head shaped MRI container is capable of holding various submersion liquids and can be be placed under vacuum pressure to minimize air bubbles while decreasing the distance between the coils and tissue for optimized positioning. We demonstrate the use of the container in a large bore 9.4T MRI system. This container optimizes MR imaging conditions for whole human brain post mortem imaging, while allowing efficient and flexible use in standard head-coils.

Methods

Construction of container

A container was developed in collaboration with the Instrument Development Engineering and Evaluation (IDEE) department at Maastricht University. The dimensions for the space inside a 7T 32 channel Nova Medical MRI head coil (Nova Medical, Wilmington, MA) where digitally rendered using Creo Parametric 3D Modeling Software 3.0 (Parametric Technology Corporation, PTC, USA) (Figure 1B). A cardboard model with the gross

dimensions of the container was laser cut and tested within multiple 7T and 9.4T head-coils available at the local MRI facility (Scannexus; Maastricht University campus; www.scannexus.nl),. The container consisted from two halves (shells) and a lid milled from polymethylmethacrylaat (PMMA) using a Fehlmann P82 computer numerical control (CNC) milling machine over the course of 20 hours with ESPRIT 2016 software (DP Technology Corporation, USA), a high-performance computer-aided manufacturing (CAM) system. After being shaped and smoothed the two shells were clamped and glued together using ACRIFIXÒ 1S 0117, a solvent acrylic cement. The container was then dried at 70°C for 18 hours in a Memmert UN110, a universally applicable lab oven, to anneal the stress after milling, then cooled down to room temperature over a six-hour period. Finally, the container was smoothed and polished by hand in order to achieve complete transparency of the PMMA. The outside diameter is 177mm and the length of the container is 245mm (Figure 1A).

A PMMA lid was constructed with a silicon sealing-ring on the bottom. Two polycarbonate 3-way stopcock Luer-lok® valves were installed on top of the lid for the removal of air bubbles and to pump in liquid (Figure 1C, Figure 2A). Polyamide (nylon) screws were

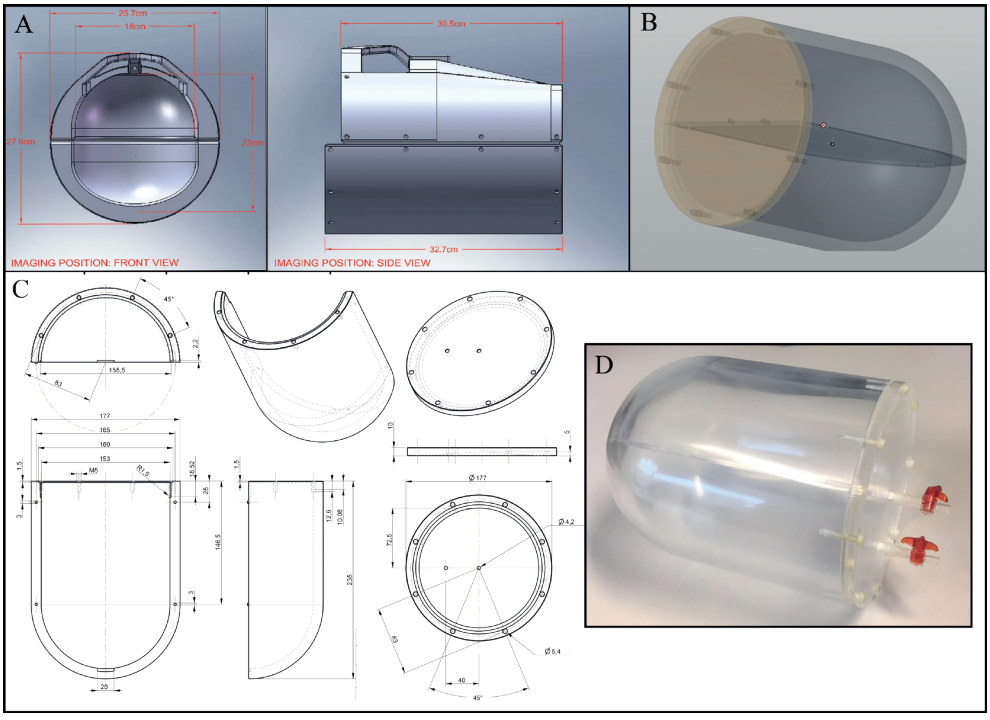

Figure 1. A) Geometric dimensioning and tolerancing of the container; 245mm full-length, 177mm width. B) 3D rendering using Creo Parametric 3D Modeling Software 3.0 (Parametric Technology Corporation, PTC, USA). C) Completed container including the lid, screws [yellow], sealing ring, and values [red].

used to secure the lid to the container and provide additional sealing tension (Figure 1C, Figure 2D). A flat removable PMMA separator was created and placed down the middle of the inside of the container for situations where two separate hemispheres are scanned simultaneously. The separator can be removed for larger samples such as whole brains.

Tissue preparation protocol

Two whole hemisphere tissue samples, one Parkinson's disease (PD) patient and one healthy control, were obtained from the Multiple Sclerosis and Parkinson's Tissue Bank located at Imperial College London. Ethical approval was given for the use of tissue in research projects by the Research Ethics Committee for Wales, which was additionally approved by the Maastricht University medical ethical committee. Tissue samples were stored in 10% formaldehyde in PBS at room temperature. The protocol of preparing the tissue within the container was as follows:

1) Remove tissue from storage and wash in 3 liters of PBS for 3 x 5 minutes.
2) Place tissue sample into the PMMA container.
3) Fill container with 3M Fluorinert™ FC-770 (perfluorocarbon).
4) Place six open 50ml Falcon centrifuge tubes made from polypropylene loosely on top of the tissue to keep samples fully submerged.
5) Close container and screw shut.
6) Further seal with KaptonÒ tape (DuPontÔ) (Figure 2B).
7) Position sealed container upright on custom-built metal stand in a vacuum chamber (Figure 2E).
8) Open values and set vacuum to a pressure of -1 bar; leave overnight.
9) Slowly bring pressure back to 1 bar in order to keep the tissue stable.
10) Remove container from the chamber and fill with additional Fluorinert™ via the valves and siphon residue fixative solution.
11) Wipe container down and tape values into the close position.
12) Place container within a linear low-density polyethylene (LLDPE) bag to safeguard against any possible leaks during transportation and scanning.
13) Place bagged container within a nonferromagnetic container in the MRI scanning room (adjacent to magnet) to have the material and tissue reach temperature equilibrium.

Within this set up, KaptonÒ tape was used for it is an unfilled thermoplastic polyimide film material with silicon adhesive used as a high-grade electrical insulator. Also to note, the vapor pressure of Fluorinert FC-770 is 0.056 bar which causes a minimal amount of evaporation to occur when under negative pressure. As residue fixative solution will be freed from tissue during set up and scanning, one should be mindful of the position of the container within the MR scanner along with the field-of-view (FoV) created on the MR console.

Figure 2. Custom postmortem MRI container with two postmortem hemispheres submerged in Fluorinert™. A) Three-way stopcock valves. B) Kapton tape. C) Rubber seal. D) Nylon screws. E) Custom built metal stand. F) PMMA separator in between hemispheres.

MRI acquisition and data reconstruction

Samples were scanned on a 9.4T Magnetom MRI scanner (Siemens Healthcare, Erlangen, Germany) equipped with a 16 channel parallel transmit (pTx) and 31 channel receive head coil (Max Planck Institute, Tübingen, Germany).[17] First, a localizer scan with 11 slices in all three orthogonal directions was acquired for planning. Next a 2mm isotropic field map[18] and dual refocusing echo acquisition mode (DREAM)[19] sequence were obtained to characterize B0 and B1+ map profiles, respectively. B0 and B1+ offline shimming was performed using in house custom build MATLAB scripts.[20]

The main acquisitions were performed with a custom 3D gradient echo (GRE) pulse sequence, modified to use a composite parallel excitation pulse using kT-points shimming for B1+ homogenization.[20] The 3D GRE sequence was used to acquire high resolution isotropic T2* weighted data at 250µm (FoV read; 172mm, FoV phase; 71.2%, Repetition Time (TR); 42ms, TE; 6.98ms, 11.00ms, 16.21ms, 20.23ms, 24.46ms and 30.00ms, Flip Angle (FA); 15deg. The GRE acquisition time (TA) was 05:10:58.

Diffusion-weighted imaging (DWI) scans were obtained with the 3D kT-point diffusion weighted STimulated Echo Acquisition Mode (kT-dSTEAM) sequence[12] along 48 directions, distributed with an electrostatic repulsion algorithm for optimal whole sphere coverage, in six groups of eight directions with a B-value of 5009 s/mm^2 with four B0 volumes (at a low B-value of 318 s/mm^2). The voxel size was 1mm isotropic with a matrix size of 144x180x116, TR 450ms, TE 28ms, mixing time 135ms, and a five lines per shot segmented echo planar imaging (EPI) readout. The TA was 29:10 per volume, with diffusion-weighted volumes acquired in series of eight. Total TA for all diffusion volumes was 23:22:36. Raw data was exported offline to undergo reconstruction using in-house build reconstruction software in a Python environment using NumPy and SciPy packages[21,22] and in MATLAB (v2015) running on a Windows 2012 R2 server, as previously reported.[12]

Results

T2 Weighted Images*

T2-weighted scans showed a clear visualization of the grey and white matter structures of the neuronal tissue (Figure 3). The brain container and spacer were invisible in the MR image and the proton free liquid showed no signal. Visual representations of the GRE scans are provided in Figure 3; six echoes at 6.98ms, 11.00ms, 16.21ms, 20.23ms, 24.46ms and 30.00ms are provided and show different contrasts with variable structural visibility. The echo at 16.21ms clearly shows grey and white matter borders due to it being the closest to the T2* of these tissues. Using the six echoes a quantitative T2* (qT2*) image was computed (Figure 4). Signal loss can be seen in the occipital lobe due a combination of low transmit B1 and low receive sensitivity, the latter resulting from that area being more distant to receiver coils.

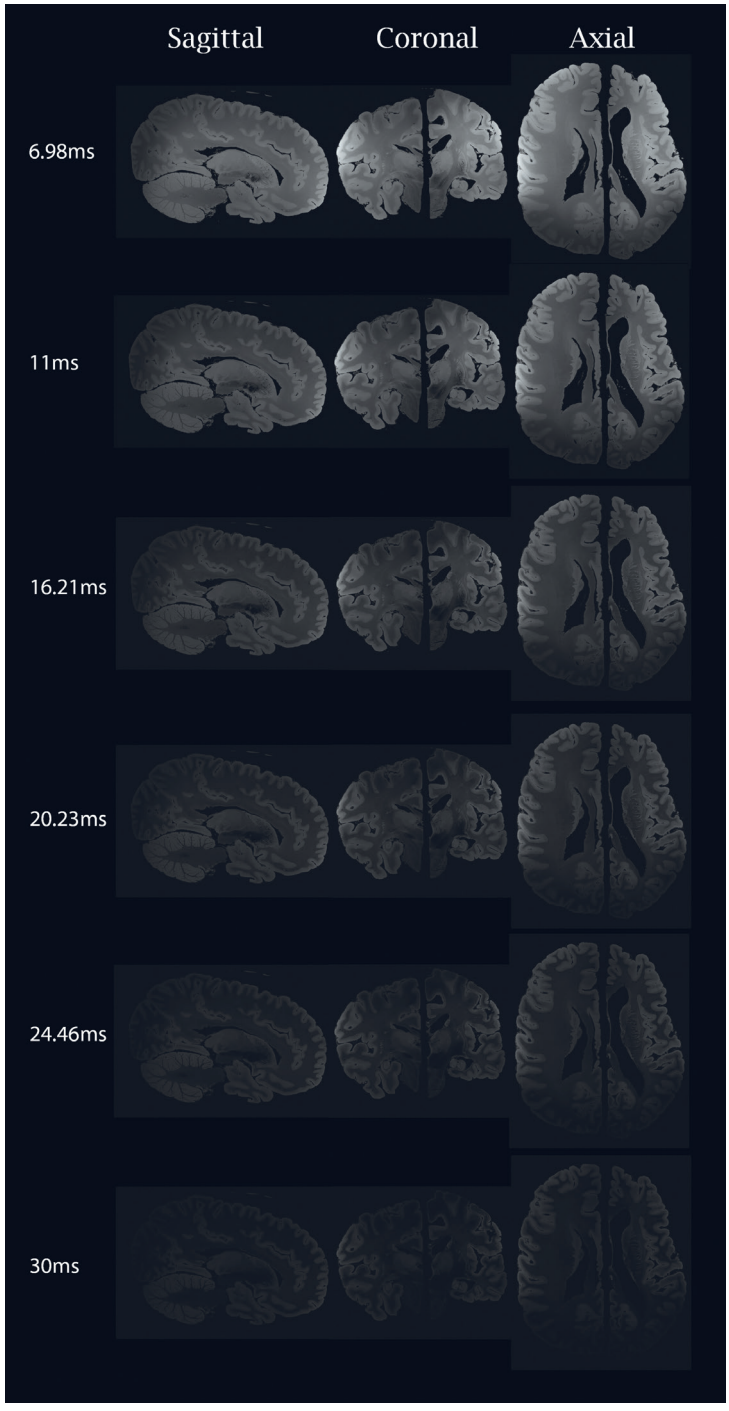

Figure 3. T2* Weighted Gradient Echo scans in ascending order of 6.98ms, 11ms, 16.21ms, 20.23ms, 24.46ms and 30ms showing the T2* decay of the signal. Healthy control on far left and left sides, PD patient on the right sides.

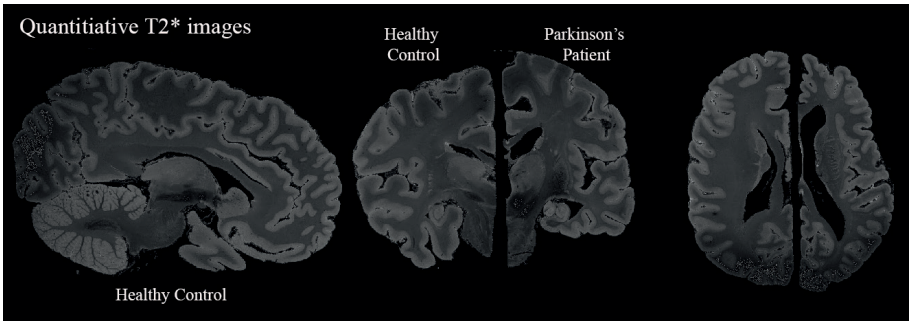

Figure 4. Quantitative T2* (qT2*) images estimated from six T2* weighted gradient echo volumes.

Diffusion weighted scans

A raw B0 image and directionally-encoded colour (DEC) FA map are provided in Figure 5. The raw DWI scans had enough information to reconstruct the structural white matter connections; an overview of the entire tractogram is provided in Figure 6. It should be noted that within the occipital lobe there was not enough signal to reconstruct fiber tracts. This was in part due to our scanning protocol having the main region of interest be the mesencephalon (basal ganglia) and motor cortex, i.e. *parkinsonian* regions.

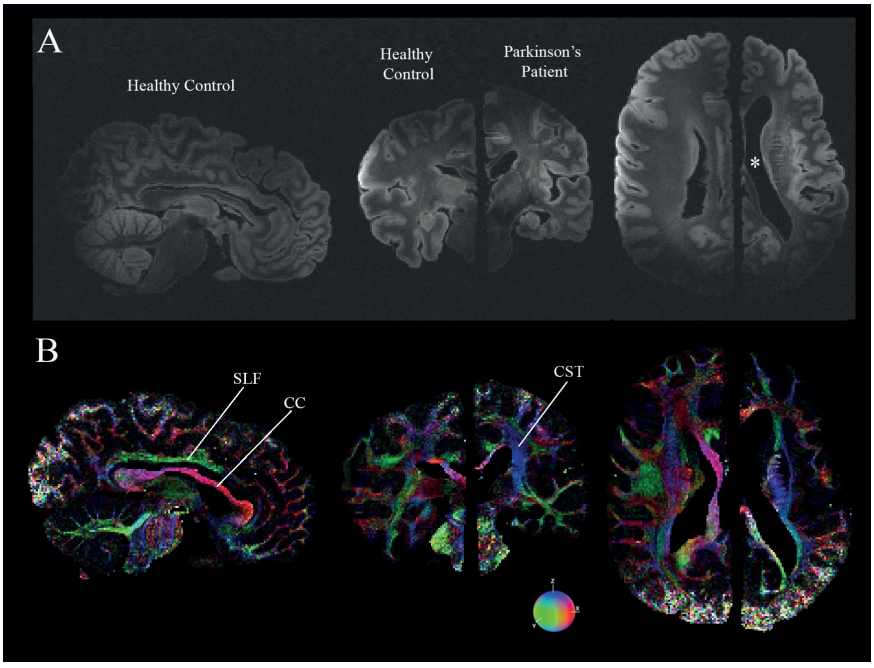

Figure 5. A: Raw B0 image of healthy control (far left and left side) and PD patient (right side). *Atrophy in the Parkinson's patient's third ventricle. B: directionally-encoded colour (DEC) FA map. SLF = superior longitudinal fasciculus. CC = corpus callosum. CST = corticospinal tract. Color coding sphere depicts the standard DEC diffusion orientations along the left/right axis in red, diffusion along the anterior/posterior axis in green and diffusion along the inferior/superior axis in blue.

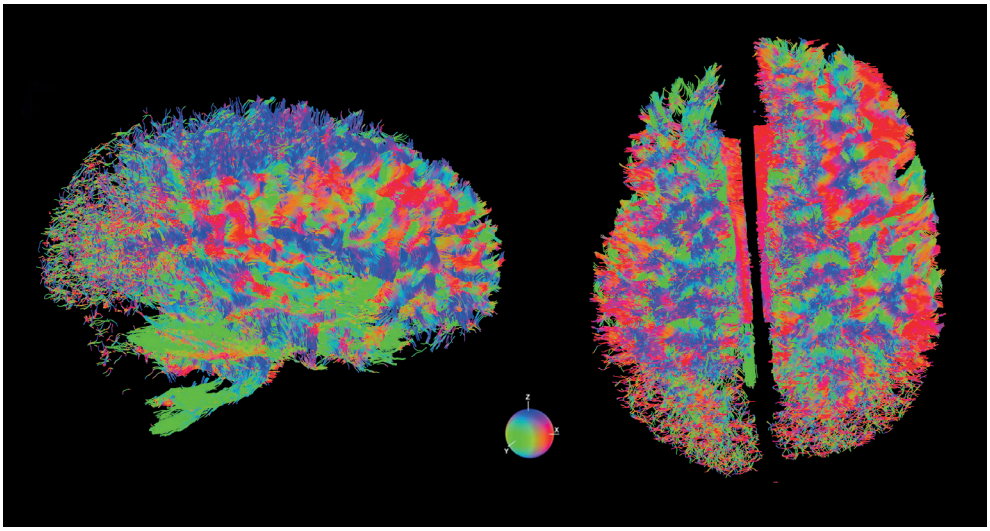

Figure 6. Diffusion weighted imaging tractography showing white matter bundles. Left: lateral view of PD patient. Right: superior view showing both health control (left) and PD patient (right).

Discussion

A dedicated container was designed for scanning postmortem brains in UHF-MR scanners. In the development process, several considerations were made to optimize the container to be easy to use within MR facilities and engender high quality images with a low number of artefacts. While postmortem imaging holds several challenges including altered T1 and T2 relaxation times as well as achieving optimized imaging contrasts at high resolution, it also grants advantages to *in vivo* measurements including longer scan times, less motion and physiological noise artifacts, and greater SNR.

The container here proved to have the necessary qualifications needed for postmortem imaging including ease of transportation, vacuum sealing capabilities, and compatibility with previously designed sequences and procedures. Imaging procedures using a custom GRE pulse sequence that utilize composite parallel excitation pulses with kT-points proved effective in acquiring high resolution T2* weighted data at 250μm and DWI data at 1mm.

Air bubbles within ventricles and cortical surfaces compromise regional information and are one of the major issues for *ex vivo* imaging. Likewise, as fixative solution will continuously seep from the tissue during scanning, additional measures should be made to reduce such interference. Further improvements can be made to obtain even greater image quality including improved positioning of the tissue within the container and

longer scanning times. Additionally, the feasibility of this method is not limited by MRI magnet field strength allowing images to be acquired on traditional 1.5 and 3T scanners and even stronger ultra-high field systems (≥ 10T) provided the bore of the magnet affords large enough RF-coils.

In the future, the use of this container alongside modified separators can be further customized to improve positioning and submersion of tissue, hold single or multiple brain slices or separate biological tissue segmentations, and reduce bulk motion and scanner-related vibrations to increase stability while scanning. This postmortem scanning methodology has proven advantageous and can be used to improve the ability in achieving high-quality low artifact MR images of large postmortem brain tissue.

References

1. Mori, S., Y. Kageyama, Z. Hou, et al., *Elucidation of White Matter Tracts of the Human Amygdala by Detailed Comparison between High-Resolution Postmortem Magnetic Resonance Imaging and Histology.* Front Neuroanat, 2017. **11**: p. 16.
2. Seehaus, A.K., A. Roebroeck, O. Chiry, et al., *Histological validation of DW-MRI tractography in human postmortem tissue.* Cereb Cortex, 2013. **23**(2): p. 442-50.
3. Roebroeck, A., K.L. Miller, and M. Aggarwal, *Ex vivo diffusion MRI of the human brain: Technical challenges and recent advances.* NMR Biomed, 2019. **32**(4): p. e3941.
4. Augustinack, J.C., A.J. van der Kouwe, and B. Fischl, *Medial temporal cortices in ex vivo magnetic resonance imaging.* J Comp Neurol, 2013. **521**(18): p. 4177-88.
5. Miller, K.L., J.A. McNab, S. Jbabdi, and G. Douaud, *Diffusion tractography of post-mortem human brains: optimization and comparison of spin echo and steady-state free precession techniques.* Neuroimage, 2012. **59**(3): p. 2284-97.
6. Miller, K.L., C.J. Stagg, G. Douaud, et al., *Diffusion imaging of whole, post-mortem human brains on a clinical MRI scanner.* Neuroimage, 2011. **57**(1): p. 167-181.
7. Plantinga, B.R., A. Roebroeck, V.G. Kemper, et al., *Ultra-High Field MRI Post Mortem Structural Connectivity of the Human Subthalamic Nucleus, Substantia Nigra, and Globus Pallidus.* Front Neuroanat, 2016. **10**: p. 66.
8. Sengupta, S., F.J. Fritz, R.L. Harms, et al., *High resolution anatomical and quantitative MRI of the entire human occipital lobe ex vivo at 9.4T.* Neuroimage, 2018. **168**: p. 162-171.
9. Dyrby, T.B., W.F. Baare, D.C. Alexander, et al., *An ex vivo imaging pipeline for producing high-quality and high-resolution diffusion-weighted imaging datasets.* Hum Brain Mapp, 2011. **32**(4): p. 544-63.
10. Iglesias, J.E., S. Crampsie, C. Strand, et al., *Effect of Fluorinert on the Histological Properties of Formalin-Fixed Human Brain Tissue.* J Neuropathol Exp Neurol, 2018. **77**(12): p. 1085-1090.
11. Edlow, B.L., A. Mareyam, A. Horn, et al., *7 Tesla MRI of the ex vivo human brain at 100 micron resolution.* Sci Data, 2019. **6**(1): p. 244.
12. Fritz, F.J., S. Sengupta, R.L. Harms, et al., *Ultra-high resolution and multi-shell diffusion MRI of intact ex vivo human brains using kT-dSTEAM at 9.4T.* Neuroimage, 2019. **202**: p. 116087.
13. Shatil, A.S., K.M. Matsuda, and C.R. Figley, *A Method for Whole Brain Ex Vivo Magnetic Resonance Imaging with Minimal Susceptibility Artifacts.* Front Neurol, 2016. **7**: p. 208.
14. Iglesias, J.E., R. Insausti, G. Lerma-Usabiaga, et al., *A probabilistic atlas of the human thalamic nuclei combining ex vivo MRI and histology.* Neuroimage, 2018. **183**: p. 314-326.
15. Schmierer, K., C.A. Wheeler-Kingshott, P.A. Boulby, et al., *Diffusion tensor imaging of post mortem multiple sclerosis brain.* Neuroimage, 2007. **35**(2): p. 467-77.
16. Foxley, S., S. Jbabdi, S. Clare, et al., *Improving diffusion-weighted imaging of post-mortem human brains: SSFP at 7 T.* Neuroimage, 2014. **102 Pt 2**: p. 579-89.
17. Shajan, G., M. Kozlov, J. Hoffmann, et al., *A 16-channel dual-row transmit array in combination with a 31-element receive array for human brain imaging at 9.4 T.* Magn Reson Med, 2014. **71**(2): p. 870-9.
18. Cusack, R. and N. Papadakis, *New robust 3-D phase unwrapping algorithms: application to magnetic field mapping and undistorting echoplanar images.* Neuroimage, 2002. **16**(3 Pt 1): p. 754-64.
19. Nehrke, K. and P. Bornert, *DREAM--a novel approach for robust, ultrafast, multislice B(1) mapping.* Magn Reson Med, 2012. **68**(5): p. 1517-26.
20. Tse, D.H., C.J. Wiggins, D. Ivanov, et al., *Volumetric imaging with homogenised excitation and static field at 9.4 T.* MAGMA, 2016. **29**(3): p. 333-45.
21. Virtanen, P., R. Gommers, T.E. Oliphant, et al., *SciPy 1.0: fundamental algorithms for scientific computing in Python.* Nat Methods, 2020. **17**(3): p. 261-272.
22. Harris, C.R., K.J. Millman, S.J. van der Walt, et al., *Array programming with NumPy.* Nature, 2020. **585**(7825): p. 357-362.

CHAPTER 4

Diffusion connectivity disparities across Parkinson's disease motor subtypes and non-demented controls: a postmortem ultra high field MRI study

Boonstra JT, Michielse S, Temel Y, Jahanshahi A, and Roebroeck A**
*These authors contributed equally to this work.

Abstract

The structural correlates of Parkinson's disease with tremor-dominance and those with non-tremor dominance are not fully differentiated. Ultra-high field magnetic resonance imaging (UHF-MRI) allows the human brain to be imaged at a higher resolution compared to traditional scanner strengths but has largely been underutilized. Scanning post-mortem tissue additionally allows for increased scan times and fewer movement issues leading to improved image quality. We performed diffusion MRI on twelve post-mortem hemispheres (eight parkinsonian (four tremor-dominant, four non-tremor-dominant) and four non-demented controls) scanned with a specialized 9.4T human post-mortem brain radiofrequency coil. Diffusion tensor analysis was performed for local scalar diffusion metrics and constrained spherical deconvolution tractography was performed for global connectivity metrics. Compared to both non-tremor-dominant patients and non-demented controls, tremor-dominant patients displayed greater hemispheric fractional anisotropy. Motor subtypes did not differ from each other in multiple regional diffusion metrics but differentially varied compared to non-demented controls. Interconnections within basal ganglia circuitry mainly involving the internal capsule showed disparities across both subtypes and non-demented controls. Our findings show motor subtype specific circuitopathies in Parkinson's disease and improve the mapping of neuronal *fingerprints* potentially relevant in the planning of treatment regimes.

Keywords: Parkinson's disease; neuroimaging; motor subtypes; post-mortem; diffusion

Introduction

Parkinson's disease (PD) is a progressive and complex neurodegenerative disorder with heterogeneous clinical characteristics and various movement symptoms including tremors and kinesia paradoxa. Based on clinical evaluations different PD subtypes can be distinguished by separate motor symptoms including tremor-dominance (TD) and non-tremor dominance (nTD) that suggest dissimilar pathophysiologies in neuronal motor circuitry.[1-4] nTD patients have shown a longer course of disease, higher disease severity, and a need for higher daily dosages of levodopa.[5] Greater distinction between the pathophysiology of PD subtypes can help improve disease monitoring and treatment regimens including deep brain stimulation (DBS) that uses surgically implanted electrodes to target basal ganglia/thalamic structures involved in motor circuitry to reduce PD symptoms.[6]

Subcortical structures can be challenging to visualize using conventional MRI scanners at field strengths of 1.5 and 3 Tesla. Ultra-high field MRI (UHF-MRI, 7 Tesla and higher) generates higher resolution images from improved contrast- and signal-to-noise ratios (SNR) holding potential to capture novel fine-grained neurological information to improve the clinical targeting of DBS.[7] Furthermore, UHF imaging may expand disease progression monitoring, potentially starting from premotor stages, and work to understand disease etiology with improved detail.[8] There is an ongoing observational study aiming to identify distinctive characteristics in PD patients using UHF and correlate MRI characteristics to clinical phenotype, genetics, and symptom progression.[9] Scanning post-mortem PD brains has additionally proven of great value in understanding pathophysiologies due to the ability to scan for longer periods (hours/days) compared to *in vivo* investigations[10,11] leading to higher quality images through improved spatial resolution and greater SNR.[12-14] Post-mortem MRI with subsequent histology can additionally aid in the development of translational radiological sequences used to detect pathology *in vivo* and in the differentiation of PD to that of other parkinsonisms.[15,16]

Degradation of the basal ganglia is the main pathological hallmark of PD leading to microstructural integrity alterations in cortical and subcortical neuronal white matter. Several imaging sequences are available in MRI to detail white matter alterations in brain tissue and hold potential to differentiate PD subtypes with sufficient accuracy.[17] Diffusion weighted imaging (DWI) measures random water molecule movement restricted by myelin and white matter architecture, and is used as an indirect marker for white matter integrity and axonal organization in the brain. Diffusion Tensor Imaging (DTI) measurements can be performed with DWI to obtain markers of the demyelination, axonal density, and fiber configuration of white matter. Standard diffusion metrics include fractional anisotropy (FA) that measures the extent diffusion is restricted or unrestricted in specific directions,

radial diffusivity (RD) as the diffusion coefficient perpendicular to axonal fibers, axial diffusivity (AD) that measures the magnitude of diffusion parallel to fibers, and mean diffusivity (MD, i.e., mean apparent diffusion coefficient (ADC)) as the average diffusion within a voxel.[18]

PD is associated with decreases in FA in many white matter tracts indicating an increase in fiber complexity, a decrease in axons, and greater demyelination.[19] Decreases in FA along with increases in MD in the substantia nigra[20] have additionally proven to distinguish PD patients from healthy controls *in vivo*.[19] TD patients generally show increased MD and AD along multiple white matter tracts mainly in the cerebello-thalamocortical (CTC) pathway compared to nTD[21,22], while those with postural instability and gait difficulty (PIGD, i.e., nTD) show increased MD in the SN and bilateral globus pallidus (GP) that correlate with disease stage and motor severity.[19] TD patients have shown greater FA and attenuated RD and AD in major commissural, projection, and association tracts compared to PIGD patients, while PIGD patients show more white matter deterioration in those areas reflected by decreased FA and increased RD and AD compared to TD.[23]

Using connectivity indices derived from DWI, previous research has shown lower structural connectivity in nTD patients compared to TD patients in interconnected motor areas such as the GP–SN tract, GP–thalamus tract, putamen–precentral cortex tract, thalamus–precentral cortex tract, and the caudate nucleus–supplementary motor area tract.[24] TD patients show enhanced causal connectivity from the bilateral ventral intermediate nucleus (Vim) to the bilateral paracentral gyrus, M1, and cerebellum compared with health controls, while PIGD show increased causal connectivity from the bilateral Vim to the bilateral premotor cortex and putamen.[25] PIGD patients show significantly increased local and global efficiencies in a thalamic network of nodes (a structurally weighted connectivity matrix of individual thalamic volumes) compared to healthy controls, while TD did not, denoting increased segregation of intrinsic thalamic network breakdowns in nTD.[26]

Interpreting diffusion alterations calculated with a standard tensor model in brain regions containing crossing fibers can be challenging[27] as studies show 33-90% of all white matter voxels contain crossing fibers largely invalidating the conventional tensor model that proposes white matter to be in specific bundles.[28-30] The technique of Constrained Spherical Deconvolution (CSD) can better detect crossing fibers within voxels and be further improved upon with the application of higher b-values[31]; higher b-values lead to stronger diffusion weighting providing sensitivity to diffusion effects at smaller length scales as well as more precise tensor estimation.[32] Probabilistic CSD tracking has shown to provide an improved sensitivity in identifying white matter connectivity disruptions associated with PD and in detecting group differences in topological measurements and

connectivity strengths.[33] Currently, there is little evidence from post-mortem PD material imaged with UHF CSD in discerning and quantifying white matter alterations related to PD and PD subtypes.

In this study, we employed tractography analysis on post-mortem hemispheres of PD and non-demented controls imaged with an ultra-high field (9.4T) MRI using a dedicated radiofrequency coil.[34] The interconnections of basal ganglia regions were quantified in all samples. We hypothesized PD brains would show lower universal connectivity indices compared to non-demented controls, with nTD patients having multiple lower interconnected motor system related nuclei compared to TD. We further hypothesized previous research to be supported with more fine-grained resolution and novel detail wherein nTD patients show greater alterations in multiple projection, association, and commissural tracts compared to TD patients in line with greater microstructural white matter abnormalities in the cortico-basal ganglia-thalamocortical tract.[17] Differentiating PD motor subtype pathophysiologies under this paradigm can work to better delineate afflicted networks and develop robust PD models.[8,9,14]

Materials and methods

Sample acquisition

Twelve post-mortem hemispheres (four TD, four nTD, and four non-demented controls) were obtained from the Multiple Sclerosis and Parkinson's Tissue Bank located at Imperial College London, UK. Ethical approval was given for the use of tissue in research projects by the Research Ethics Committee for Wales reference number 08/MRE09/31+5. Clinical data for each patient was checked to ensure they displayed rigidity without any tremors or tremors with limited rigidity, consistent with a diagnosis of either TD or nTD subtypes of Parkinson's disease. The most affected hemisphere of each PD patients (contralateral to symptoms) was selected based on clinical reports of lateral symptoms. None of the patients included in the study had a diagnosis of dementia, nor had they undergone brain surgery. The control group consisted of non-demented individuals with no history of neurological disease.

See Table 1.1 and 1.2 for a demographic overview and comparisons of the samples used.

Table 1.1: Demographic overview of post-mortem hemispheres

Case	Group	Hem	Sex	PD Duration (years)	Age	PMI (hours)	Storage Time (years)	Volume (ml)
#1	TD	Left	M	20	83	45	3	567
#2	TD	Left	M	21	88	16	3	606
#3	TD	Right	M	6	80	17	2	672
#4	TD	Left	M	19	86	48	3	560
#5	nTD	Left	F	18	87	46	3	540
#6	nTD	Left	M	6	79	43	2	553
#7	nTD	Right	M	4	88	39	1	641
#8	nTD	Right	M	18	79	28	2	639
#9	Control	Right	M	x	72	40	3	650
#10	Control	Left	M	x	87	8	3	545
#11	Control	Right	F	x	92	21	1	390
#12	Control	Right	F	x	81	19	2	561

Table 1.2: Demographic comparisons of post-mortem hemispheres

	TD	nTD	HC	*p*
N	4	4	4	
Age (years)	84.50 [82.25, 86.50]	83.00 [79.00, 87.25]	84.00 [78.75, 88.25]	0.939
Sex	4 (100.0)	3 (75.0)	2 (50.00)	0.264
PMI (hours)	31.00 [16.75, 45.75]	41.00 [36.25, 43.75	20.00 [16.25, 25.75]	0.334
DoD	2017 [2017, 2017]	2018 [2017, 2018]	2017 [2017, 2018]	0.373

Note: Median values and [interquartile ranges] are reported. TD: tremor-dominance, nTD: non-tremor dominance, PD: Parkinson's disease, Sex: Biological sex (Male, Female), PMI: post-mortem interval (hours), DoD: Date of death (year). Hem: Hemisphere (left, right). mL: milliliters.

Sample preparation

Tissue samples were stored in 10% formalin in phosphate buffered saline (PBS) at room temperature. The tissue preparation protocol was adjusted from a published methodology[36] and was as follows:

(1) Remove tissue from storage and wash in 3 liters of PBS for 3 × 5 min.
(2) Place tissue sample into a custom 3D printed container.
(3) Close and seal container with silicone adhesive sealant. Let dry for 24 hours.
(4) Fill container with 3M Fluorinert™ FC-770 (perfluorocarbon) via top opening.
(5) Position shell upright in a 12-liter vacuum chamber.
(6) Set vacuum to a pressure of –1 bar and slowly bring pressure back to atmospheric pressure.

(7) Apply and release additional negative vacuum pressure in ten-minute intervals until no further bubbles are seen surfacing in the container. Rotate and gently shake the container between intervals to dislodge any air or fixative.
(8) Remove container from the vacuum; fill with additional Fluorinert™, siphon residue fixative solution if needed and seal the top opening with silicone.
(10) Place shell within a plastic bag for secondary concealment and put it in the MRI room 12 hours prior to scanning to reach temperature equilibrium.

Image acquisition

Imaging was carried out on a 9.4T Magnetom MRI scanner (Siemens Healthineers, Erlangen, Germany) using a dedicated 9.4T 8 channel parallel transmit (pTx), 24 channel receive RF-coil.[34] After a localizer scan and 11 slice localizer, a 2mm isotropic field map[37] and dual refocusing echo acquisition mode (DREAM)[38] sequence were obtained to characterize B_0 and B_1^+ map profiles, respectively. B_0 shimming was performed including 3rd order shim coils and kT-point composite RF pulses for B_1^+ homogenization were calculated offline using in-house build MatLab scripts.[39] Image acquisition was performed with a custom 3D gradient echo[40] pulse sequence, modified to use a composite parallel excitation (kT-points) pulse for B1+ homogenization.[39] A multi-echo 3D GRE (GRadient Echo) sequence was used to acquire high resolution isotropic T2* weighted data at 250µm (FoV read; 170mm, FoV phase; 83.2%, Repetition Time (TR); 37ms, echo time (TE); 5.90ms, 12.00ms, 20.00ms, and 28.00ms, flip angle; 28°. The acquisition time (TA) was 05:50:50.

Diffusion-weighted imaging (DWI) scans were obtained with a 3D kT-point diffusion weighted STimulated Echo Acquisition Mode (kT-dSTEAM) sequence[10] along 48 random directions, distributed with an electrostatic repulsion algorithm for optimal whole sphere coverage, in twelve sets of four directions with a B-value of 5007 s/mm^2 and five B0 volumes (Table 2). The voxel size was 1mm isotropic with a matrix size of 144x170x148, TR 400ms, flip angle 90°, TE 28ms, mixing time (TM) 135ms, and a five lines per shot segmented echo planar imaging readout. The TA was 29:10 per volume making a total TA of 23:22:36.

Table 2. Overview of MR sequences

Sequence	Resolution (mm^3)	Matrix size (x-y-z)	TE (ms)	TR (ms)	Flip angle (°)	Scan Time (hh:mm:ss)
GRE	0.25	640x680x566	5.9/12/20/28	37	28	05:50:50
DWI	1	144x170x148	28	400	90	23:22:36

Note. GRE: Gradient Echo, DWI: Diffusion Weighted Imaging, TE: Echo Time, TR: Repetition Time

Data preprocessing

Processing steps were completed on the Data Science Research Infrastructure (DSRI) cluster, a distributed and scalable computational infrastructure for data science

experiments at Maastricht University. Raw data first underwent reconstruction using in-house build reconstruction software in a Python environment using NumPy and SciPy packages[41,42] and in MatLab (v2015) running on a Windows 2012 R2 server, as previously reported[10]. Data were independently inspected by two researchers (J.T.B., S.M.) to check for artifacts and assure optimal image data quality. Several specimen had miniscule residual fixative solution or air bubbles in ventricles where proton-free fluid was unable to infiltrate, but this did not impact overall image quality. Analyses were completed using software tools from the Berkeley Advanced Reconstruction Toolbox (BART, Göttingen University)[43], Oxford Centre for Functional MRI of the Brain (FMRIB) Software Library Version 5.0.9 (FSL)[40] and MRtrix3 (http://www.mrtrix.org/). All images were oriented to standard FSL orientation via a custom MatLab script (Supplementary material).

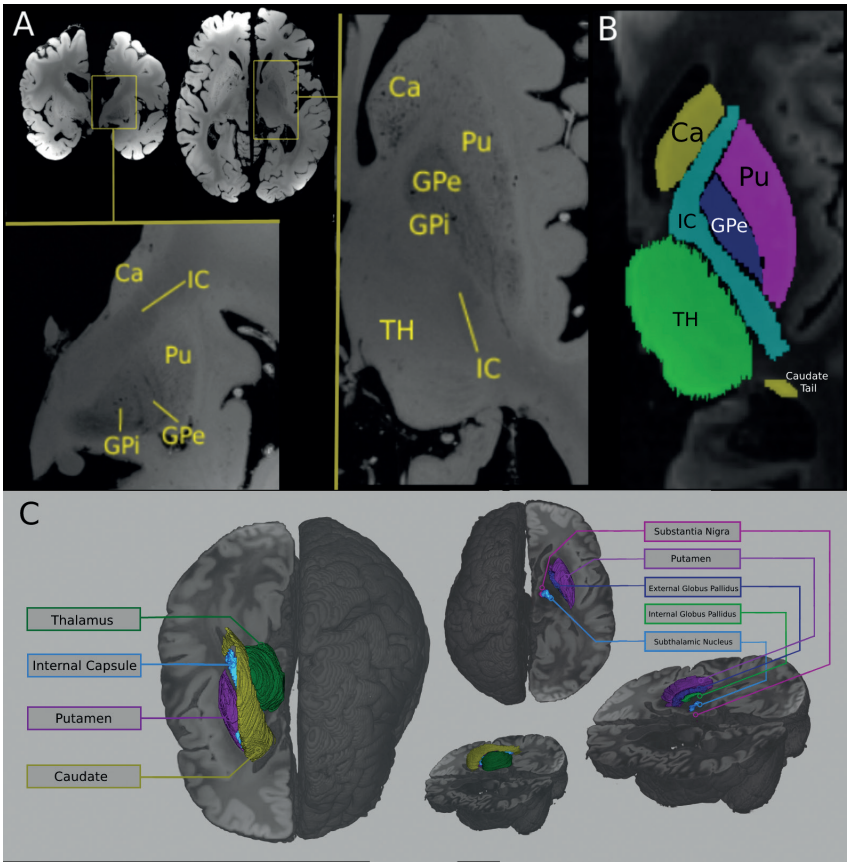

Figure 1. Manually segmented regions of interest. A) GRadient Echo images with windowing and leveling to highlight midbrain regions; CA; caudate, GPe; globus pallidus externa, GPi; globus pallidus interna, IC; internal capsule, Pu; putamen, and TH; thalamus. B) Manually segmented regions-of-interest (ROIs) in a 2D axial plane overlaid on upsampled diffusion-weighted space. C) Segmented ROIs visualized in 3D space.

Region of interest definition

A binary mask of each hemisphere was created from respected GREs using FMRIB's Automated Segmentation Tool (FAST)[44] and manually edited to remove small non-tissue artifacts (*e.g.,* silicone) originating from the container. The mask was used to select all tissue voxels and calculate DTI metrics for whole hemisphere statistics. Quantitative analysis was conducted in native imaging space. The regions of interest (ROIs) mainly within the basal ganglia and brainstem included the red nucleus (RN), putamen (PU), anterior commissure (AC), internal capsule (IC), sublenticular internal capsule (sIC), interthalamic adhesion[45], subthalamic nucleus (STN), substantia nigra [20], globus pallidus interna (GPi), globus pallidus externa (GPe), locus coeruleus (LC), caudate (CA), and thalamus (TH). All ROIs were manually delineated using fsleyes by means of respective high-resolution GRE images in various contrasts and high-resolution probabilistic *in vivo* MRI atlases of the human subcortex[46,47] as anatomical references (Fig. 1).

Response function and fODF estimation

Diffusion data were checked visually in all three orthogonal directions and did not reveal any severe artifacts related to gross geometric alterations, signal dropout, or bulk motion. DWI data were up-sampled from 1.0mm^3 to 0.25mm^3 resolution[48] and then corrected for eddy current- and susceptibility-induced geometric distortions[49] based on GREs. The response function estimation for Constrained Spherical Deconvolution (CSD) was calculated using MRtrix3 utilizing the *Tournier* iterative algorithm for single-fiber voxel selection[50]. Estimation of the fiber distribution was completed using the CSD response function to estimate a voxel-wise white matter fiber Orientation Distribution Function (fODF) (Fig. 2).

DTI & Fiber tracking

DTI parameters including fractional anisotropy (FA), axial diffusivity (AD), radial diffusivity (RD), mean diffusivity (MD/ADC), planar tensor coefficient (Cp), spherical tensor coefficient (Cs), and linear tensor coefficient (CL) of each ROI were obtained[51]. CSD probabilistic fiber tracking with a maximum harmonic order (Imax) of 8 was accomplished with MRtrix3 on each hemisphere per ROI. The protocol to determine optimal parameter values was adjusted from a published methodology[52] that excluded sets resulting in unrealistically long, short, and straight and/or noisy fiber tracks. One hundred thousand randomly selected streamlines seeding from each ROI limited to each hemisphere were generated. ROI fiber counts are the total streamlines intersecting with the ROI as a seed region (Fig. 3).

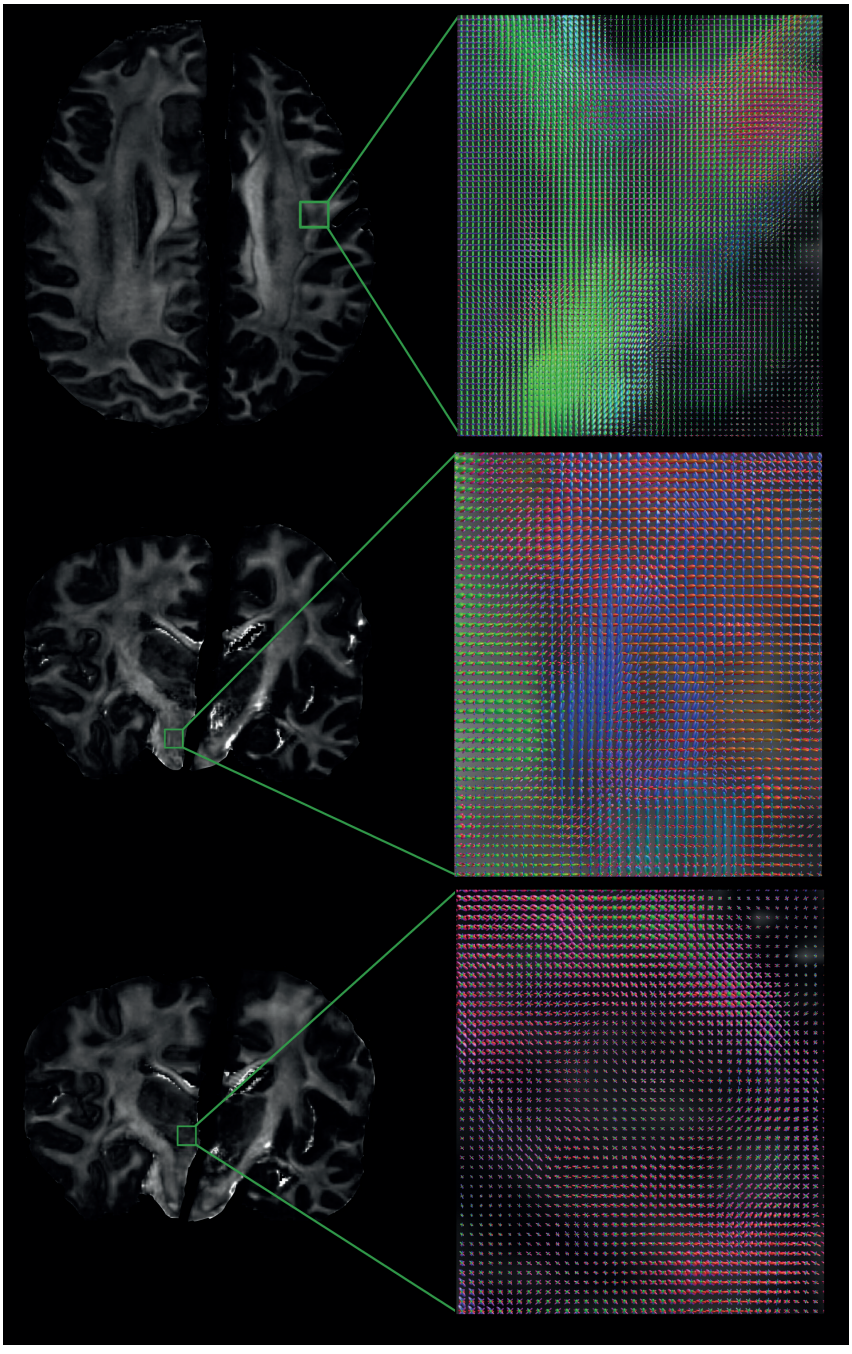

Figure 2. Reconstructed fiber orientation distribution functions (FOD) in three distinct brain regions. The upper panel at an axial plane superior of the corpus callosum showing large angular orientations changing from an anterior-posterior orientation and bending medio-laterally, the middle panel in the pons showing medio-laterally based orientations, and the lower panel showing a complex region in the superior pons mainly aligned anterior-posteriorly.

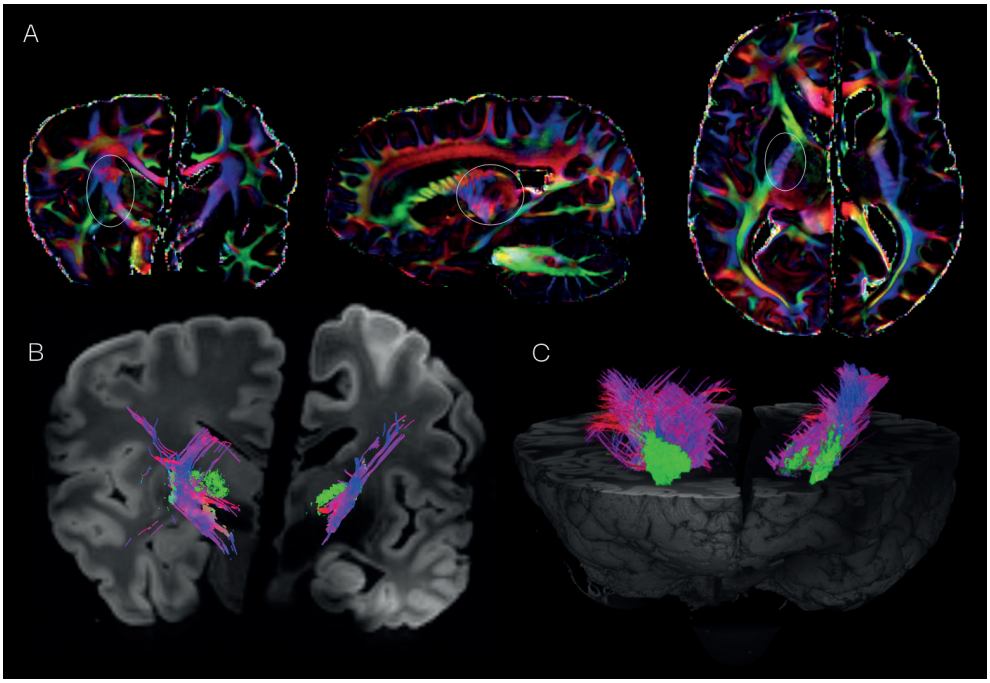

Figure 3. Internal capsule tractography. A) Representative DTI fractional anisotropy (FA) map with the internal capsule circled; fiber directions are color-coded based on main eigenvector (red; left-right, green; anteroposterior, blue; superior-inferior). **B)** Internal capsule (IC) streamline tractography from two hemispheres (one scanning session) obtained using manually delineated IC regions of interest (ROI) as seed voxels. Tractography results are overlaid on an upscaled coronal DWI image. **C)** 3D reconstruction of internal capsule streamline tractography overlaid on axial sliced gradient echo sequence (GRE). All color-coding indicate fiber orientations in the same convention.

Interconnectivity analysis

To investigate connectivity patterns in ROIs, connections were generated by seeding from one region to another using the CSD algorithm in the same way as fiber tracking for the individual ROIs was performed. Connections are bi-directional and do not provide information of directionality. Connectivity outputs were mapped in matrices for visualization mirrored across top left and bottom right; diagonals have zeros as self-loops are excluded (Supplementary Figure 1).

Statistical analysis

All statistical analyses were performed using Rstudio Version 2021.9.1.372 software. Because of small sample sizes and non-normal distributions, nonparametric test were used. Demographics data between groups (nTD, TD, HC) were compared using Kruskal-Wallis H test for continuous variables and Chi-square tests for categorical variables, with statistical significance set to $p < 0.05$. For all DTI metrics (FA, ADC, AD, RD, Cl, Cp, Cs)

mean values from the whole hemispheres were compared between groups using *Rank-based Estimation for Linear Models* (RFit)[53], with age, biological sex, post-mortem interval (PMI), and total hemisphere volume as covariates[54]. Mean values of all diffusion metrics sampled along streamlines that seed from each ROI were computed along with grand means of DTI metrics constrained within the specified binary brain masks. Pair-wise group comparisons were completed for the mean values of each diffusion metric sampled from the streamlines that seed on each ROI using *RFit*, controlling for age, biological sex, PMI, and mean value of the respective diffusion metric. Data and code are openly shared under CC BY-NC-ND license via GitHub (Supplementary material).

Data availability

Raw data were generated at the Department of Cognitive Neuroscience, Maastricht University. Derived data supporting the findings of this study are available from the corresponding author on request.

Results

Whole hemispheric volumes were comparable across groups (Table 3). Whole hemispheric mean FA values showed to be significantly different across groups (HC = 0.19, nTD = 0.17, TD = 0.15, $p = 0.049$). No other diffusion metric showed significant statistical differences across groups at the whole hemisphere level.

Table 3. Hemispheric diffusion metrics.

	nTD	HC	TD	p
N	4	4	4	
Volume	596.05 [549.74, 639.46]	552.88 [506.31, 583.23]	587.64 [568.78, 622.28]	0.437
FA	0.17 [0.16, 0.18]	0.19 [0.18, 0.19]	0.15 [0.14, 0.15]	0.049*
ADC	0.26 [0.25, 0.29]	0.28 [0.27, 0.28]	0.28 [0.27, 0.29]	0.694
AD	0.30 [0.28, 0.33]	0.32 [0.31, 0.32]	0.31 [0.30, 0.32]	0.618
RD	0.24 [0.23, 0.27]	0.26 [0.25, 0.26]	0.26 [0.25, 0.27]	0.735
CL	0.06 [0.06, 0.07]	0.07 [0.07, 0.08]	0.06 [0.06, 0.06]	0.116
CP	0.09 [0.08, 0.09]	0.10 [0.09, 0.10]	0.08 [0.08, 0.09]	0.174
CS	0.84 [0.84, 0.86]	0.83 [0.82, 0.84]	0.85 [0.85, 0.86]	0.118

Note. Volume is denoted in milliliters. Median values & [interquartile ranges] for each diffusion metric is reported. Statistically significant values ($p < 0.05$) are denoted with an asterisk. ADC, AD, and RD are multiplied by a factor 1000 to remove leading zeros. TD; tremor-dominance, nTD; non-tremor dominance, HC; healthy non-demented control. FA; fractional anisotropy, AD; axial diffusivity, ADC; apparent diffusion coefficient, RD; radial diffusivity. Cp; planar tensor coefficient, Cs; spherical tensor coefficient, Cl; linear tensor coefficient.

Region of interest volume and fiber counts

All volumes and fiber counts in each ROI were controlled for age, biological sex, PMI, and hemispheric volume when compared across groups (Supplementary Table 2). TD showed larger putamen volumes (p=0.027) and higher putamen fiber counts (p= 0.027) compared to non-demented controls. Similarly, TD showed larger GPe volumes (p=0.029) and ITA volumes (p=0.037) but lower GPe fiber counts (p=0.029) compared to controls.

Region of interest diffusion metrics

All diffusion metrics in each ROI were also controlled for age, biological sex, PMI, and hemispheric volume when compared across groups (Table 4). TD showed lower AD (p=0.020), ADC (p=0.021), and RD (p=0.010) ITA values compared to HC. TD also showed lower AD (p=0.024) and ADC (p=0.033) values in the thalamus and lower AD (p=0.000) and ADC (p=0.033) values in the locus coeruleus (LC) compared to HC. While TD showed lower FA in the STN (p=0.002) compared to HC, nTD showed lower ADC in the STN (p=0.030) compared to HC. nTD showed significantly higher FA values in the caudate (p=0.030) but lower FA values in the sublenticular internal capsule (p=0.049) (Fig. 4) as well as lower ADC values in the STN (p=0.030) and SN (p=0.041) compared to HC.

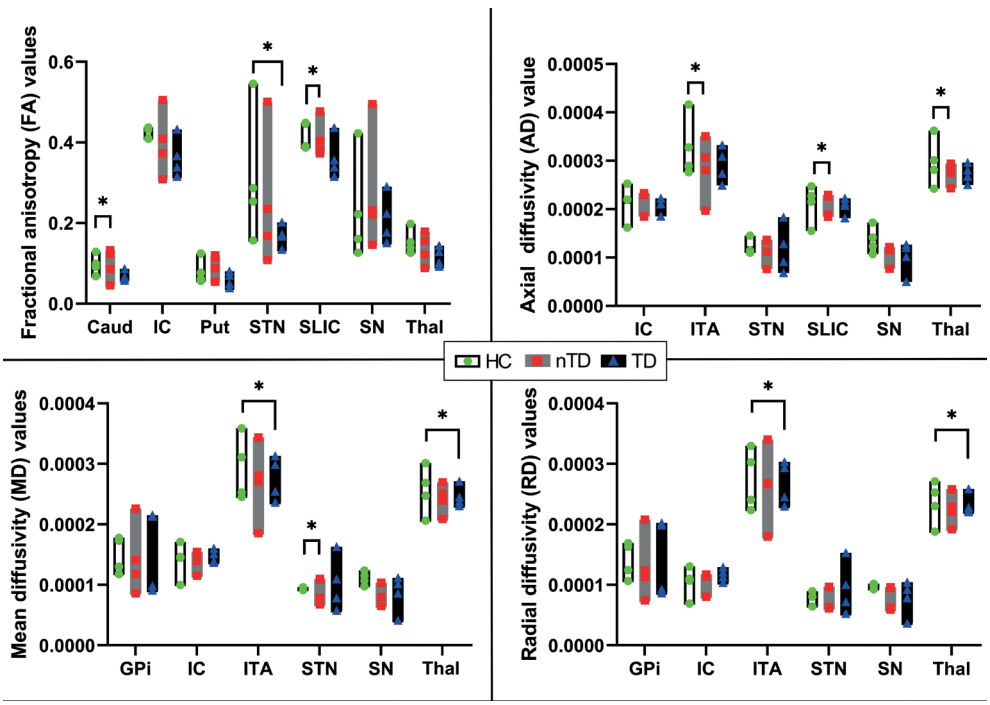

Figure 4. Bar plots illustrating diffusivity and anisotropy data across samples. Healthy non-demented controls (HC, white-green), non-tremor dominant (nTD, gray-red), and tremor-dominant (TD, black-blue). $p < 0.05$. Between group analyses were performed using age, biological sex, PMI, total hemispheric volume, and respective mean diffusion value as covariates. Caud; caudate. GPi; internal globus pallidus. IC; internal capsule. Put; Putamen. SLIC; sublenticular internal capsule. SN; substanta nigra. STN; subthalamic nucleus. Thal; Thalamus.

Table 4. Region of interest diffusion metric variation between groups

	FA			AD			ADC			RD		
Region	nTD-HC	nTD-TD	HC-TD	nTD-HC	nTD-TD	HC-TD	nTD-HC	nTD-TD	HC-TD	nTD-HC	nTD-TD	HC-TD
AC	0.592	0.163	0.601	0.784	0.598	0.947	0.570	0.981	0.951	0.565	0.713	0.952
Caudate	**0.030**↑	0.861	0.609	0.784	0.699	0.265	0.972	0.926	0.123	0.979	0.850	0.106
GPe	0.718	0.861	0.434	0.432	0.154	0.480	0.801	0.615	0.568	0.743	0.644	0.657
GPi	0.434	0.949	0.840	0.645	0.448	0.502	0.598	0.808	0.453	0.587	0.992	0.493
IC	0.127	0.092	0.962	0.137	0.351	0.075	0.232	0.217	0.361	0.303	0.168	0.953
ITA	0.561	0.688	0.784	0.976	0.880	**0.020**↓	0.721	0.767	**0.021**↓	0.722	0.724	**0.010**↓
LC	0.071	0.657	0.958	0.706	0.987	**0.000**↓	0.616	0.318	**0.033**↓	0.224	0.146	0.258
Putamen	0.183	0.240	0.903	0.670	0.876	0.984	0.639	0.662	0.877	0.754	0.652	0.816
RN	0.294	0.607	0.439	0.740	0.639	0.723	0.961	0.774	0.577	0.870	0.701	0.774
STN	0.398	0.637	**0.002**↓	0.050	0.487	0.978	**0.030**↓	0.611	0.341	0.230	0.845	0.356
sIC	**0.049**↓	0.154	0.893	0.167	0.299	**0.043**↓	0.382	0.397	0.090	0.369	0.275	0.630
SN	0.651	0.853	0.362	0.588	0.846	0.346	**0.041**↓	0.622	0.533	0.132	0.894	0.986
Thalamus	0.667	0.992	0.432	0.484	0.738	**0.024**↓	0.794	0.578	**0.033**↓	0.811	0.170	**0.005**↓

Note. P-values of non-parametric tests between groups. Statistically significant values ($p < 0.05$) are signified in bold. Arrows denote motor subtypes having lower ↓ or higher ↑ diffusion values compared to non-demented controls. Motor subtypes did not significantly differ from each other in regional diffusion metrics. FA; fractional anisotropy, AD; axial diffusivity, ADC; apparent diffusion coefficient, RD; radial diffusivity. RN; red nucleus, AC; anterior commissure, GPe; globus pallidus externa, GPi; globus pallidus interna, IC; internal capsule, ITA; interthalamic adhesion, LC; locus coeruleus, STN; subthalamic nucleus, sIC; sublenticular internal capsule, SN; substantia nigra.

When compared, nTD and TD patients' ROIs did not differ across any diffusion metric (Table 4). Cs, Cl, and Cp diffusion values did not differ between groups in any ROI (Supplementary Table 4-6).

Tractography connectivity metrics

Consistent across all samples were nine white matter fiber connections; 1) The caudate connected to the thalamus (Fig. 5C), internal capsule (Fig. 5A), and sublenticular internal capsule (Fig. 5E) The internal capsule connected to the thalamus (Fig. 5D), globus pallidus externa (Fig. 5B), putamen (Fig. 5G), and to its sublenticular section (Fig. 5F), and 3) The sublenticular internal capsule to the putamen (Fig. 5J) and thalamus (Fig. 5I). Results based on non-parametric tests including age, biological sex, PMI, and ROI volume as confounders show nTD had a lower number of streamlines between the Caudate ↔ Internal Capsule (p=0.038) compared to TD, and a significantly higher number of streamlines connecting the Internal Capsule ↔ Putamen (p=0.041), Internal Capsule ↔ Thalamus (p=0.012), and Sublenticular Internal Capsule ↔ Thalamus (p=0.019) compared to HC.

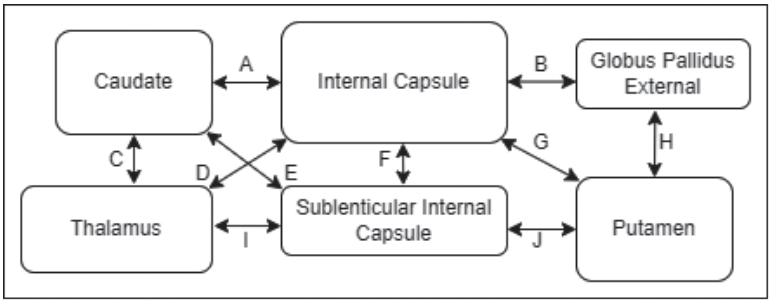

Figure 5. Consistent white matter fiber connections across samples. nTD had a lower number of streamlines in *A* and a higher number of streamlines in *G*, *E*, and *I* compared to HC.

Fractional anisotropy in white matter connections

Subsequent results are based on non-parametric tests with age, biological sex, PMI, and corresponding mean diffusion value per hemisphere as confounders (Supplementary Table 7). TD showed to have higher FA in the Caudate ↔ Thalamus connection compared to both nTD and HC (p=0.004, p=0.006, respectively). The nTD group had significantly higher FA connecting the Internal Capsule ↔ Thalamus compared to both TD and HC (p>0.001, p=0.012), and higher FA connecting the Sublenticular Internal Capsule ↔ Thalamus compared to both TD and HC (p>0.001, p=0.005), while TD had significantly lower FA in these connections (p>0.001). The Putamen ↔ Sublenticular Internal Capsule connection shows higher FA in nTD compared to HC (p=0.023).

Axial-, radial-, and apparent diffusion coefficient connectivity

TD showed lower AD in the Caudate ↔ Internal Capsule (p=0.046) streamlines and Caudate ↔ Sublenticular Internal Capsule (p=0.035) streamlines compared to HC. TD had lower ADC in the Caudate ↔ Internal Capsule (p=0.048) and Internal Capsule ↔ Putamen (p=0.033) connection compared to HC. TD showed lower RD in the Caudate ↔ Sublenticular Internal Capsule (p=0.028) and Putamen ↔ Sublenticular Internal Capsule (p=0.023) connections compared to HC.

Linear shape connectivity

Results show connections between groups have no significant differences in Cl. Notwithstanding this, Cp was lower for TD in the Caudate ↔ Thalamus connection compared to HC and nTD (p=0.005, p=0.001, respectively), and when compared to HC and nTD, TD showed higher Cs in the Caudate ↔ Thalamus (p=0.007, p=0.002), Internal Capsule ↔ Thalamus (p=0.011, p=0.028) and Sublenticular Internal Capsule ↔ Thalamus connections (p=0.016, p=0.045). nTD additionally had lower Cs in the Putamen ↔ Sublenticular Internal Capsule connection (p=0.019) compared to HC.

Discussion

After controlling for age, biological sex, PMI, and hemispheric volume, tremor-dominant (TD) samples showed larger putamen volumes and higher putamen fiber counts compared to non-demented controls as well as larger GPe volumes. Although previous research has found small but significant reductions in caudate and putamen volume, independent of age and biological sex, occurring in PD brains, such volumetrics were not correlated with motor or cognitive decline.[55] Post-mortem studies have also shown dendritic spine density reductions and medium spiny neuron dendritic length shortenings within the striatum[56], as well as direct loss of striatal cells occurring in PD[57] which could contribute to striatal volume reductions and influence cortical projection functionality, although whether such pathologies occur as a direct result of PD dopaminergic cell loss remains unknown.[55] While a negative association between putamen volume and H&Y stage (*i.e.,* Hoehn and Yahr scale, a system for describing PD symptom progression) has been previously shown[58], H&Y stages correlating with age serves as a methodological limitation, as non-diseased brains atrophy around 0.5% of their volume per year[59] and nigra-striatal neuron loss is approximately 60% by the time of PD symptom onset[60], therefore, small magnitudes of striatal volume variation is challenging to separate from normal aging and PD dopaminergic cell loss.

Compared to both non-tremor dominant (nTD) samples and non-demented controls, TD samples displayed greater hemispheric fractional anisotropy (FA). FA is sensitive

to a broad spectrum of pathological conditions but generally deduces microstructural integrity, indicates nerve fiber arrangements, axonal degeneration and the extent of axonal myelination, and commonly decreases from a loss of coherence in the principle diffusion direction.[61] Decreases in FA and increases in mean diffusivity have also shown to correlate with neuronal degeneration[62] and degeneration from dopamine loss.[63] A previous *in-vivo* study using the Parkinson's Progression Markers Initiative (PPMI) dataset found FA to be increased in TD but not in the postural instability and gait difficulty (PIGD. i.e., nTD) subtype, similar to our results, and suggested this was from compensatory white matter reorganization specific to TD.[23] An earlier study was in disagreement to this, showing increased whole-brain FA in only the akinetic-rigid (AR, i.e., nTD) phenotype.[64] Notably, their study included *de novo* drug naïve patients diagnosed with PD as compared to our current study where patients were at a disease endpoint. Divergences associated with global FA regression across specific PD motor subtypes are then difficult to reconcile without longitudinal data.[65]

Mean diffusivity (MD, i.e., mean apparent diffusion coefficient (ADC)) has generally shown to be higher in damaged tissues as a result of increased free water movement.[66] In previous *in-vivo* studies, TD have shown increased MD in the thalamus compared to nTD[67] and in the cerebello-thalamo-cortical (CTC) pathway[21], while nTD showed increased MD in the left and right substantia nigra and bilateral globus pallidus that correlated with disease stage and motor severity[19] as well as increased MD in the putamen.[68] Another study showed no differences in histogram-derived MD metrics between TD and nTD.[64] In this current study, no differences in MD were seen between TD and nTD on a whole hemispheric level nor within individual regions of interest. These results could be explained by the aforementioned compensatory white matter reorganization specific to TD[23] as neural reorganization is speculated to compensate PD pathology and dopamine deficits within TD. Similarity, AD is sensitive to axonal pathologies and decreases in axonal injury while RD has shown to increase in white matter with demyelination.[69] In this study, TD showed both lower AD and lower RD in internal capsule streamlines that could indicate either selective neurodegeneration or a mixed compensatory neuronal reorganization of this white matter macrostructure. Prior post-mortem studies showed TD having less cell loss in multiple neuronal systems compared to nTD[70,71] while a clinical study also showed specific increased pallidal gray matter volumes in TD compared to healthy controls[72] both of which support such cerebral compensation and white matter enhancement, and alongside the greater degenerative metrics seen in nTD, elucidate anatomical support for TD patients having a more benign course of disease progression.[23,73] Although the concept of neural compensation and plasticity in PD is relatively young and not well recognized, as previous studies towards the characterization of microstructural compensation could be reporting incidental findings or post hoc interpretations[74], such biomarkers can still be operationalized and improve understandings of PD circuitopathies that underpin symptomology.

Previous research has shown nTD patients have striato-thalamo-cortical (STC) circuitry and other thalamocortical projection deficits related to cognitive and sensorimotor function, while TD patients have greater cerebello-thalamo-cortical (CTC) circuitry dysfunctions.[17] Effective connectivity and clinical intervention studies further suggest tremor may result from a pathological interaction between basal ganglia and the cerebellothalamic circuitry[75] arising in the internal globus pallidus and being propagated to the CTC circuit via the motor cortex.[76] These studies are in line with the "*dimmer-switch model*" of PD resting tremor where pathological activity in the STC from dopaminergic denervation of the GP triggers tremor-related responses in the CTC while the BG act as a light switch triggering tremors on and off and the CTC modulates tremor intensity similar to a light dimmer.[73,75] Studies have demonstrated benefits in tremor from deep brain stimulation (DBS) of posterior subthalamic areas, primarily the subthalamic nucleus (STN) and the zona incerta.[77] From this, the efficacy of thalamotomy and DBS for the treatment of tremors has traditionally focused on the CTC network for its multifaceted involvement in tremor genesis.[73,78,79] Our results related to internal capsule streamlines are then of particular interest, as the internal capsule is part of the corticospinal tract and contains large concentrations of motor and sensory fibers that project to and from various cortical areas in a vertical manner.[80] The anterior limb of the internal capsule contains fibers running from the thalamus to the frontal lobe as well as thalami pontine fibers.[81] Two pivotal nuclei involved in PD, the substantia nigra pars reticulata (SNpr) and the internal globus pallidus (GPi), are further separated by internal capsule white matter.[45] While higher FA values have previously been shown in the anterior limb of the internal capsule in PD when compared to healthy controls[82], in this current study nTD similarly showed higher FA in internal capsule-thalamus streamlines compared to both TD and controls indicating circuitopathy specific to motor subtype. Furthermore, TD showed lower AD in internal capsule-caudate streamlines and lower RD in sublenticular internal capsule-caudate and sublenticular internal capsule-putamen streamlines compared to controls possibly indicating axonal damage specific to the TD subtype.[83]

In general, TD patients show an improved response towards DBS whereas those with axial subtypes and gait problems benefit less favorably.[84-86] Differences in DBS outcomes have been shown to relate to connectivity alterations between motor subtypes within tremor and non-tremor circuits.[87-91] Patient-specific dissections of DBS targets facilitate individualized surgical planning[92] while overlapping DBS target locations and their cortical connectivity patterns have been associated with various improvements in tremor, rigidity, and bradykinesia.[93] Previous findings further suggest Parkinson's disease patients benefit more from stimulation settings that balance effects of multiple symptoms and side effects[94] while DBS in the dorsal or ventral regions of the internal capsule has shown to both improve and worsen mood through limbic-motor networks via capsular connections interfacing with multiple striatal regions.[95] Therefore, a more refined understanding of

motor subtype specific circuitopathies may help create predictors for DBS efficacy; several variations specific to PD motor subtypes found in this study could thus be quantifiable *in vivo* with clinical MR sequences and hold translational value in detecting a *fingerprint* of specific circuitopathy underlying motor subtype degeneration. This fingerprint would encompass integrated anatomical, functional, and network influences to generate more specified circuitopathy models for personalized information-based neurostimulation.[96] Correspondingly, localizing neuromodulatory effects mediated by the internal capsule in non-motor basal ganglia loops is therapeutically beneficial to DBS clinical planning.[97,98] We therefore hope future clinical DBS tractography studies will further elaborate on the role capsular fibers play during patient target selection and network analysis.

High-field MRI holds further potential in improving DBS targeting and surgical planning[99] as high-resolution tractography moves to become sensitive enough to measure neuronal network abnormalities that can engender personalized psychiatry and disease treatments.[100] Moreover, post-mortem MRI imaging (in further combination with microscopy) works to bring anatomical ground truth to the neuroimaging field with unbridled spatial resolution and contrast.[101] As the level of anatomical detail granted by both *ex vivo* and *in vivo* imaging will continue to improve in concert, it will allow for *in vivo* scan resolutions of subcortical nuclei and small fiber bundles at the individual level to potentially approach the level of ex vivo[101] further facilitating patient-specific DBS targeting methodologies.

Strengths and limitations

Our study is not without limitations innate to post-mortem neuroimaging regimes, principally involving cohorts being donors at the furthest stages of aging and disease, as well as processes of autolysis and tissue fixation affecting several neuroimaging markers.[11,102,103] Therefore, disparities between our e*x vivo* results to that of previous *in vivo* diffusion data could be contributed to the post-mortem nature of our study; our samples were kept in fixative for four/five years prior to being scanned causing principle diffusion characteristics of the tissue to shift.[11,104] Still, while many *ex vivo* imaging studies attribute small sample sizes to be a limitation in regards to statistical power, as a strength, this study has a comparatively larger post-mortem sample sizes (n=12) than previous *ex vivo* studies. Furthermore, our imaging was performed on a 9.4T MRI system, which are of limited availability, and utilized a dedicated bespoke RF-coil and post-mortem diffusion-imaging pipeline.[10]

Translational capabilities could theoretically improve from a more refined parcellation scheme, as regions of interest were manually delineated in native image space to ensure accuracy and avoid effects of potential misalignment to MRI atlases. Nevertheless, a more standardized and automatic approach to nuclei delineations may prove more scalable

within clinical practice, even though *ex vivo* scans registered to MNI-space are subject to similar registration limitations that are present *in vivo*.[101] Similarly, greater intranuclear divisions of the thalamus could be obtained utilizing this methodology with a more refined and focused field of view. The stability of all motor and nonmotor subtypes of PD should be taken under further consideration as PD patients have shown shift from one subtype to another as the disease progresses.[105,106] Moving forward, greater translational and reverse translational investigations involving *in vivo* neuroimaging regimes in combination with subsequent *ex vivo* imaging and histological analysis are needed to validate findings and parcellate potential distortions each imaging paradigm possess.

Conclusion

This study supports ultra-high field magnetic resonance imaging of large post-mortem tissue samples being efficacious for reconstructing assorted anatomical defects between Parkinson's disease motor subtypes and healthy non-demented controls. Previous studies investigating PD subtypes mainly employed lower field strengths (1.5-3T) *in vivo* while here we utilized 9.4T *ex vivo* imaging granting better resolution and allowing us to measure diffusion related discrepancies with refined spatial detail. The ability to map specific white matter circuitopathies underlying PD motor symptomology is imperative to enhance multimodal biomarkers assessing diverse PD trajectories. Our findings imply fundamental differences in neural mechanisms between motor subtypes in the latest stages of PD and support subtypes undergoing varied therapeutic approaches given their diverse etiologies. Our results further support the notion that TD patients may show less negative alternations compared to nTD through neural reorganization. Based on our findings the internal capsule acts as a crossroads in networks involved in tremor symptoms while its diffusion variations may be a key pattern in the *fingerprint* of anatomical circuitopathy distinguishing PD motor subtypes. Continued translational research involving clinical studies, *in vivo* and *ex vivo* neuroimaging, and histology will expand the ability to principally track, trace, target, and treat Parkinson's disease.

Acknowledgements: The authors would like to thank Stichting Beheer Vermogen De Weijerhorst for their funding and Ashly Pineda for her contribution during the feasibility analysis.
Funding: This work was funded by a Stichting Beheer Vermogen De Weijerhorst research grant to YT and AJ.

References

1. He, N., P. Huang, H. Ling, et al., *Dentate nucleus iron deposition is a potential biomarker for tremor-dominant Parkinson's disease.* NMR Biomed, 2017. **30**(4).
2. Rajput, A.H., A. Voll, M.L. Rajput, C.A. Robinson, and A. Rajput, *Course in Parkinson disease subtypes: A 39-year clinicopathologic study.* Neurology, 2009. **73**(3): p. 206-12.
3. van Rooden, S.M., W.J. Heiser, J.N. Kok, et al., *The identification of Parkinson's disease subtypes using cluster analysis: a systematic review.* Mov Disord, 2010. **25**(8): p. 969-78.
4. Zaidel, A., D. Arkadir, Z. Israel, and H. Bergman, *Akineto-rigid vs. tremor syndromes in Parkinsonism.* Curr Opin Neurol, 2009. **22**(4): p. 387-93.
5. Wu, Y., Y.W. Yang, S.C. Gu, et al., *The Importance of Early Identification for Parkinson's Disease Patients with Postural Instability and Gait Disturbance.* Comput Intell Neurosci, 2022. **2022**: p. 6701519.
6. Temel, Y., A. Blokland, H.W. Steinbusch, and V. Visser-Vandewalle, *The functional role of the subthalamic nucleus in cognitive and limbic circuits.* Prog Neurobiol, 2005. **76**(6): p. 393-413.
7. Forstmann, B.U., B.R. Isaacs, and Y. Temel, *Ultra High Field MRI-Guided Deep Brain Stimulation.* Trends Biotechnol, 2017. **35**(10): p. 904-907.
8. Lehericy, S., D.E. Vaillancourt, K. Seppi, et al., *The role of high-field magnetic resonance imaging in parkinsonian disorders: Pushing the boundaries forward.* Mov Disord, 2017. **32**(4): p. 510-525.
9. Wolters, A.F., M. Heijmans, S. Michielse, et al., *The TRACK-PD study: protocol of a longitudinal ultra-high field imaging study in Parkinson's disease.* BMC Neurol, 2020. **20**(1): p. 292.
10. Fritz, F.J., S. Sengupta, R.L. Harms, et al., *Ultra-high resolution and multi-shell diffusion MRI of intact ex vivo human brains using kT-dSTEAM at 9.4T.* Neuroimage, 2019. **202**: p. 116087.
11. Roebroeck, A., K.L. Miller, and M. Aggarwal, *Ex vivo diffusion MRI of the human brain: Technical challenges and recent advances.* NMR Biomed, 2019. **32**(4): p. e3941.
12. Miller, K.L., J.A. McNab, S. Jbabdi, and G. Douaud, *Diffusion tractography of post-mortem human brains: optimization and comparison of spin echo and steady-state free precession techniques.* Neuroimage, 2012. **59**(3): p. 2284-97.
13. Miller, K.L., C.J. Stagg, G. Douaud, et al., *Diffusion imaging of whole, post-mortem human brains on a clinical MRI scanner.* Neuroimage, 2011. **57**(1): p. 167-181.
14. Plantinga, B.R., Y. Temel, A. Roebroeck, et al., *Ultra-high field magnetic resonance imaging of the basal ganglia and related structures.* Front Hum Neurosci, 2014. **8**: p. 876.
15. Meijer, F.J. and B. Goraj, *Brain MRI in Parkinson's disease.* Front Biosci (Elite Ed), 2014. **6**(2): p. 360-9.
16. Jonkman, L.E., B. Kenkhuis, J.J.G. Geurts, and W.D.J. van de Berg, *Post-Mortem MRI and Histopathology in Neurologic Disease: A Translational Approach.* Neurosci Bull, 2019. **35**(2): p. 229-243.
17. Boonstra, J.T., S. Michielse, Y. Temel, G. Hoogland, and A. Jahanshahi, *Neuroimaging Detectable Differences between Parkinson's Disease Motor Subtypes: A Systematic Review.* Mov Disord Clin Pract, 2021. **8**(2): p. 175-192.
18. Winklewski, P.J., A. Sabisz, P. Naumczyk, et al., *Understanding the Physiopathology Behind Axial and Radial Diffusivity Changes-What Do We Know?* Front Neurol, 2018. **9**: p. 92.
19. Nagae, L.M., J.M. Honce, J. Tanabe, et al., *Microstructural Changes within the Basal Ganglia Differ between Parkinson Disease Subtypes.* Front Neuroanat, 2016. **10**: p. 17.
20. Boutet, A., I. Hancu, U. Saha, et al., *3-Tesla MRI of deep brain stimulation patients: safety assessment of coils and pulse sequences.* J Neurosurg, 2019. **132**(2): p. 586-594.
21. Luo, C., W. Song, Q. Chen, et al., *White matter microstructure damage in tremor-dominant Parkinson's disease patients.* Neuroradiology, 2017. **59**(7): p. 691-698.
22. Vervoort, G., I. Leunissen, M. Firbank, et al., *Structural Brain Alterations in Motor Subtypes of Parkinson's Disease: Evidence from Probabilistic Tractography and Shape Analysis.* PLoS One, 2016. **11**(6): p. e0157743.

23. Wen, M.C., H.S.E. Heng, Z. Lu, et al., *Differential White Matter Regional Alterations in Motor Subtypes of Early Drug-Naive Parkinson's Disease Patients.* Neurorehabil Neural Repair, 2018. **32**(2): p. 129-141.
24. Barbagallo, G., M.E. Caligiuri, G. Arabia, et al., *Structural connectivity differences in motor network between tremor-dominant and nontremor Parkinson's disease.* Hum Brain Mapp, 2017. **38**(9): p. 4716-4729.
25. Zeng, Q., X. Guan, T. Guo, et al., *The Ventral Intermediate Nucleus Differently Modulates Subtype-Related Networks in Parkinson's Disease.* Front Neurosci, 2019. **13**: p. 202.
26. Park, J., K.M. Park, G. Jo, et al., *An investigation of thalamic nuclei volumes and the intrinsic thalamic structural network based on motor subtype in drug naive patients with Parkinson's disease.* Parkinsonism Relat Disord, 2020. **81**: p. 165-172.
27. Tournier, J.D., S. Mori, and A. Leemans, *Diffusion tensor imaging and beyond.* Magn Reson Med, 2011. **65**(6): p. 1532-56.
28. Behrens, T.E., H.J. Berg, S. Jbabdi, M.F. Rushworth, and M.W. Woolrich, *Probabilistic diffusion tractography with multiple fibre orientations: What can we gain?* Neuroimage, 2007. **34**(1): p. 144-55.
29. Grazioplene, R.G., C.E. Bearden, K.L. Subotnik, et al., *Connectivity-enhanced diffusion analysis reveals white matter density disruptions in first episode and chronic schizophrenia.* Neuroimage Clin, 2018. **18**: p. 608-616.
30. Jeurissen, B., A. Leemans, J.D. Tournier, D.K. Jones, and J. Sijbers, *Investigating the prevalence of complex fiber configurations in white matter tissue with diffusion magnetic resonance imaging.* Hum Brain Mapp, 2013. **34**(11): p. 2747-66.
31. Wilkins, B., N. Lee, N. Gajawelli, M. Law, and N. Lepore, *Fiber estimation and tractography in diffusion MRI: development of simulated brain images and comparison of multi-fiber analysis methods at clinical b-values.* Neuroimage, 2015. **109**: p. 341-56.
32. Burdette, J.H., D.D. Durden, A.D. Elster, and Y.F. Yen, *High b-value diffusion-weighted MRI of normal brain.* J Comput Assist Tomogr, 2001. **25**(4): p. 515-9.
33. Kamagata, K., A. Zalesky, T. Hatano, et al., *Connectome analysis with diffusion MRI in idiopathic Parkinson's disease: Evaluation using multi-shell, multi-tissue, constrained spherical deconvolution.* Neuroimage Clin, 2018. **17**: p. 518-529.
34. A. Roebroeck, S. Sengupta, M. Bastiani, et al., *High resolution MRI neuroanatomy of the whole human brain post mortem with a specialized 9.4T RF-coil*, in *Annual Meeting of the Organization for Human Brain Mapping*. 2015: Honolulu.
35. Kirrane, E.F., C. Bowman, J.A. Davis, et al., *Associations of Ozone and PM2.5 Concentrations With Parkinson's Disease Among Participants in the Agricultural Health Study.* J Occup Environ Med, 2015. **57**(5): p. 509-17.
36. Boonstra, J.T., S. Michielse, A. Roebroeck, Y. Temel, and A. Jahanshahi, *Dedicated container for postmortem human brain ultra-high field magnetic resonance imaging.* Neuroimage, 2021. **235**: p. 118010.
37. Cusack, R. and N. Papadakis, *New robust 3-D phase unwrapping algorithms: application to magnetic field mapping and undistorting echoplanar images.* Neuroimage, 2002. **16**(3 Pt 1): p. 754-64.
38. Nehrke, K. and P. Bornert, *DREAM--a novel approach for robust, ultrafast, multislice B(1) mapping.* Magn Reson Med, 2012. **68**(5): p. 1517-26.
39. Tse, D.H., C.J. Wiggins, D. Ivanov, et al., *Volumetric imaging with homogenised excitation and static field at 9.4 T.* MAGMA, 2016. **29**(3): p. 333-45.
40. Greve, D.N. and B. Fischl, *Accurate and robust brain image alignment using boundary-based registration.* Neuroimage, 2009. **48**(1): p. 63-72.
41. Virtanen, P., R. Gommers, T.E. Oliphant, et al., *SciPy 1.0: fundamental algorithms for scientific computing in Python.* Nat Methods, 2020. **17**(3): p. 261-272.
42. Harris, C.R., K.J. Millman, S.J. van der Walt, et al., *Array programming with NumPy.* Nature, 2020. **585**(7825): p. 357-362.
43. Uecker, M., F. Ong, J. Tamir, et al., *BART Toolbox for Computational Magnetic Resonance Imaging.* Annual Meeting International Society for Magnetic Resonance in Medicine, 2015(23): p. 2486.

44. Zhang, Y., M. Brady, and S. Smith, *Segmentation of brain MR images through a hidden Markov random field model and the expectation-maximization algorithm.* IEEE Trans Med Imaging, 2001. **20**(1): p. 45-57.
45. H. Kita and D. Jaeger, *Organization of the Globus Pallidus*, in *Handbook of Behavioral Neuroscience*. 2016. p. 259-276.
46. Alkemade, A., M.J. Mulder, J.M. Groot, et al., *The Amsterdam Ultra-high field adult lifespan database (AHEAD): A freely available multimodal 7 Tesla submillimeter magnetic resonance imaging database.* Neuroimage, 2020. **221**: p. 117200.
47. Pauli, W.M., A.N. Nili, and J.M. Tyszka, *A high-resolution probabilistic in vivo atlas of human subcortical brain nuclei.* Sci Data, 2018. **5**: p. 180063.
48. Dyrby, T.B., H. Lundell, M.W. Burke, et al., *Interpolation of diffusion weighted imaging datasets.* Neuroimage, 2014. **103**: p. 202-213.
49. Andersson, J.L.R. and S.N. Sotiropoulos, *An integrated approach to correction for off-resonance effects and subject movement in diffusion MR imaging.* Neuroimage, 2016. **125**: p. 1063-1078.
50. Tournier, J.D., F. Calamante, and A. Connelly, *Determination of the appropriate b value and number of gradient directions for high-angular-resolution diffusion-weighted imaging.* NMR Biomed, 2013. **26**(12): p. 1775-86.
51. Westin, C.F., S.E. Maier, H. Mamata, et al., *Processing and visualization for diffusion tensor MRI.* Med Image Anal, 2002. **6**(2): p. 93-108.
52. Plantinga, B.R., A. Roebroeck, V.G. Kemper, et al., *Ultra-High Field MRI Post Mortem Structural Connectivity of the Human Subthalamic Nucleus, Substantia Nigra, and Globus Pallidus.* Front Neuroanat, 2016. **10**: p. 66.
53. Kloke, J. and J. McKean, *Rfit: Rank-based Estimation for Linear Models.* The R Journal, 2012. **4**(2): p. 57--64.
54. Simuni, T., C. Caspell-Garcia, C. Coffey, et al., *How stable are Parkinson's disease subtypes in de novo patients: Analysis of the PPMI cohort?* Parkinsonism Relat Disord, 2016. **28**: p. 62-7.
55. Pitcher, T.L., T.R. Melzer, M.R. Macaskill, et al., *Reduced striatal volumes in Parkinson's disease: a magnetic resonance imaging study.* Transl Neurodegener, 2012. **1**(1): p. 17.
56. Stephens, B., A.J. Mueller, A.F. Shering, et al., *Evidence of a breakdown of corticostriatal connections in Parkinson's disease.* Neuroscience, 2005. **132**(3): p. 741-54.
57. Bugiani, O., F. Perdelli, S. Salvarani, A. Leonardi, and G.L. Mancardi, *Loss of striatal neurons in Parkinson's disease: a cytometric study.* Eur Neurol, 1980. **19**(5): p. 339-44.
58. Geng, D.Y., Y.X. Li, and C.S. Zee, *Magnetic resonance imaging-based volumetric analysis of basal ganglia nuclei and substantia nigra in patients with Parkinson's disease.* Neurosurgery, 2006. **58**(2): p. 256-62; discussion 256-62.
59. Sluimer, J.D., W.M. van der Flier, G.B. Karas, et al., *Whole-brain atrophy rate and cognitive decline: longitudinal MR study of memory clinic patients.* Radiology, 2008. **248**(2): p. 590-8.
60. Fearnley, J.M. and A.J. Lees, *Ageing and Parkinson's disease: substantia nigra regional selectivity.* Brain, 1991. **114 (Pt 5)**: p. 2283-301.
61. Basser, P.J. and D.K. Jones, *Diffusion-tensor MRI: theory, experimental design and data analysis - a technical review.* NMR Biomed, 2002. **15**(7-8): p. 456-67.
62. Thomalla, G., V. Glauche, M.A. Koch, et al., *Diffusion tensor imaging detects early Wallerian degeneration of the pyramidal tract after ischemic stroke.* Neuroimage, 2004. **22**(4): p. 1767-74.
63. Boska, M.D., K.M. Hasan, D. Kibuule, et al., *Quantitative diffusion tensor imaging detects dopaminergic neuronal degeneration in a murine model of Parkinson's disease.* Neurobiol Dis, 2007. **26**(3): p. 590-6.
64. Tessa, C., M. Giannelli, R. Della Nave, et al., *A whole-brain analysis in de novo Parkinson disease.* AJNR Am J Neuroradiol, 2008. **29**(4): p. 674-80.
65. Alexander, G.E., *Biology of Parkinson's disease: pathogenesis and pathophysiology of a multisystem neurodegenerative disorder.* Dialogues Clin Neurosci, 2004. **6**(3): p. 259-80.

66. Narr, K.L., N. Hageman, R.P. Woods, et al., *Mean diffusivity: a biomarker for CSF-related disease and genetic liability effects in schizophrenia.* Psychiatry Res, 2009. **171**(1): p. 20-32.

67. Lenfeldt, N., W. Hansson, A. Larsson, et al., *Diffusion tensor imaging and correlations to Parkinson rating scales.* J Neurol, 2013. **260**(11): p. 2823-30.

68. Surova, Y., B. Lampinen, M. Nilsson, et al., *Alterations of Diffusion Kurtosis and Neurite Density Measures in Deep Grey Matter and White Matter in Parkinson's Disease.* PLoS One, 2016. **11**(6): p. e0157755.

69. Alexander, A.L., J.E. Lee, M. Lazar, and A.S. Field, *Diffusion tensor imaging of the brain.* Neurotherapeutics, 2007. **4**(3): p. 316-29.

70. Jellinger, K.A., *Post mortem studies in Parkinson's disease--is it possible to detect brain areas for specific symptoms?* J Neural Transm Suppl, 1999. **56**: p. 1-29.

71. Paulus, W. and K. Jellinger, *The neuropathologic basis of different clinical subgroups of Parkinson's disease.* J Neuropathol Exp Neurol, 1991. **50**(6): p. 743-55.

72. Rosenberg-Katz, K., T. Herman, Y. Jacob, et al., *Subcortical Volumes Differ in Parkinson's Disease Motor Subtypes: New Insights into the Pathophysiology of Disparate Symptoms.* Front Hum Neurosci, 2016. **10**: p. 356.

73. Helmich, R.C., M. Hallett, G. Deuschl, I. Toni, and B.R. Bloem, *Cerebral causes and consequences of parkinsonian resting tremor: a tale of two circuits?* Brain, 2012. **135**(Pt 11): p. 3206-26.

74. Sanjari Moghaddam, H., M. Dolatshahi, F. Mohebi, and M.H. Aarabi, *Structural white matter alterations as compensatory mechanisms in Parkinson's disease: A systematic review of diffusion tensor imaging studies.* J Neurosci Res, 2020. **98**(7): p. 1398-1416.

75. Helmich, R.C., M.J. Janssen, W.J. Oyen, B.R. Bloem, and I. Toni, *Pallidal dysfunction drives a cerebellothalamic circuit into Parkinson tremor.* Ann Neurol, 2011. **69**(2): p. 269-81.

76. Dirkx, M.F., H. den Ouden, E. Aarts, et al., *The Cerebral Network of Parkinson's Tremor: An Effective Connectivity fMRI Study.* J Neurosci, 2016. **36**(19): p. 5362-72.

77. Krack, P., P. Pollak, P. Limousin, A. Benazzouz, and A.L. Benabid, *Stimulation of subthalamic nucleus alleviates tremor in Parkinson's disease.* Lancet, 1997. **350**(9092): p. 1675.

78. Lyons, K.E. and R. Pahwa, *Deep brain stimulation and tremor.* Neurotherapeutics, 2008. **5**(2): p. 331-8.

79. Benabid, A.L., P. Pollak, C. Gervason, et al., *Long-term suppression of tremor by chronic stimulation of the ventral intermediate thalamic nucleus.* Lancet, 1991. **337**(8738): p. 403-6.

80. Ghazi Sherbaf, F., M. Mojtahed Zadeh, M. Haghshomar, and M.H. Aarabi, *Posterior limb of the internal capsule predicts poor quality of life in patients with Parkinson's disease: connectometry approach.* Acta Neurol Belg, 2019. **119**(1): p. 95-100.

81. Mikula, S., I. Trotts, J.M. Stone, and E.G. Jones, *Internet-enabled high-resolution brain mapping and virtual microscopy.* Neuroimage, 2007. **35**(1): p. 9-15.

82. Shen, T., Y. Yue, S. Zhao, et al., *The role of brain perivascular space burden in early-stage Parkinson's disease.* NPJ Parkinsons Dis, 2021. **7**(1): p. 12.

83. Wheeler-Kingshott, C.A. and M. Cercignani, *About "axial" and "radial" diffusivities.* Magn Reson Med, 2009. **61**(5): p. 1255-60.

84. Neudorfer, C., M. Hinzke, S. Hunsche, et al., *Combined Deep Brain Stimulation of Subthalamic Nucleus and Ventral Intermediate Thalamic Nucleus in Tremor-Dominant Parkinson's Disease Using a Parietal Approach.* Neuromodulation, 2019. **22**(4): p. 493-502.

85. Neumann, W.J., H. Schroll, A.L. de Almeida Marcelino, et al., *Functional segregation of basal ganglia pathways in Parkinson's disease.* Brain, 2018. **141**(9): p. 2655-2669.

86. Xu, C., P. Zhuang, M. Hallett, et al., *Parkinson's Disease Motor Subtypes Show Different Responses to Long-Term Subthalamic Nucleus Stimulation.* Front Hum Neurosci, 2018. **12**: p. 365.

87. Wong, J.K., V.T. Viswanathan, K.S. Nozile-Firth, et al., *STN Versus GPi Deep Brain Stimulation for Action and Rest Tremor in Parkinson's Disease.* Front Hum Neurosci, 2020. **14**: p. 578615.

88. Chen, Y., S. Ge, Y. Li, et al., *Role of the Cortico-Subthalamic Hyperdirect Pathway in Deep Brain Stimulation for the Treatment of Parkinson Disease: A Diffusion Tensor Imaging Study.* World Neurosurg, 2018. **114**: p. e1079-e1085.

89. Zhang, D., H. Lin, J. Liu, et al., *Electrode Reconstruction Assists Postoperative Contact Selection in Deep Brain Stimulation.* World Neurosurg, 2019. **125**: p. e442-e447.

90. Vanegas-Arroyave, N., P.M. Lauro, L. Huang, et al., *Tractography patterns of subthalamic nucleus deep brain stimulation.* Brain, 2016. **139**(Pt 4): p. 1200-10.

91. Horn, A., M. Reich, J. Vorwerk, et al., *Connectivity Predicts deep brain stimulation outcome in Parkinson disease.* Ann Neurol, 2017. **82**(1): p. 67-78.

92. Plantinga, B.R., Y. Temel, Y. Duchin, et al., *Individualized parcellation of the subthalamic nucleus in patients with Parkinson's disease with 7T MRI.* Neuroimage, 2018. **168**: p. 403-411.

93. Akram, H., S.N. Sotiropoulos, S. Jbabdi, et al., *Subthalamic deep brain stimulation sweet spots and hyperdirect cortical connectivity in Parkinson's disease.* Neuroimage, 2017. **158**: p. 332-345.

94. Louie, K.H., M.N. Petrucci, L.L. Grado, et al., *Semi-automated approaches to optimize deep brain stimulation parameters in Parkinson's disease.* J Neuroeng Rehabil, 2021. **18**(1): p. 83.

95. Okun, M.S., G. Mann, K.D. Foote, et al., *Deep brain stimulation in the internal capsule and nucleus accumbens region: responses observed during active and sham programming.* J Neurol Neurosurg Psychiatry, 2007. **78**(3): p. 310-4.

96. Rajamani, N., A. Horn, and B. Hollunder, *Outlook: Towards personalized connectomic deep brain stimulation.* Connectomic Deep Brain Stimulation, 2022: p. 527-542.

97. Baldermann, J.C., L. Hahn, T.A. Dembek, et al., *Weight Change after Striatal/Capsule Deep Brain Stimulation Relates to Connectivity to the Bed Nucleus of the Stria Terminalis and Hypothalamus.* Brain Sci, 2019. **9**(10).

98. Zhang, C., D. Li, H. Jin, K. Zeljic, and B. Sun, *Target-specific deep brain stimulation of the ventral capsule/ventral striatum for the treatment of neuropsychiatric disease.* Ann Transl Med, 2017. **5**(20): p. 402.

99. Patriat, R., S.E. Cooper, Y. Duchin, et al., *Individualized tractography-based parcellation of the globus pallidus pars interna using 7T MRI in movement disorder patients prior to DBS surgery.* Neuroimage, 2018. **178**: p. 198-209.

100. Callaghan, F., J.J. Maller, T. Welton, et al., *Toward personalised diffusion MRI in psychiatry: improved delineation of fibre bundles with the highest-ever angular resolution in vivo tractography.* Transl Psychiatry, 2018. **8**(1): p. 91.

101. Alkemade, A., J.M. Groot, and B.U. Forstmann, *Do We Need a Human post mortem Whole-Brain Anatomical Ground Truth in in vivo Magnetic Resonance Imaging?* Front Neuroanat, 2018. **12**: p. 110.

102. Boon, B.D.C., P.J.W. Pouwels, L.E. Jonkman, et al., *Can post-mortem MRI be used as a proxy for in vivo? A case study.* Brain Commun, 2019. **1**(1): p. fcz030.

103. Dyrby, T.B., W.F. Baare, D.C. Alexander, et al., *An ex vivo imaging pipeline for producing high-quality and high-resolution diffusion-weighted imaging datasets.* Hum Brain Mapp, 2011. **32**(4): p. 544-63.

104. Tendler, B.C., F. Qi, S. Foxley, et al., *A method to remove the influence of fixative concentration on postmortem T2 maps using a kinetic tensor model.* Hum Brain Mapp, 2021. **42**(18): p. 5956-5972.

105. Eisinger, R.S., D. Martinez-Ramirez, A. Ramirez-Zamora, et al., *Parkinson's disease motor subtype changes during 20 years of follow-up.* Parkinsonism Relat Disord, 2020. **76**: p. 104-107.

106. Xiao, Y., Q. Wei, R. Ou, et al., *Stability of motor-nonmotor subtype in early-stage Parkinson's disease.* Front Aging Neurosci, 2022. **14**: p. 1040405.

CHAPTER 5

Nigral neuropathology of Parkinson's motor subtypes coincide with circuitopathies: a scoping review

Boonstra JT, McGurran H, Temel Y, Jahanshahi A.

Nigral neuropathology of Parkinson's motor subtypes coincide with circuitopathies: A scoping review. Brain Struct Funct. 2022;227:2231–42.

Abstract

The neuropathological substrates of Parkinson's disease (PD) patients with motor subtypes tremor-dominance (TD), non-tremor dominance (nTD), postural instability and gait difficulty (PIGD), and akinetic-rigid (AR) are not completely differentiated. While extensive pathological research has been conducted on neuronal tissue of PD patients, data has not been discussed in the context of mechanistic circuitry theories differentiating motor subtypes. It is therefore expected that a more specific and tailored management of PD symptoms can be accomplished by understanding symptom-specific neuropathological mechanisms with the detail histology can provide. This scoping review gives an overview of the literature comparing TD and nTD PD motor subtypes by clarify observed pathology with underlying physiological circuitry theories. Studies using an array of pathological examination techniques have shown significant differences between TD and nTD PD subtypes. nTD PD patients show higher neuronal loss, gliosis, extraneuronal melanin deposits, and neuroaxonal dystrophy in multiple subregions of the substantia nigra (SN) related to the overactivity of the *indirect* motor loop. TD patients show more severe cell loss specifically in medial SN subdivisions, and have damage in the retrorubral field A-8 that projects to the dorsolateral striatum and ventromedial thalamus in the *direct* motor loop. Pathological studies are consistent with neuroimaging data and support contemporary mechanistic circuitry theories of PD motor symptom genesis. Further multimodal neuroimaging and histological studies are required to validate and expand upon these findings.

Introduction

Parkinson's disease (PD) is a progressive neurodegenerative disorder that affects more than 10 million people worldwide.[1] Clinical diagnoses of PD are based on the identification of cardinal motor symptoms including bradykinesia, postural instability, rigidity, and tremor. Motor symptom subtypes can be clinically determined with the Movement Disorder Society Unified Parkinson's Disease Rating Scale (MDS-UPDRS), an assessment of motor and non-motor PD symptoms[2]. The ratio of the mean tremor score to the mean score of their postural instability and gait difficulty (PIGD) score can be used to differentiate tremor-dominance (TD) patients (ratio ≥1.5), from PIGD patients (ratio ≤1), and from intermediate or 'mixed-type' patients (ratios >1.0 and <1.5)[3]. Those patients diagnosed with PIGD have been called akinetic-rigid (AR) with both subtypes often denoted as non-tremor dominant (nTD).

Heterogeneous motor symptom presentation between PD motor subtypes suggest correspondingly diverse pathophysiologies.[4-7] Previous research reviews both TD and nTD PD patients differing in various neuroanatomical and neurofunctional domains[8] as well as in non-motor symptoms and quality of life.[9] Patients with nTD have shown accelerated motor, functional, and cognitive decline compared to TD, resulting in TD to be considered the less severe subtype.[9] In line with differing symptoms and disease severity, histological data shows TD and nTD subtypes have '*specific morphological lesion patterns of pathophysiological relevance*'[10,11]. It is therefore expected that a more specific and tailored management of PD symptoms can be accomplished by understanding symptom-specific neuropathological mechanisms with the detail histology can provide. Pathological examinations further contribute to the validation of *in vivo* neuroimaging readouts by virtue of resolution as the imaging modalities assist each other in a complementary nature.

Despite a plethora of research investigating the pathophysiological bases of PD[12-14], particularly regarding the degeneration of midbrain dopamine (DA) neurons in the substantia nigra pars compacta (SNc), the full extent of PD pathology is poorly understood and even less is known about pathological differences between PD motor subtypes. Moreover, how previously described pathophysiological alterations between PD motor subtypes fit into contemporary mechanistic circuitry theories of PD symptoms genesis has yet to be described. The aim of this scoping review is to fill the gap between pathology and circuitry by consolidating previous studies that characterize pathological variances between TD and nTD subtypes of PD with contemporary mechanistic circuitry theories of PD symptom genesis.

Methods

We conducted and reported this study adhering to the PRISMA-ScR (PRISMA Extension for Scoping Reviews) guidelines and following the scoping review framework developed by Arksey and O'Malley and advanced by Levac et al.[15,16], a six-stage methodological framework involving (1) identifying the research question, (2) searching for relevant studies, (3) selecting studies, (4) charting the data, (5) collating, summarizing, and reporting the results, and (6) consulting with stakeholders.

Identifying relevant studies

A PubMed string search was iteratively developed with keywords "Parkinson's disease", "tremor-dominant", and "neuropathology" and variations thereof. The final string was used to identify all English-language abstracts containing human pathological data comparing the TD subtype to nTD subtype(s) within the NBIC database published up to December 2020. Additional articles were found from manual collation and supplemented references. The search string is provided in the Supplementary Material.

Selecting studies and charting the data

Eligibility was assessed via abstract and full-text screenings. Articles containing human pathological data comparing the TD PD subtype to the nTD subtype(s) directly were taken for further review. Data from all eligible studies pertaining to the tremor dominant, non-tremor dominant, and healthy control sample sizes, methodology used during pathological data collection, and conclusionary results was extracted and tabled.

Collating, summarizing, and reporting results

Results are grouped in the text by cardinal PD hallmarks including the dysfunction of the substantia nigra (SN) and dopaminergic system and the aggregation of Lewy bodies and Amyloid-β plaques. We first discuss basal ganglia circuitry and the data, then describe how results coincide with neuroimaging research and fit into circuitopathy theories, as well as future clinical implications. While critical appraisal of studies is not required for scoping reviews, the main source of bias we identified were potential false positives stemming from small sample sizes. Additional plausible sources of bias include differential use of the MDS-UPDRS; practitioner- and patient-reported outcomes may vary between consolidated studies.

Consulting with relevant stakeholders

It is recommended under the scoping review guidelines to involve stakeholders throughout the review process.[16] During the design and implementation, our project team regularly discussed the review strategy and our interpretations with experts in various clinical, technical, and academic fields including with authors of the reviewed studies. While

there were no patients involved with this review, results will be shared with any patients involved in future clinical exercises supported from this work.

The substantia nigra

The SN is a bilateral nucleus in the basal ganglia (BG*)* and plays an important role in modulating movement. As the SN is a major source of dopamine, degeneration of dopamine neurons in the SN is the main pathological hallmark of PD.[17] The SN can be divided into two subsections, the pars reticulata (SNr) that predominantly contains gamma-aminobutyric acid (GABA)-ergic neurons, mainly serving as an output nucleus in the cortico-basal ganglia loop conveying signals to the thalamus, superior colliculus, and to midbrain motor nuclei, and the pars compacta (SNc) projecting along the nigrostriatal pathway to the dorsal striatum (i.e., the caudate nucleus and putamen). SNc subdivisions innervate ventrally to the adjacent SNr[18] and modulate dopaminergic activity via axon collaterals. Fibers in the SNc have been shown to travel on average in a superior-posterior direction, whereas those in the SNr travel more in superior-medial/inferior-lateral directions.[19] Medial, dorsal, and ventral SN dopaminergic regions generally project to the central and dorsal caudate, while caudal, lateral, and ventrolateral SN regions project more to the putamen.[18,20-23]

The ventral region of the SNc is more vulnerable in numerous neurodegenerative diseases compared to the dorsal region partly due to the ventral tier being less melanised; vulnerability is concentrated ventrolaterally in PD and ventromedially in progressive supranuclear palsy (PSP).[21,24] Functional neuroimaging has identified a tripartite connectivity-based parcellation of the SN; the *medial SN* functionally correlated to limbic striatal and cortical regions, the *ventral SN* to associative regions of cortex and striatum, and the *lateral SN* to somatomotor regions of striatum and cortex.[25] The medial SN could overlap with ventral tegmental area (VTA) as the VTA similarly projects via mesolimbic and mesocortical pathways to limbic and cortical areas. Due to a lack of clear tissue boundaries this is sometimes referred to as the 'SN/VTA' complex.

Parkinsonian circuitry models; direct, indirect, hyperdirect pathways

Motor circuitry organization of BG pathways include the *direct* pathway (striatum-SNr/globus pallidus interna (GPi)-thalamus-cortex, responsible for motor excitation), the *indirect* pathway (striatum-globus pallidus externa (GPe)-subthalamic nucleus (STN)-SNr/GPi-thalamus-cortex, for motor inhibition), the *hyperdirect* pathway (STN-SNr/GPi-thalamus-cortex, as baseline motor inhibition), and the nigrostriatal projection (SNc-striatum, that is modulatory).[26] The striatum is the main input for the SNr via the *direct*

(striatum-SNr) and *indirect* (striatum-GPe-STN-SNr) pathways. However, the *direct* and *indirect* pathways are neurochemically distinct; *direct* pathway neurons express high levels of DA subtype-1 receptor (D1) while neurons in the *indirect* pathway express more D2 receptors[27]. Because of this, striatal activity via the *direct* pathways has an inhibitory effect on the SNr, while *indirect* pathway activity has an excitatory effect; a decrease in striatal DA leads to hyperactivity in D2 containing neurons and hypoactivity in D1 neurons[27]. Therefore, it was generally thought that hypotonic-hyperkinetic symptoms of PD such as tremors are caused by dysfunction of the *indirect* loop, leading to the loss of movement inhibition, while hypertonic-hypokinetic symptoms such as bradykinesia (a slowing of movement) are caused by dysfunction of the *direct* pathway that typically serves to plan and execute movements[28], but neuropathological evidence for this is inconclusive.

Two classical functional hypotheses explaining the pathophysiological circuitry underlying movement dysfunction in PD include the 'firing rate' model and the 'firing pattern' model[29]. In the 'firing rate' model, dopamine depletion in the BG reduces excitation to striatal *direct* pathways that project to the GPi and reduces tonic inhibition to striatal *indirect* pathways that project to the GPe. This leads to an increase in the firing rates of the GPi and SNr via the inhibition of the striato-GPi/SNr *direct* pathway, excitation of the striato-GPe-STN-GPi/SNr *indirect* pathway, and subsequent decreased thalamic and cortical activity resulting in akinesia. A key limitation of the 'firing rate' model is that it does not explain tremor circuitries. The 'firing pattern' model suggests oscillatory and/or synchronized firing patterns in the BG disables the processing and relaying of motor-related information leading to movement dysfunction. These abnormal firing patterns exist in the form of bursts (a series of firings in short time periods) and oscillations (periodic bursts, ranging from 4-9Hz 'tremor frequency' and 10-30Hz 'beta frequency')[30]. It is thought that dopamine depletion could enhance reciprocal connections between the GPe and the STN and lead to increased synchronized oscillatory activity resulting in motor dysfunction[31]. While the 'firing pattern' model partially explains tremors, its explanation for akinesia is less clear.

Nambu et al., 2015 proposed a novel '*dynamic activity*' model to reconcile the *firing rate* and *firing pattern* models, where signals from the *direct* pathway disinhibit thalamic neurons in a *center* thalamic area, *hyperdirect* and *indirect* pathways inhibit the *center* area, and *hyperdirect* and *direct* pathways inhibit the *surround* thalamic area (Figure 1)[29]. The *center-surround* composition is based on an anatomical study showing excitatory STN–GPi fibers arborize more extensively and terminate more proximally in the thalamus than inhibitory striato–GPi fibers[32], although the authors acknowledge that different studies suggest highly specific STN–GPi and striato-GPi projections.[33,34] In this model, dopamine depletion is thought to reduce GPi inhibition via the *direct* pathway to the *center* area and facilitate GPi excitation via the *hyperdirect* and *indirect* pathways to the *center*

and *surround* areas, leading to a reduction of thalamic and cortical disinhibition and subsequent akinesia. Furthermore, hyperkinetic disorders like tremors are said to result from the combination of enhanced inhibition to the *center* area of the GPi via the *direct* pathway and reduced excitation via the *hyperdirect* and *indirect* pathways to the *center* and *surround* area causing uncontrolled thalamic and cortical disinhibition. Further electrophysiological and anatomical studies investigating movement-related BG activity are needed to verify the '*dynamic activity*' model. Moreover, how specific pathological differences between PD motor subtypes correspond to circuitry theories are prominently missing from all models.

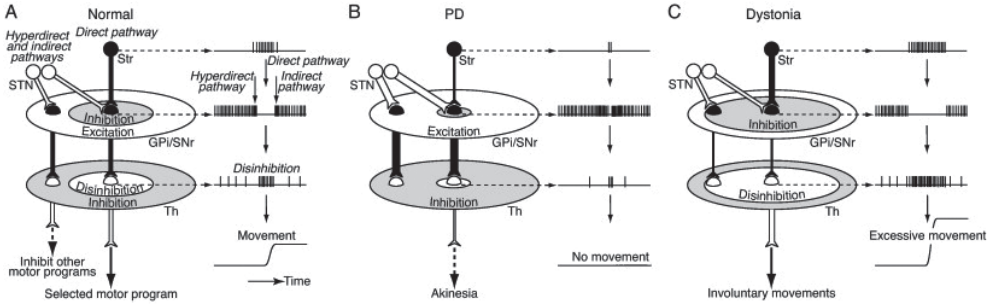

Figure 1. *'Dynamic activity model'* diagraming voluntary control of movement. A; Normal state, B; Parkinson's disease, C; Dystonia. Spatial distributions (left) and temporal patterns (right) of neuronal activity are illustrated in each panel. STN; subthalamic nucleus, GPi/SNr; internal global pallidus/substantia nigra, Th; thalamus. Reprinted with permission from Nambu et al., 2015.[29]

Results

Basal ganglia degeneration between subtypes

An array of quantitative histological differences in basal nuclei degeneration have been shown between PD motor subtypes (Table 1). Histological research examining extensive clinical documentation of forty-five autopsy confirmed PD patients with AR subtype show higher neuronal loss in the medial and lateral SN (devised by a line through the cerebral aqueduct) and the locus coeruleus (LC) compared to TD, as well as more severe SN gliosis, extraneuronal melanin deposits, and neuroaxonal dystrophy.[11] In this study, neuroaxonal dystrophy of the SNr was seen in 10 out of 28 AR patients but in none of the 15 TD patients, while neuronal reduction in the dorsal raphe nucleus (DRN) was equal between subtypes.[11]

In another study on pathologically confirmed PD patients with severe Parkinsonian AR syndrome, examinations showed that cell loss in the dorsolateral SN correlated with

the duration of PD symptoms, while cell loss in the dorsomedial SN correlated with the presence of tremor.[21] TD showed more neuronal loss in the medial rather than in the lateral SNc, an area that projects to the caudate nucleus and anterior putamen.[22] The ventrolateral part of the SNc typically degenerates faster in AR PD relative to the medial SNc, with negative correlations between SNc cell counts, severity of AR symptoms, and dopamine loss in the posterior putamen.[22] When quantifying neuronal densities from the medial to lateral part of the SN in idiopathic PD brains and controls, a positive association was seen between rigidity and hypokinesia and low neuronal densities in the lateral SN, but tremor was less severe in patients with similarly low neuronal densities.[23] As the SN is the neuronal region where the enzyme tyrosine hydroxylase (TH) is most abundant, TH deficiency has shown to be associated with hypokinetic-rigid symptoms while other features like tremor are largely absent in patients with TH deficiency.[35]

Although TD patients have shown less severe total SN cell loss (60%) compared to nTD (68%), TD patients have more cell loss in the periretrorubal field A8 in the lateral reticular formation.[36] A8 is located in the midbrain reticular formation dorso-caudal laterally to the SN and projects to the dorsolateral striatum and ventromedial thalamus.[37] Interestingly, in a study of seven autopsy confirmed AR patients with resting tremor, the A8 region appeared to be largely unaffected, with equal volume and neuronal count between the PD cases (those with only nigrostriatal pathway degeneration), Parkinson plus syndromes (those with additional degeneration elsewhere), or healthy controls.[38] The degree of PD akinesia has been shown to correlate with decreased dopamine and its inactive metabolite homovanillic acid in the caudate nucleus, while tremor severity correlates more with reduced homovanillic acid in the pallidum.[20] Additionally, using high performance liquid chromatography AR patients have shown to have a greater loss of dopamine in both the dorsal and ventral regions of the rostral GPi compared to TD and mixed subtypes.[39]

It is clear that quantitative differences in BG degeneration are visible on histological levels between PD motor subtypes. Pathological results indicate a multitude of nigrostriatal degenerative processes innate to PD are less severe in TD compared to nTD; nTD patients show more severe degeneration in the lateral parts of the SN, while TD patients show more alterations in medial SN regions.

Cortical Lewy bodies and Amyloid-β plaques between subtypes

Parkinsonian diseases involve abnormal accumulation of α-synuclein proteins within neuronal, glial, and nerve fiber cells. The progressive aggregation of Lewy bodies (LB), Lewy neurites, and amyloid-β plaques (Aβ) are additional hallmark histological markers of PD [17]. In one study of 70 autopsy-verified PD patients, the majority of tremor-onset cases (55.9%) had LB disease while the majority of PIGD-onset cases (73%) had other or additional forms of pathology including multiple system atrophy and PSP.[40] This study

aimed to evaluate the mode of onset and prognosis in autopsy confirmed PD cases and showed PIGD manifestations in PD were not due to age of onset as previously thought, but resulted from dissimilar neuropathology.

nTD patients have shown higher mean pathological grading of cortical LB, more cortical Aβ load, and more cerebral amyloid angiopathy compared to early-onset disease (EOD, <45years of age) and TD patients [41]. In this study the age of death was equal between cohorts indicating the higher cortical LB seen in nTD were not effects of age. Additionally, nTD showed higher cortical LB in the frontal regions and more severe plaque formation in the neocortex compared to EOD and TD who were more likely to have brainstem and limbic LB disease. Neocortical LB class was also related more to severe bradykinesia and falls than localized or limbic LB disease was.[41] In De Pablo-Fernández et al., the staging of Lewy pathology and Alzheimer's disease–related pathology did not differ between PD subtypes, but showed different rates of progression.[42] Although this study did not group according to TD and nTD subtypes, instead using mild-motor predominant, intermediate, and diffuse malignant groupings, 79% of those in the mild motor-predominant subtype were TD and 33% of the diffuse malignant subtype were PIGD, and it demonstrated that the speed of pathological accumulation in certain neuronal areas varies between PD subtypes.[43]

From these studies, it appears that patients with the nTD PD subtypes suffer more from cortical LB depositions and carry additional diverse forms of pathologies while TD patients have more localized pathology in the brainstem and limbic LB disease. Using cluster analyses, the authors suspect that a spectrum exists between a SN origin and a multi-pathway diffuse neurodegenerative process that is coupled with individual variation in progression and pathological patterns.[43] As PD pathology gradually progresses from the brainstem to higher cortical layers as the disease advances, nTD patients with comparable disease duration to TD patients may be demonstrating greater and faster degeneration along this specific network that is not simply due to age or different stages of the disease.

Neuroimaging findings support pathology

Neuroimaging studies examining nTD and TD patients support findings of pathology variance in the SN. In Table 2 an overview is provided. Diffusion tensor imaging (DTI) measures water molecule diffusion and directionality and is an indirect marker for white matter composition. PD patients show reduced diffusion measurements in the ventrolateral SN in keeping with dopaminergic cell loss.[44] Reductions of the DTI measurement fractional anisotropy (FA, reflecting a combination of axonal density, fiber mixture, and density) in the SN and putamen correlate with increased UPDRS motor scores in PD patients.[45] DTI has also shown increased mean diffusivity and radial diffusivity relating to structural disintegration in the SN being driven largely by the PIGD subtype.[46] Additionally, using

Table 1 Neuropathological variances in Parkinson's disease motor subtypes

Article	Patient numbers per subtype							Methods	Findings
	PD	TD	nTD	PIGD	AR	Mixed	HC		
Bernheimer et al. (1973)	28						28	IHC	Degree of akinesia correlated with DA and HVA decreases in the caudate nucleus, while the degree of tremor matched best with the degree of HVA decrease in the pallidum
Rinne et al. (1989)	12						18	IHC	Positive association found between rigidity and hypokinesia and low neuronal densities in the SNL
Paulus et al. (1991)		18			27			IHC	AR had a higher degree of gliosis in the SNM and SNL and more intense extraneuronal melanin deposits in the SNL. Neuroaxonal dystrophy of the SN reticula was seen in 10/28 AR but not in any of the 15 TD. AR have higher neuronal loss in the SNL and SNM and LC. Neuronal reduction in the DRN did not differ between AR and TD
Jellinger and Paulus (1992)		18			27			IHC	AR show degeneration of the striatonigral dopaminergic system and neuronal loss in SNL, SNM, and noradrencrgic LC. Tremor was related to other anatomo-pathophysiological substrates
Rajput et al. (1993)		34		11				x	The majority of tremor-onset cases had Lewy body disease while the majority of PIGD-onset cases had other forms of pathology
Halliday et al. (1996)					20		15	IHC	Greater dorsomedial SN cell loss was seen in PD patients with resting tremor than in those without tremor (85% loss compared to 70%, respectively)
McRitchie et al. (1997)					7		5	IHC	A8 regions appear largely unaffected in AR PD
Rajput et al. (2008)		3			3	2	5	HPLC	AR have greater loss of DA in both the dorsal and ventral regions of the rostral GPi compared to TD and Mixed
Selikhova et al. (2009)	242	88	93					Review	nTD have higher mean pathological grading of cortical Lewy bodies, more cortical amyloid-b plaque load, and more cerebral amyloid angiopathy compared to the EDO onset group and to TD. nTD have higher burdens of cortical Lewy bodies in the frontal regions and more severe plague formation in the neocortex compared to EOD and TD. EOD and TD were more likely to have brainstem and limbic Lewy body disease compared to nTD. Neocortical Lewy body class was more related to sever bradykinesia and falls than localized or limbic Lewy body disease was
Selikhova et al. (2013)	15	15 BT PD						IHC	Benign tremulous PD had less global neuronal loss in the substantia nigra compared to pathological controls. Benign tremulous PD had less cell loss in all nigral subregions compared to pathological controls. The most severe cell loss was seen in the ventrolateral nigra, while the medial nigra showed the greatest difference between benign tremulous PD and pathological controls
De Pablo-Fernandez et al. (2019)	111							Review	Staging of Lewy pathology and Alzheimer disease–related pathology did not differ between unique PD subtypes, but showed different rates of progression

A8 dopaminergic cell group A8, *AR* akinetic-rigid, *BT* benign tremulous, *DA* dopamine, *DRN* dorsal raphe nucleus, *EOD* early onset disease, *GPi* global pallidus internal, *HC* healthy control, *HPLC* high-performance liquid chromatography, *HVA* homovanillic acid, *IHC* immunohistochemistry, *LC* locus coeruleus, *Mixed* mixed-ratio subtype, *nTD* non-tremor dominant, *PD* Parkinson's disease, *PIGD* postural instability and gait difficulty, *SNL* substantia nigra lateral, *SN* substantia nigra, *SNM* substantia nigra medial, *TD* tremor-dominant.

neuromelanin-sensitive magnetic resonance imaging (NM-MRI) to detect dopamine metabolism, researchers found NM contrast-to-noise ratio (CNR) values in the lateral SN to decrease linearly with PD progression, while PIGD patients show larger decreases in CNR values in the lateral SN compared to TD.[47] PIGD have also shown more severe NM signal attenuation in the medial SN compared to TD with the medial SN ipsilateral to the most clinically affected side showing the greatest power to discriminate PD motor subtypes.[48]

High-pass filtered phase MRI used to measure iron depositions show SN phase shifts to be positively correlated with UPDRS-III and bradykinesia-rigidity subscores but not with tremor subscores.[49] Additionally, MRI has found positive correlations between motor subtype ratio and measures of iron via transverse relaxation rates (R2*) in the putamen, caudate, and thalamus but not in the SN with larger TD motor phenotype ratios having higher R2* suggesting putaminal over nigral iron accumulation as an early TD predictor.[50] Taken together these results suggest that regional patterns of microstructural degradation found via various neuroimaging techniques in the SN prove to accurately distinguish between PD motor subtypes and support histological findings assessing PD-related neurodegeneration. In short, neuroimaging shows nTD subtypes to have more laterally concentrated SN related severities compared to TD. Production of an accurate and detailed description of complete SN anatomy based on histological and immunohistochemistry stainings (*e.g.,* Perl, Luxol fast blue/Cresyl violet, substance P, and Calbindin) of PD tissue conjointly imaged with high-field MRI (i.e., *MR microscopy*) has proven successful[51] warranting similar examination across PD subtypes.

How cortical neuritic plaque differences between PD subtypes correspond to neuroimaging data is less clear. Although MRI typically shows more severe cortical volumetric changes in PIGD compared to TD, on a whole volumetric variations between PD motor subtypes are mixed[8]; TD patients have shown to have higher gray matter volumes (GMV)[52-55], lower GMV[56,57], and similar GMV[58-63] in cerebellular and cortical regions when compared to nTD subtypes. Correspondingly, greater attention should be granted towards cerebellular and brainstem pathways, as heterogeneous imaging acquisitions applied to all PD patients may lead to critical subcortical variations being overlooked. Parkinsonian resting tremor has shown to be related to cerebellar receiving thalamus activity[8,64] although to our knowledge no histological work has been done to support various neuroimaging studies that investigated cerebellar circuitopathies. This exact line of research will be a focus in our departments' future work.

Table 2. Substantia nigra neuroimaging findings in Parkinson's disease motor subtypes

Article	Patient numbers per subtype							Methods	Findings
	PD	TD	nTD	PIGD	AR	Mixed	HC		
[44]	14						14	DTI	Reduced FA in PD patients SN was greater in the caudal region compared with the middle and rostral regions
[45]	12						20	DTI	Alterations of FA in the SN and putamen correlate with increased UPDRS motor scores
[46]	9	12					20	DTI	Reduced FA and increased MD and RD in the SN was largely driven by PIGD. Increased diffusivity in the globus pallidus correlated with disease stage and motor severity in PIGD
[48]		9		14			20	NM-MRI	PIGD have more severe signal attenuation in the medial SN of compared to TD, with the medial SN ipsilateral to the MAH having the greatest power to discriminate PD motor subtypes
[49]	70						20	MR	SN MR phase shifts are positively correlated with UPDRS-III and bradykinesia-rigidity subscores but not with tremor subscores
[50]		10			10		20	MR	Positive correlation between motor subtype ratio and R2* in the putamen, caudate, and thalamus but not in SN, with larger TD ratios having higher R2*

DTI diffusion tensor imaging, *HC* healthy control, *Mixed* mixed-ratio subtype, *nTD* non-tremor dominant, *PD* Parkinson's disease, *PIGD* postural instability and gait difficulty, *SN* substantia nigra, *TD* tremor-dominant, *MD* mean diffusivity, *RD* radial diffusivity, *MAH* most affected hemisphere, *MR* magnetic resonance imaging, *NM-MRI* neuromelanin-sensitive magnetic resonance imaging, *R2** relaxometry rate, *FA* fractional anisotropy, *UPDRS* Unified Parkinson's Disease Rating Scale

Pathology supports circuitry models

Evidence from pathological research does not definitively support the notion that tremor symptoms of PD are mainly caused by dysfunction of the *indirect* loop while bradykinesia is caused by dysfunction of the *direct* pathway. nTD patients show more severe cell loss in the ventrolateral part of the SN that projects to the dorsal putamen, while SNc cell loss has also shown to negatively correlate to severity of akinesia-rigidity and DA loss in the posterior putamen.[22] The ventrolateral SNc in nTD has additionally shown to degenerate more severely than the medial SN[20] in contrast to TD patients, who exhibit less severe total and lateral SNc cell loss, but more severe cell loss in the medial SNc, as well as damage to the A8 region not seen in AR/nTD.[10,37,65]

nTD SN deficits could underpin pathological hyperactivity of the GABAergic *indirect* motor loop. GABAergic projections of the putamen have an inhibitory effect on the thalamus providing neuronal deficits in SN areas that project to the putamen to cause pathological thalamocortical pathway inhibition leading to reduced cortical activation. TD patients show pathological deficits in matrices of the dorsolateral striatum and ventromedial thalamus *direct* motor loop that could relate to hyperactivity in thalamomotor and cerebellar projections underpinning tremors. Such differential degeneration seen between PD motor subtypes could prove to be anatomical support for the Nambu et al., 2015 '*dynamic activity*' model in how the GPi/SNr receives differential and competitive inputs from the *hyperdirect*, *direct*, and *indirect* pathways that modulate movement.[29] Variations within the proposed *center-surround* topographical distribution of striatum-derived inhibition on the GPi/SNr[29] and its functional consequences could partly be explained by dissimilar neuropathological depositions in subpopulations of dopamine cells in the SN. nTD deficits in the ventrolateral SN could partly explain the proposed reduction in GPi/SNr inhibition in the *center* area and facilitation of GPi/SNr excitation in the *center* and *surround* areas that are suspected to lead to akinesia. Likewise, TD deficits in the medial SN could enhance inhibition in the *center* area of the GPi/SNr and reduced GPi/SNr excitation in the *center* and *surrounding* areas said to lead to involuntary movements.

Further research is needed to verify topographical distributions of SN subregion pathology. Investigations involving both subcortical and cortical stimulation are further required to functionally map striatum-derived inhibition and STN-derived excitation in the GPi to characterize '*dynamic activity*' alterations between PD motor subtypes.[29] Tracing studies in non-human primates using cell-type specific viral tools[68] can also shed light on projection patterns of medial and lateral SN dopamine cells. Additionally, how basal-brainstem pathways relate to diverse symptoms of PD remains to be studied in equal detail.

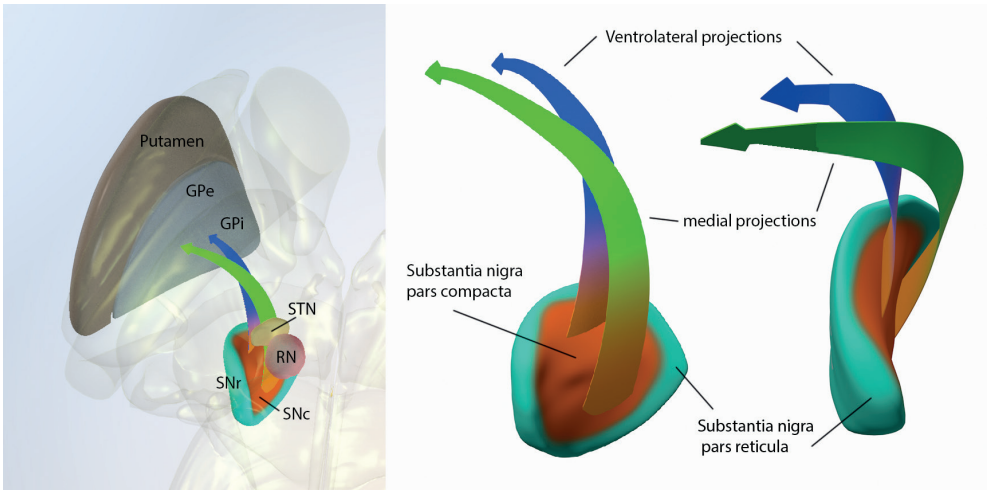

Figure 2. 3D renderings of MRI probability maps of the SNc = substantia nigra pars compacta (red) and SNr = substantia nigra pars reticulata (light blue) with ventrolateral (blue arrow) and medial projections (green arrow) towards the dorsal pallidum (grey). GPe = global pallidus external. GPi = global pallidus internal. STN = subthalamic nucleus. RN = red nucleus. The three-dimensional Cartesian coordinate axes indicate superior-dorsal (blue), posterior-caudal (red), and lateral (green) planes of the middle image. Renderings are modeled after two high-resolution probabilistic *in vivo* MRI atlases of the human subcortex.[66,67]

Clinical application

Modeling discrepancies between PD subtypes should have the ultimate aim to improve fundamental understandings of the disease and promote clinical success. Cortical pathological alternations could relate to the non-motor symptoms often seen more in nTD than in TD.[9] In cognitively normal elderly individuals increased global amyloid pathology showed to be associated with alterations in gray matter networks indicative of network breakdowns that lead to dementia.[69] Although correlations of Aβ deposition with cognitive decline in PD is still a matter of debate[70-72] a better understanding of variations in dopaminergic cell loss, plaque, and Lewy body depositions within PD patients has the potential to lead to more tailored treatment regimens and opens the opportunity to repurpose existing drug treatments, including dopamine (L-DOPA) based and amyloid targeted therapies (apomorphine).[73]

Results hold further clinical implications in the field of deep brain stimulation (DBS) as TD patients tend to respond better to DBS, whereas those with axial subtypes and gait problems benefit less favorably[26,74,75] demonstrating a clear need for improved diagnoses between PD subtypes. The SN is being studied as a DBS target region for PD motor symptom alleviation.[76,77] Low frequency SNr-DBS has shown to result in a significant improvement in PD patient's freezing of gait although its global antiparkinsonian effects were lower

than that of the more common high frequency STN-DBS[77]. STN-DBS has shown to have a protective effect on SNc neuron apoptosis in PD animal models conceivably resulting from neurotransmitter distribution and metabolism alterations[78] while supportive clinical data remains sparse.

Clinical limitation

It should be noted that the PD motor subtypes of TD and nTD have shown to have substantial clinical variability over time, specifically for the PIGD subtype.[79] After a four-year follow-up in 325 PD patients, the proportion of recorded PIGD patients was shown to have increased significantly, from 23.1% at baseline to 44.2%.[80] Controversies exist that TD and PIGD are not different PD subtypes but instead are different clinical PD stages with dissimilar disease progression features.[80] Correspondingly, the positive correlation between SN neurons and tremor may have been due to patients having not yet shifted from a TD subtype to nTD.[23] It is then reasonable to question if conventional PD motor subtyping has proficient clinical applicability. While authors found that 79% of those in the mild motor-predominant subtype were TD and 33% of the diffuse malignant subtype were PIGD, the tremor/PIGD classifications alone could not predict prognosis unlike their global subtyping solution that integrated additional daily living and cognition factors.[43] These results speak towards the utility of incorporating various motor and non-motor symptoms as well as other biomarkers in the identification of PD subtypes, as more multivariate groupings may produce greater clinical applications and prove more stable over time.[81] It is still unknown why certain subpopulations of cells undergo different degeneration patterns within each PD subtype, what initiates these divergences, whether they are a cause or a consequence of other co-occurring pathogenic mechanisms, and how they may be best targeted for treatment.

Conclusion

The purpose of scoping reviews is to chart a field within research and aid practitioners in constructing future research agendas.[15] Clustering pathological differences between PD motor subtypes by combining MRI and histology to understand neuroanatomical pathways underlying clinical symptoms is essential in clarifying PD etiology. Literature displays a vast array of SN variation across PD subtypes, showing nTD to have more severe damage in the ventrolateral part of the SN while TD patients show less severe total SN cell loss but more severe medial SN alterations.[10,37,65] Patients with the nTD subtype further suffer from more cortical LB depositions and additional pathologies while TD patients have more brainstem and limbic LB disease.[40,41]

Neuroimaging studies support pathological findings between PD subtypes showing alterations within SN subsections[47-49] although support for cortical plaque depositions is less clear.[8] Pathological differences between PD subtypes in the SN support the '*dynamic*

activity' model of PD symptom genesis; SN pathology may sustain the proposed *center-surround* topographical distribution of striatum-derived inhibition on the GPi/SNr that is correlated to motor disabilities.[29] Findings hold clinical implications in support of pathocircuitries and towards novel targets for treatment and interventions.[76-78]

Translational neuroscience works to disentangle the relationship between pathological data found *ex vivo* and clinically relevant *in vivo* data to innovate towards earlier PD diagnostic tools, better monitoring, and improved treatment approaches. Further research should continue to improve upon the creation of sustainable multivariate PD subtypes. As histology confers specificity by virtue of resolution neuroimaging should be inspired by postmortem findings and direct examinations with greater detail towards distinct neuronal pathway deficits.

References

1. Marras, C., J.C. Beck, J.H. Bower, et al., *Prevalence of Parkinson's disease across North America*. NPJ Parkinsons Dis, 2018. 4: p. 21.
2. Goetz, C.G., S. Fahn, P. Martinez-Martin, et al., *Movement Disorder Society-sponsored revision of the Unified Parkinson's Disease Rating Scale (MDS-UPDRS): Process, format, and clinimetric testing plan.* Mov Disord, 2007. 22(1): p. 41-7.
3. Jankovic, J., J. Carter, S. Gauthier, et al., *Variable expression of Parkinson's disease: A base-line analysis of the DATATOP cohort*. 1990(October).
4. He, N., P. Huang, H. Ling, et al., *Dentate nucleus iron deposition is a potential biomarker for tremor-dominant Parkinson's disease.* NMR Biomed, 2017. 30(4).
5. Rajput, A.H., A. Voll, M.L. Rajput, C.A. Robinson, and A. Rajput, *Course in Parkinson disease subtypes: A 39-year clinicopathologic study*. Neurology, 2009. 73(3): p. 206-12.
6. van Rooden, S.M., W.J. Heiser, J.N. Kok, et al., *The identification of Parkinson's disease subtypes using cluster analysis: a systematic review.* Mov Disord, 2010. 25(8): p. 969-78.
7. Zaidel, A., D. Arkadir, Z. Israel, and H. Bergman, *Akineto-rigid vs. tremor syndromes in Parkinsonism.* Curr Opin Neurol, 2009. 22(4): p. 387-93.
8. Boonstra, J.T., S. Michielse, Y. Temel, G. Hoogland, and A. Jahanshahi, *Neuroimaging Detectable Differences between Parkinson's Disease Motor Subtypes: A Systematic Review.* Mov Disord Clin Pract, 2021. 8(2): p. 175-192.
9. Wu, Y., X.Y. Guo, Q.Q. Wei, et al., *Non-motor symptoms and quality of life in tremor dominant vs postural instability gait disorder Parkinson's disease patients*. Acta Neurol Scand, 2016. 133(5): p. 330-7.
10. Jellinger, K.A. and W. Paulus, *Clinico-pathological correlations in Parkinson's disease.* Clin Neurol Neurosurg, 1992. 94 Suppl: p. S86-8.
11. Paulus, W. and K. Jellinger, *The neuropathologic basis of different clinical subgroups of Parkinson's disease*. J Neuropathol Exp Neurol, 1991. 50(6): p. 743-55.
12. Borghammer, P., *How does parkinson's disease begin? Perspectives on neuroanatomical pathways, prions, and histology.* Mov Disord, 2018. 33(1): p. 48-57.
13. Braak, H., K. Del Tredici, U. Rub, et al., *Staging of brain pathology related to sporadic Parkinson's disease*. Neurobiol Aging, 2003. 24(2): p. 197-211.
14. Hornykiewicz, O., *Biochemical aspects of Parkinson's disease*. Neurology, 1998. 51(2 Suppl 2): p. S2-9.
15. Arksey, H. and L. O'Malley, *Scoping studies: towards a methodological framework*. International Journal of Social Research Methodology, 2005. 8(1): p. 19-32.
16. Levac, D., H. Colquhoun, and K.K. O'Brien, *Scoping studies: advancing the methodology.* Implement Sci, 2010. 5: p. 69.
17. Alexander, G.E., *Biology of Parkinson's disease: pathogenesis and pathophysiology of a multisystem neurodegenerative disorder.* Dialogues Clin Neurosci, 2004. 6(3): p. 259-80.
18. Haber, S.N. and B. Knutson, *The reward circuit: linking primate anatomy and human imaging.* Neuropsychopharmacology, 2010. 35(1): p. 4-26.
19. Plantinga, B.R., A. Roebroeck, V.G. Kemper, et al., *Ultra-High Field MRI Post Mortem Structural Connectivity of the Human Subthalamic Nucleus, Substantia Nigra, and Globus Pallidus.* Front Neuroanat, 2016. 10: p. 66.
20. Bernheimer, H., W. Birkmayer, O. Hornykiewicz, K. Jellinger, and F. Seitelberger, *Brain dopamine and the syndromes of Parkinson and Huntington. Clinical, morphological and neurochemical correlations.* J Neurol Sci, 1973. 20(4): p. 415-55.
21. Halliday, G.M., D.A. McRitchie, H. Cartwright, et al., *Midbrain neuropathology in idiopathic Parkinson's disease and diffuse Lewy body disease.* J Clin Neurosci, 1996. 3(1): p. 52-60.
22. Jellinger, K. *Post mortem studies in Parkinson's disease - Is it possible to detect brain areas for specific symptoms*. in *Journal of Neural Transmission, Supplement*. 1999.
23. Rinne, J.O., J. Rummukainen, L. Paljarvi, and U.K. Rinne, *Dementia in Parkinson's disease is related to neuronal loss in the medial substantia nigra*. Ann Neurol, 1989. 26(1): p. 47-50.

24. Gibb, W.R. and A.J. Lees, *Anatomy, pigmentation, ventral and dorsal subpopulations of the substantia nigra, and differential cell death in Parkinson's disease.* J Neurol Neurosurg Psychiatry, 1991. 54(5): p. 388-96.
25. Zhang, Y., K.M. Larcher, B. Misic, and A. Dagher, *Anatomical and functional organization of the human substantia nigra and its connections.* Elife, 2017. 6.
26. Neumann, W.J., H. Schroll, A.L. de Almeida Marcelino, et al., *Functional segregation of basal ganglia pathways in Parkinson's disease.* Brain, 2018. 141(9): p. 2655-2669.
27. Cazorla, M., U.J. Kang, and C. Kellendonk, *Balancing the basal ganglia circuitry: a possible new role for dopamine D2 receptors in health and disease.* Mov Disord, 2015. 30(7): p. 895-903.
28. Obeso, J.A., M.C. Rodriguez-Oroz, M. Rodriguez, et al., *Pathophysiology of the basal ganglia in Parkinson's disease.* Trends Neurosci, 2000. 23(10 Suppl): p. S8-19.
29. Nambu, A., Y. Tachibana, and S. Chiken, *Cause of parkinsonian symptoms: Firing rate, firing pattern or dynamic activity changes?* Basal Ganglia, 2015. 5(1): p. 1-6.
30. Ashkan, K., P. Rogers, H. Bergman, and I. Ughratdar, *Insights into the mechanisms of deep brain stimulation.* Nat Rev Neurol, 2017. 13(9): p. 548-554.
31. Hutchison, W.D., J.O. Dostrovsky, J.R. Walters, et al., *Neuronal oscillations in the basal ganglia and movement disorders: evidence from whole animal and human recordings.* J Neurosci, 2004. 24(42): p. 9240-3.
32. Parent, A. and L.N. Hazrati, *Functional anatomy of the basal ganglia. II. The place of subthalamic nucleus and external pallidum in basal ganglia circuitry.* Brain Res Brain Res Rev, 1995. 20(1): p. 128-54.
33. Smith, Y., M.D. Bevan, E. Shink, and J.P. Bolam, *Microcircuitry of the direct and indirect pathways of the basal ganglia.* Neuroscience, 1998. 86(2): p. 353-87.
34. Shink, E., M.D. Bevan, J.P. Bolam, and Y. Smith, *The subthalamic nucleus and the external pallidum: Two tightly interconnected structures that control the output of the basal ganglia in the monkey.* Neuroscience, 1996. 73(2): p. 335-357.
35. Willemsen, M.A., M.M. Verbeek, E.J. Kamsteeg, et al., *Tyrosine hydroxylase deficiency: a treatable disorder of brain catecholamine biosynthesis.* Brain, 2010. 133(Pt 6): p. 1810-22.
36. Hirsch E. C., M.A., Graybiel A. M., Javoy-Agid F., Agid Y., *The loss of catecholami-nergic neurons in Parkinson's disease is heterogeneous in the midbrain. 10th International Symposium on Parkinson's disease.* 10th International Symposium on Parkinson's disease, 1991.
37. Deutch, A.Y., M. Goldstein, F. Baldino, Jr., and R.H. Roth, *Telencephalic projections of the A8 dopamine cell group.* Ann N Y Acad Sci, 1988. 537: p. 27-50.
38. McRitchie, D.A., H.R. Cartwright, and G.M. Halliday, *Specific A10 dopaminergic nuclei in the midbrain degenerate in Parkinson's disease.* Exp Neurol, 1997. 144(1): p. 202-13.
39. Rajput, A.H., H.H. Sitte, A. Rajput, et al., *Globus pallidus dopamine and Parkinson motor subtypes: clinical and brain biochemical correlation.* Neurology, 2008. 70(16 Pt 2): p. 1403-10.
40. Rajput, A.H., R. Pahwa, P. Pahwa, and A. Rajput, *Prognostic significance of the onset mode in parkinsonism.* Neurology, 1993. 43(4): p. 829-30.
41. Selikhova, M., D.R. Williams, P.A. Kempster, et al., *A clinico-pathological study of subtypes in Parkinson's disease.* Brain, 2009. 132(Pt 11): p. 2947-57.
42. De Pablo-Fernandez, E., A.J. Lees, J.L. Holton, and T.T. Warner, *Prognosis and Neuropathologic Correlation of Clinical Subtypes of Parkinson Disease.* JAMA Neurol, 2019. 76(4): p. 470-479.
43. Fereshtehnejad, S.M., Y. Zeighami, A. Dagher, and R.B. Postuma, *Clinical criteria for subtyping Parkinson's disease: biomarkers and longitudinal progression.* Brain, 2017. 140(7): p. 1959-1976.
44. Vaillancourt, D.E., M.B. Spraker, J. Prodoehl, et al., *High-resolution diffusion tensor imaging in the substantia nigra of de novo Parkinson disease.* Neurology, 2009. 72(16): p. 1378-84.
45. Zhan, W., G.A. Kang, G.A. Glass, et al., *Regional alterations of brain microstructure in Parkinson's disease using diffusion tensor imaging.* Mov Disord, 2012. 27(1): p. 90-7.
46. Nagae, L.M., J.M. Honce, J. Tanabe, et al., *Microstructural Changes within the Basal Ganglia Differ between Parkinson Disease Subtypes.* Front Neuroanat, 2016. 10: p. 17.

47. Wang, L., Y. Yan, L. Zhang, et al., *Substantia nigra neuromelanin magnetic resonance imaging in patients with different subtypes of Parkinson disease.* J Neural Transm (Vienna), 2021. 128(2): p. 171-179.
48. Xiang, Y., T. Gong, J. Wu, et al., *Subtypes evaluation of motor dysfunction in Parkinson's disease using neuromelanin-sensitive magnetic resonance imaging.* Neurosci Lett, 2017. 638: p. 145-150.
49. Martin-Bastida, A., N.P. Lao-Kaim, C. Loane, et al., *Motor associations of iron accumulation in deep grey matter nuclei in Parkinson's disease: a cross-sectional study of iron-related magnetic resonance imaging susceptibility.* Eur J Neurol, 2017. 24(2): p. 357-365.
50. Bunzeck, N., V. Singh-Curry, C. Eckart, et al., *Motor phenotype and magnetic resonance measures of basal ganglia iron levels in Parkinson's disease.* Parkinsonism Relat Disord, 2013. 19(12): p. 1136-42.
51. Massey, L.A., M.A. Miranda, O. Al-Helli, et al., *9.4 T MR microscopy of the substantia nigra with pathological validation in controls and disease.* Neuroimage Clin, 2017. 13: p. 154-163.
52. Al-Bachari, S., R. Vidyasagar, H.C. Emsley, and L.M. Parkes, *Structural and physiological neurovascular changes in idiopathic Parkinson's disease and its clinical phenotypes.* J Cereb Blood Flow Metab, 2017. 37(10): p. 3409-3421.
53. Benninger, D.H., S. Thees, S.S. Kollias, C.L. Bassetti, and D. Waldvogel, *Morphological differences in Parkinson's disease with and without rest tremor.* J Neurol, 2009. 256(2): p. 256-63.
54. Herb, J.N., S. Rane, D.A. Isaacs, et al., *Cortical Implications of Advancing Age and Disease Duration in Parkinson's Disease Patients with Postural Instability and Gait Dysfunction.* J Parkinsons Dis, 2016. 6(2): p. 441-51.
55. Piccinin, C.C., L.S. Campos, R.P. Guimaraes, et al., *Differential Pattern of Cerebellar Atrophy in Tremor-Predominant and Akinetic/Rigidity-Predominant Parkinson's Disease.* Cerebellum, 2017. 16(3): p. 623-628.
56. Rosenberg-Katz, K., T. Herman, Y. Jacob, et al., *Gray matter atrophy distinguishes between Parkinson disease motor subtypes.* Neurology, 2013. 80(16): p. 1476-84.
57. Rosenberg-Katz, K., T. Herman, Y. Jacob, et al., *Subcortical Volumes Differ in Parkinson's Disease Motor Subtypes: New Insights into the Pathophysiology of Disparate Symptoms.* Front Hum Neurosci, 2016. 10(July): p. 356.
58. Karunanayaka, P.R., E.Y. Lee, M.M. Lewis, et al., *Default mode network differences between rigidity- and tremor-predominant Parkinson's disease.* Cortex, 2016. 81: p. 239-50.
59. Linder, J., R. Birgander, I. Olsson, et al., *Degenerative changes were common in brain magnetic resonance imaging in patients with newly diagnosed Parkinson's disease in a population-based cohort.* J Neurol, 2009. 256(10): p. 1671-80.
60. Nyberg, E.M., J. Tanabe, J.M. Honce, et al., *Morphologic changes in the mesolimbic pathway in Parkinson's disease motor subtypes.* Parkinsonism Relat Disord, 2015. 21(5): p. 536-40.
61. Prodoehl, J., P.J. Planetta, A.S. Kurani, et al., *Differences in brain activation between tremor- and nontremor-dominant Parkinson disease.* JAMA Neurol, 2013. 70(1): p. 100-6.
62. Tessa, C., M. Giannelli, R. Della Nave, et al., *A whole-brain analysis in de novo Parkinson disease.* AJNR Am J Neuroradiol, 2008. 29(4): p. 674-80.
63. Vervoort, G., I. Leunissen, M. Firbank, et al., *Structural Brain Alterations in Motor Subtypes of Parkinson's Disease: Evidence from Probabilistic Tractography and Shape Analysis.* PLoS One, 2016. 11(6): p. e0157743.
64. Helmich, R.C., M. Hallett, G. Deuschl, I. Toni, and B.R. Bloem, *Cerebral causes and consequences of parkinsonian resting tremor: a tale of two circuits?* Brain, 2012. 135(Pt 11): p. 3206-26.
65. Damier, P., E.C. Hirsch, Y. Agid, and A.M. Graybiel, *The substantia nigra of the human brain. II. Patterns of loss of dopamine-containing neurons in Parkinson's disease.* Brain, 1999. 122 (Pt 8): p. 1437-48.
66. Alkemade, A., M.J. Mulder, J.M. Groot, et al., *The Amsterdam Ultra-high field adult lifespan database (AHEAD): A freely available multimodal 7 Tesla submillimeter magnetic resonance imaging database.* Neuroimage, 2020. 221: p. 117200.
67. Pauli, W.M., A.N. Nili, and J.M. Tyszka, *A high-resolution probabilistic in vivo atlas of human subcortical brain nuclei.* Sci Data, 2018. 5: p. 180063.
68. El-Shamayleh, Y., A.M. Ni, and G.D. Horwitz, *Strategies for targeting primate neural circuits with viral vectors.* J Neurophysiol, 2016. 116(1): p. 122-34.

69. Ten Kate, M., P.J. Visser, H. Bakardjian, et al., *Gray Matter Network Disruptions and Regional Amyloid Beta in Cognitively Normal Adults.* Front Aging Neurosci, 2018. 10: p. 67.
70. Compta, Y., L. Parkkinen, P. Kempster, et al., *The significance of alpha-synuclein, amyloid-beta and tau pathologies in Parkinson's disease progression and related dementia.* Neurodegener Dis, 2014. 13(2-3): p. 154-6.
71. Shah, N., K.A. Frey, M.L. Muller, et al., *Striatal and Cortical beta-Amyloidopathy and Cognition in Parkinson's Disease.* Mov Disord, 2016. 31(1): p. 111-7.
72. Melzer, T.R., M.R. Stark, R.J. Keenan, et al., *Beta Amyloid Deposition Is Not Associated With Cognitive Impairment in Parkinson's Disease.* Front Neurol, 2019. 10: p. 391.
73. Titova, N. and K.R. Chaudhuri, *Personalized medicine in Parkinson's disease: Time to be precise.* Mov Disord, 2017. 32(8): p. 1147-1154.
74. Neudorfer, C., M. Hinzke, S. Hunsche, et al., *Combined Deep Brain Stimulation of Subthalamic Nucleus and Ventral Intermediate Thalamic Nucleus in Tremor-Dominant Parkinson's Disease Using a Parietal Approach.* Neuromodulation, 2019. 22(4): p. 493-502.
75. Xu, C., P. Zhuang, M. Hallett, et al., *Parkinson's Disease Motor Subtypes Show Different Responses to Long-Term Subthalamic Nucleus Stimulation.* Front Hum Neurosci, 2018. 12: p. 365.
76. Sutton, A.C., W. Yu, M.E. Calos, et al., *Deep brain stimulation of the substantia nigra pars reticulata improves forelimb akinesia in the hemiparkinsonian rat.* J Neurophysiol, 2013. 109(2): p. 363-74.
77. Valldeoriola, F., E. Munoz, J. Rumia, et al., *Simultaneous low-frequency deep brain stimulation of the substantia nigra pars reticulata and high-frequency stimulation of the subthalamic nucleus to treat levodopa unresponsive freezing of gait in Parkinson's disease: A pilot study.* Parkinsonism Relat Disord, 2019. 60: p. 153-157.
78. Wu, S.T., Y. Ma, K. Zhang, and J.G. Zhang, *Effect of deep brain stimulation on substantia nigra neurons in a rat model of Parkinson's disease.* Chin Med J (Engl), 2012. 125(22): p. 4072-5.
79. Simuni, T., C. Caspell-Garcia, C. Coffey, et al., *How stable are Parkinson's disease subtypes in de novo patients: Analysis of the PPMI cohort?* Parkinsonism Relat Disord, 2016. 28: p. 62-7.
80. Lee, J.W., Y.S. Song, H. Kim, B.D. Ku, and W.W. Lee, *Alteration of Tremor Dominant and Postural Instability Gait Difficulty Subtypes During the Progression of Parkinson's Disease: Analysis of the PPMI Cohort.* Front Neurol, 2019. 10: p. 471.
81. Ren, J., C. Pan, Y. Li, et al., *Consistency and Stability of Motor Subtype Classifications in Patients With de novo Parkinson's Disease.* Front Neurosci, 2021. 15: p. 637896.

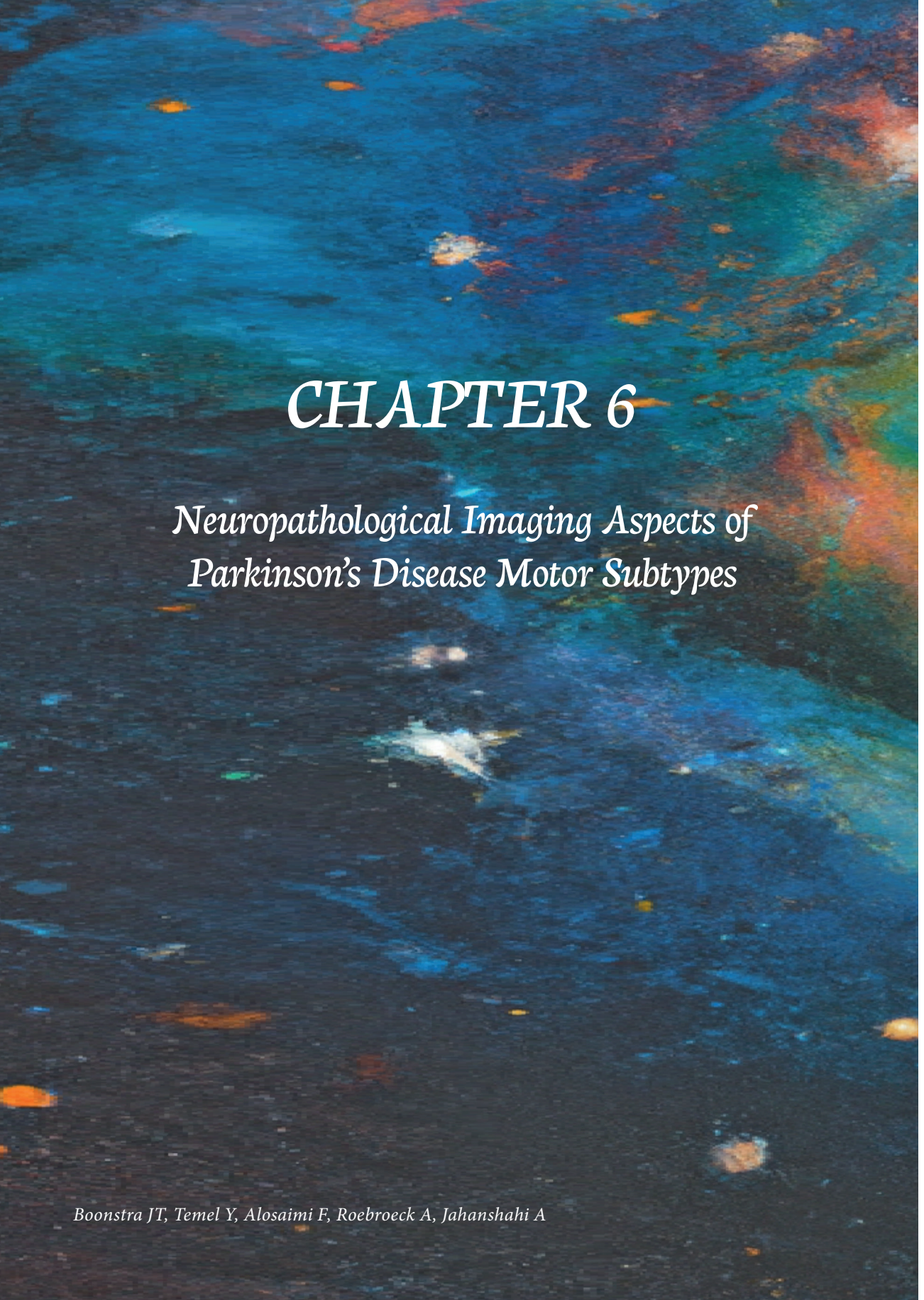

CHAPTER 6

Neuropathological Imaging Aspects of Parkinson's Disease Motor Subtypes

Boonstra JT, Temel Y, Alosaimi F, Roebroeck A, Jahanshahi A

Abstract

Parkinson's disease (PD) motor subtypes, tremor-dominant (TD) and non-tremor dominant (nTD) (including postural instability and gait difficulty (PIGD) and akinetic-rigid (AR)), are characterized by diverse motor and non-motor symptoms, but their corresponding histological markers are not well understood. A better understanding of pathological heterogeneities between these subtypes could lead to improved subtyping and enhanced treatment possibilities. Moreover, combining histological analysis with radiological imaging creates a cycle of pathological validation where ex vivo examinations can aid in the discovery of novel in vivo MR biomarkers. Here, we performed histological analysis on twelve post-mortem hemispheres (4 TD, 4 nTD, and 4 non-Parkinsonian controls) previously scanned with a specialized 9.4T human post-mortem brain MR radiofrequency coil. Measurements of nigral cell densities (Nissl), iron depositions (Pearl), and putamen and internal capsular volumetrics (Luxol Fast Blue) were completed and compared to previous MRI data. Results show that motor subtypes differ in various markers, such as cell density and iron depositions in the substantia nigra, and mixed volumetric measurements compared to MRI. This study shows Parkinson's disease motor subtype display specific postmortem circuitopathies that are potentially relevant in the planning of treatment regimes.

Introduction

Parkinson's disease (PD) is a debilitating neurodegenerative disorder and the most common movement disorder.[1] PD is clinically characterized by heterogeneous motor symptoms, including bradykinesia, tremor, and rigidity, as well as non-motor symptoms such as cognitive decline, depression, and anosmia.[2] Pathologically, PD is characterized by the loss of dopaminergic neurons in the substantia nigra, a key hallmark of the disease.[3] In addition, abnormal aggregates of α-synuclein accumulate in several regions of the brain, including the substantia nigra, locus ceruleus, dorsal motor nucleus of the vagus, raphe nuclei, and the nucleus basalis, forming intracytoplasmic neuronal inclusions called Lewy bodies and Lewy neurites.[4]

Differentiation of PD motor subtype can be clinically determined with the Movement Disorder Society Unified Parkinson's Disease Rating Scale (MDS-UPDRS), an assessment of motor and non-motor PD symptoms.[5] The ratio of the mean tremor score to postural instability and gait difficulty (PIGD) score differentiate tremor-dominance (TD) patients from PIGD patients that are also denoted akinetic-rigid (AR) or non-tremor dominant (nTD)).[6] Diverse pathologies within motor subtypes are expected due to the heterogeneous motor symptom presentation[7-10], and furthermore, TD and nTD subtypes have previously shown *'specific morphological lesion patterns of pathophysiological relevance'*.[11,12] Recent neuroimaging research has shown diverse neuroanatomical and neurofunctional dissimilarities between TD and nTD PD motor subtypes[13] while a histological data review has further shown diverging pathological markers.[14]

Despite extensive histological research towards PD[15,16], particularly regarding the degeneration of nigral dopaminergic neurons and the prevalence of Lewy bodies, little is known about pathophysiological alterations between PD motor subtypes. Moreover, how *ex vivo* MRI combined with histological techniques can be utilized in tandem to improve our understand of neurodegenerative disorder pathology is still a growing body of research (**see De Barros et al., 2019 for review**[17]**).** For example, postmortem MRI and histology have demonstrated differential iron accumulation in early- and late-onset Alzheimer's disease[18], while iron concentrations of neuromelanin have also been experimentally shown to correlate with T1 and T2 relaxation rates.[19] When 23 brains (5 PD) from the Queen Square Brain Bank were imaged using UHF MRI and subsequently stained with Luxol fast blue, Perls stain, and for substance P and Calbindin, high MR signal structures in the substantia nigra showed to correspond to histologically validated nigrosomes.[20]

Because the diagnosis of parkinsonian syndromes is entirely clinical, no imaging, biochemical, or genetic test antemortem can definitely diagnoses someone[21]; the only

definitive diagnose comes via pathological examinations postmortem[22], making continued histological evaluations imperative to differentiate disease progression paths and potentially improve treatment. Moreover, conducting postmortem MR analysis with stronger sequences coupled with designed-based histological measurements can help validate in vivo MR practices. In this paper, we aim to combine neurological imaging techniques to analyze parkinsonian tissue for variations between motor subtypes and healthy controls. A greater understanding of symptom-specific neuropathology with the detail histology provides correlated with ultra-high field MR may then translate into *in vivo* imaging regimes, improve biomarker detection, and help form differential diagnoses.[23]

Material and Methods

Specimens

Twelve brain hemispheres were collected from the Multiple Sclerosis and Parkinson's Tissue Bank located at Imperial College London, UK. Four healthy controls, four TD-PD, and four nTD-PD were selected based on retrospective review of medical records. Ethical approval was given for the use of tissue in research projects by the Research Ethics Committee for Wales reference number 08/MRE09/31+5. **Table 1** shows clinical report subtype demographics. Healthy control specimens were selected based on the absence of any neurologic disorder from clinical reports. All PD patents passed away with a diagnosis of PD and had no additional neurological disorders or brain pathologies, nor any history of neurosurgery. The most affected PD hemisphere was selected based on clinical documentation of bilateral symptom predominance. Gross visual inspections of all hemispheres were conducted to screen for an intact basal ganglia.

Table 1: Motor subtype and healthy control demographics

	_____PD_____				
	nTD (N=4)	TD (N=4)	HC (N=4)	Overall (N=12)	p-value
Sex:					
Male	1 (25%)	0 (0%)	2 (50%)	3 (25%)	0.446
Female	3 (75%)	4 (100%)	2 (50%)	9 (75%)	
Age (years)					
Median [IQR]	83 [8.3]	85 [4.3]	84 [9.5]	85 [7.5]	0.988
PMI (hours)					
Median [IQR]	41 [7.5]	31 [29]	20 [9.5]	34 [25]	0.514
Hemisphere Volume (Liters)					
Median [IQR]	0.60 [0.090]	0.59 [0.053]	0.55 [0.077]	0.57 [0.88]	0.631

Note: nTD = non-tremor dominant; TD = tremor dominant; HC = healthy control; PMI = post-mortem interval; QRI = interquartile range.

MR Imaging

Imaging was carried out on a 9.4T Magnetom MRI scanner (Siemens Healthineers, Erlangen, Germany) using a dedicated 9.4T 8 channel parallel transmit (pTx), 24 channel receive RF-coil as previous reported.[24] In short, a multi-echo 3D GRE (GRadient Echo) sequence was used to acquire high resolution isotropic T2* weighted data at 250µm while diffusion-weighted imaging (DWI) scans were obtained along 48 random directions with a voxel size of 1mm isotropic and a matrix size of 144x170x148.

Histology and immunohistochemistry

After MR scanning, each hemisphere was dissected into four tissue blocks: (1) caudate and putamen (CPu), (2) thalamus and basal ganglia, (3) midbrain, and (4) cerebellum, processed based on a previous study (see Attachment 1), and embedded in paraffin wax [63]. Blocks measured to be 4 x 2.5 x 2 cm. Histological sections were cut at 10µm thickness using a Leica RM2255 microtome with Leica 819 low profile blades. A serial 10% of sections were mounted on gelatin coated glass microscope slides; when the substantia nigra was reached, 20% were mounted.

Cresyl Violet (Nissl) Staining

Standard Nissl-staining was performed to assess neuronal cell densities; sections were deparaffinized in Xylene and rehydrated in graded ethanol and phosphate buffer saline (PBS, 3 x 20min), immersed in a aqueous solution of Sodium Acetate (Emsure 1.06267) with Acetic Acid (Merck, 10063), defatted with Triton X-100 (Sigma, T8787), and stained in Nissl solution (0.1% Cresyl violet solution; Alfa Aesar J64318) [34, 35] at 50°C for 30 minutes. Slides were then immersed three times for one minute in glacial acetic acid solution and one time in 100% ethanol before being further dehydrated in isopropanol and Xylene and coverslipped with Entellan (Sigma, 1.07961).

Luxol Fast Blue staining

Following rehydration, slides were placed in 1% LFB (solvent blue 37) for 24 hours at 60°C. After rinsing in 70% EtOH and differentiation with 0.05% lithium carbonate, slides were counterstained with Cresyl Violet for 5 minutes, and further differentiated with 70% EtOH and acetic acid EtOH before being dehydrated fully and coverslipped.

Pearl staining

Following rehydration, slides were placed in a classical aqueous Pearls solution made of equal hydrochloric acid and potassium ferrocyanide solutions and incubated for 2 hours at 37°C. After PBS washing, slides were placed in 3,3'-Diaminobenzidine (DAB) solution for ten minutes, washed with MilliQ water, dehydrated fully, and coverslipped.

Defined regions of interest

The ROIs in tissue specimen were delineated based on previous MRI delineations of a 3D GRE (GRadient Echo) sequence at 250µm. As the ROI in the MR images were delineated in standard space while utilizing two high-resolution probabilistic *in vivo* MRI atlases of the human subcortex as anatomical references[25,26], equating them with mounted tissue sections was done using simple overlapping image features **(Figure 1)**. Furthermore, the Atlas for the Human Brain by Juergen Mai (Mai Atlas)[27] was referred to during demarcation of intranuceli boundaries. To note, due to shrinkage, warping, and angular distortions innate to paraffin blocking large neuronal tissue, the delineated ROIs on tissue sections were made as cyclic polygons with respective MR ROIs serving as circumscribed circles; histological ROI were delineated slightly smaller and within matched MR ROIs to minimize inaccuracies when segmenting nuclei partitions. Across each subtype the same serial start and endpoint (rostral to caudal) per ROI was chosen in an effort to obtain anatomical consistency across sections.

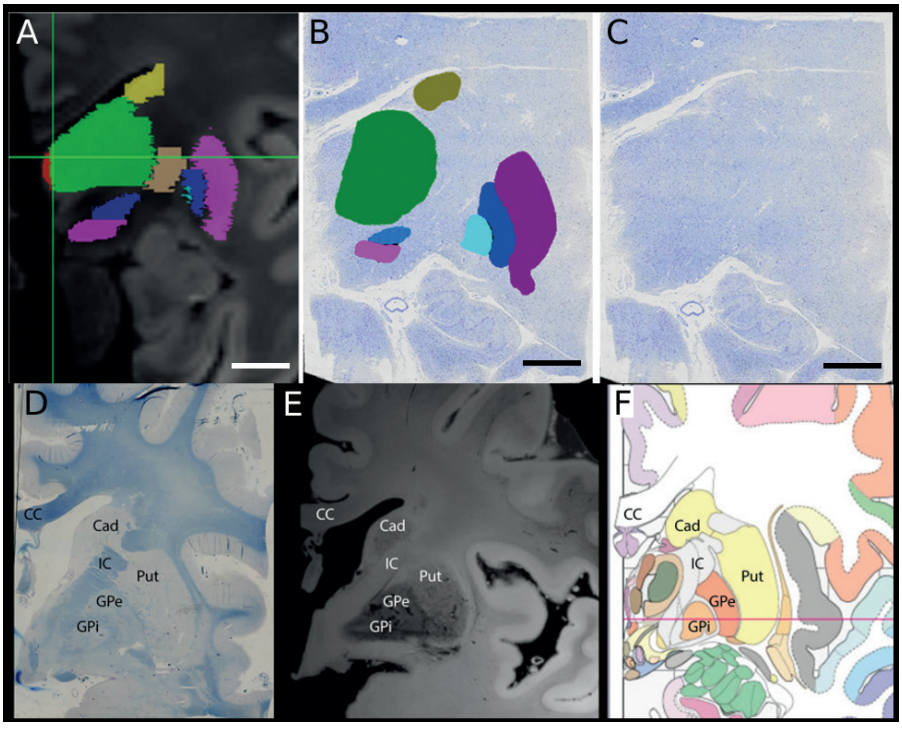

Figure 1. Delineated basal ganglia structures in magnetic resonance images, histological tissue, and brain atlases. A) Regions of interest (ROI) voxels demarcated in MR image; Caudate; yellow. Thalamus; green. Interthalmic adhesion; red. Putamen; pink (right). Globus pallidus external; dark blue (right). Globus pallidus internal; light blue. Sublenticular internal capsule; brown. Substantia nigra; pink (below). Subthalamic nucleus; blue (below). B) ROI delineated on Nissl staining with same coloration as A. C) Unmarked Nissl staining of B. D) Anterior basal ganglia nuclei labeled on Luxol fast blue staining. CC; corpus callosum. Cad; Caudate. IC; Internal capsule. Put; Putamen. GPe; Globus pallidus external. GPi; Globus pallidus internal. E) Nuclei labeled on MR image at same coronal place as D. F) Nuclei label on MAI atlas[27] at same coronal plane as D & E. Scale bar 1mm.

Data analysis

Statistical analysis was performed with Prism (Version 8, GraphPad Software LLC). A p-value of <0.05 is denoted statistically significant.

Results

Quantification of the Nissl-stained cells

Cell counting was performed on serially collected slices to assess the number of cells in the substantia nigra per square millimeter [28]. Starting at the anterior portion of the nigra the first of every fifty-one hundred serial sections was taken and quantified until the posterior section was reached. Nuclei were delineated at 10x magnification with an Olympus BX51 fluorescence microscope (Olympus, Hamburg, Germany) connected to an Olympus Camera DP72 (Olympus, Hamburg, Germany), while cell counting was performed at 40x magnification. The optical fractionator probe in the Stereo Investigator program (v2020 1.3, MBF Bio-science, USA) randomly selected 10% of the total counting frames in the delineated region based on a previously published method.[29] Counted cells and the average of counted markers divided by total surface area was used for statistical analysis.

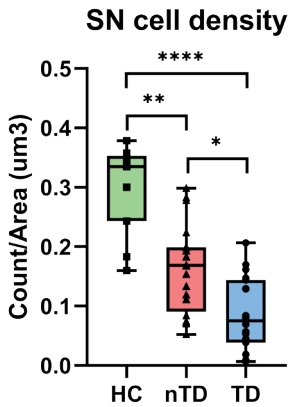

Figure 2. Cell density in the substantia nigra across Parkinson's motor subtypes and healthy controls Note. Due to a small sample sizes non-parametric Kruskal-Wallis tests were used for nigral cell counting and detected a significant difference in the mean values between the three groups (p=<0.0001) while a post-hoc Dunn's test to determine which specific pairs of groups were significantly different; HC vs. TD (p=<0.0001), HC vs. nTD (p=0.0096), and TD vs. nTD (p=0.0310).

Results show a significantly lower number of nigral neurons in the TD motor subtype compared to both nTD samples and healthy controls. Notwithstanding the higher cell density in healthy controls, these results run against our previous scoping literature review that showed nTD PD patients having greater neuronal loss (as well as greater gliosis, extraneuronal melanin deposits, and neuroaxonal dystrophy) in the SN compared to TD. More specifically, nTD patients previously showed more severe degeneration in lateral parts of the SN while TD patients show more alterations in medial SN regions.[14]

MR analysis of capsular and striatal volumes

Quantitative volumetric analysis of the MR images did not reveal any significant changes between subtypes and healthy controls in total hemisphere, internal capsule, sublenticular internal capsule, or putamen volumes. **Table 2.** However, a Dunn's multiple comparisons test did reveal variation in putamen volumes between HC and TD patients.

Table 2. MR volumetric comparisons across groups.

ROI	AR	HC	TD	*p*	AR-HC	AR-TD	HC-TD
Hemisphere	596.05 [549.74, 639.46]	552.88 [506.31, 583.23]	587.64 [568.78, 622.28]	*0.437*	/	/	/
Internal Capsule	713.51 [540.92, 997.17]	768.60 [633.25, 929.66]	922.58 [904.96, 938.73]	*0.551*	*0.251*	*0.990*	*0.886*
Sublenticular Internal Capsule	481.34 [370.19, 657.25]	551.98 [391.23, 751.55]	736.84 [723.07, 790.66]	*0.232*	*0.420*	*0.838*	*0.520*
Putamen	2769.14 [2651.73, 2924.54]	3114.67 [2661.03, 3351.09]	3318.38 [2972.89, 3657.94]	*0.390*	*0.436*	*0.926*	*0.028**

Note. Hemisphere volumetrics are given in mL. ROI volumes are denoted in voxels.

Quantification of white matter

Quantification of the internal capsule and posterior putamen volumes were completed in Stereo Investigator (ver. 2020 MBF Bioscience, USA) via the Cavalieri/Point-Counting Estimator probe. To ensure accuracy and reliability, segmentation and measurement procedures were repeated several times to assess reproducibility and then adjusted against whole MR hemispheric volume. Histological volumes were compared with MR volumes (Figure 3); while MR volumetric data revealed a significant increase in putamen volumes of TD patients compared to healthy controls, no significant differences in posterior putamen volumes were observed between any of the groups via histology, and both MR and histology showed no difference between or across groups in internal capsule volumetrics (Figure 4).

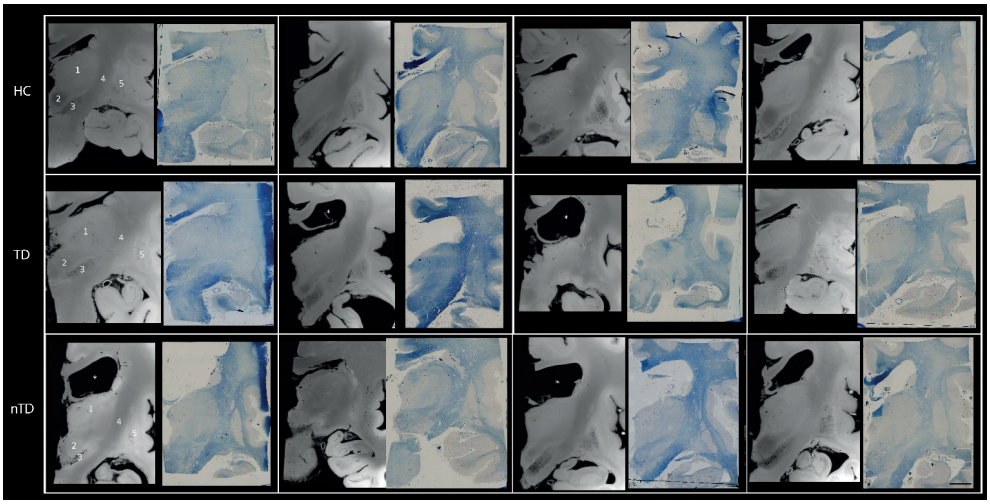

Figure 3. Magnetic resonance images of each sample with matched histological section references. Note. HC; healthy control. TD; tremor dominant PD. nTD; Nontremor dominant PD. *Atrophy of the third ventricle is evident in most TD and nTD samples while absent in HC. 1) Thalamus, 2) Red nucleus, 3) Substantia nigra, 4) Internal capsule, 5) Putamen. Scale bar 1mm.

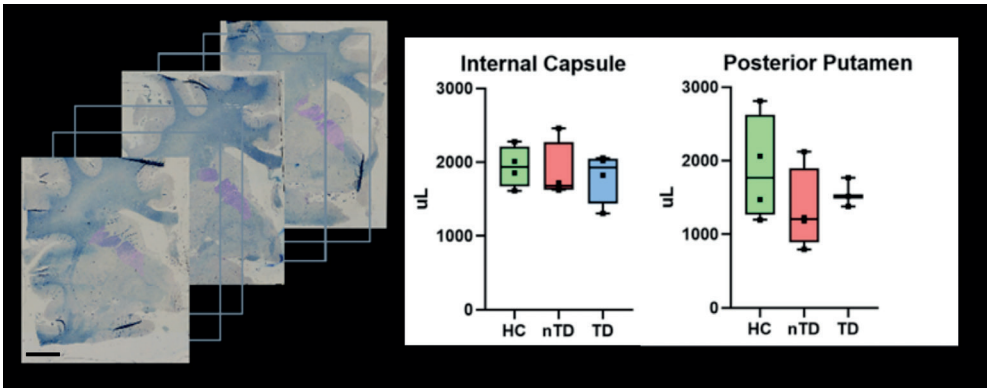

Figure 4. Volumetric analysis on histological sections. Note. Serial sectioning of neuronal tissue stained with Luxol fast blue; internal capsule highlighted in purple. Nuclei volumetric data adjusted against whole hemisphere volumes presented in uL. Scale bar 1mm.

Qualification of iron deposition

Pearls staining were imaged in the dorsal lateral and ventral medial subregions of the substantia nigra (dlSN & vmSN, respectively). Photomicrographs were taken with Cell P software (Olympus Soft Imaging Solutions, Münster, Germany) using an AX-70 microscope (Olympus, Zoeterwoude, The Netherlands). Iron deposition patterns observed in all samples ranged from a light shading to a dark stain, with varying degrees of intensity. Mean gray values were obtained in ImageJ (ImageJ software version 1.52p; NIH, Bethesda, MD, USA) using optical density (OD) measurements. The average OD of multiple sections within each subregion across all samples was calculated. Nonparametric tests showed no statistically significant differences (data not shown) but qualitative visualizations of the data revealed distinct patterns (Figure 5). In all samples, gray values corresponding to greater iron accumulation occurred in the vmSN compared to the dlSN. Healthy controls generally exhibited lower iron accumulation than both Parkinson's motor in both subregions. While TD had values above healthy controls in both subregions, nTD PD patients had larger gray value variations, ranging from health control equivalent low values to higher values to that of TD patients.

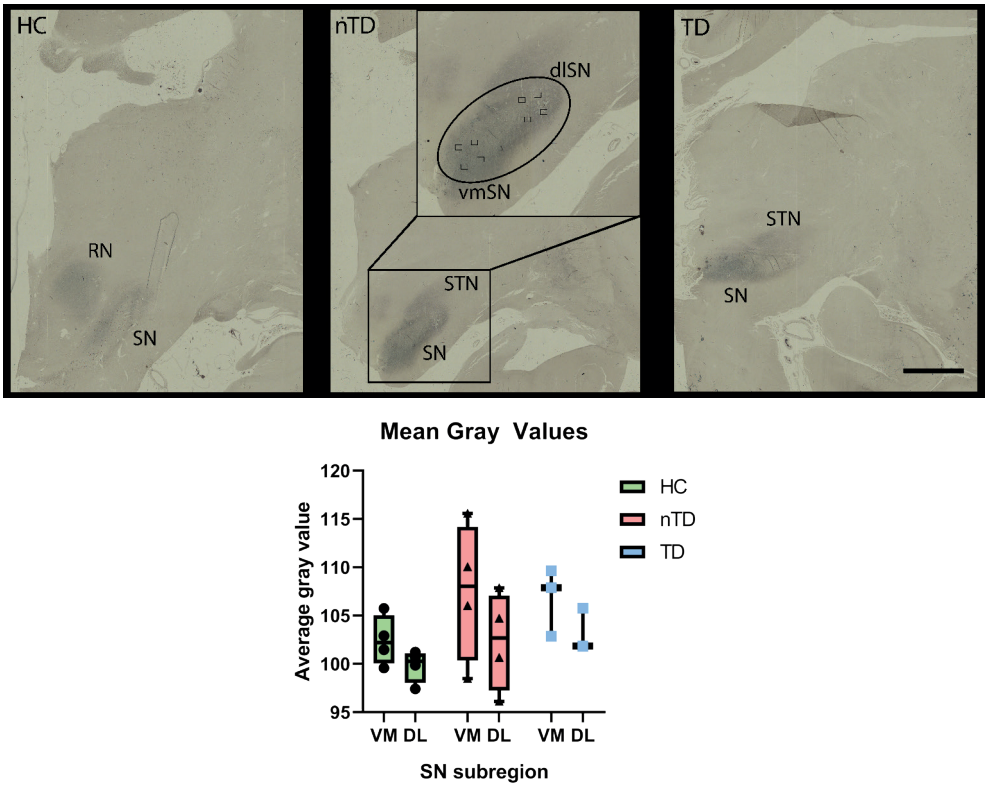

Figure 5. Pearl staining showing iron depositions across subtypes. Note. HC; healthy control. TD; tremor dominant PD. nTD; Nontremor dominant PD. RN; red nucleus. STN; subthalmic nucleus. SN; substantia nigra. vmSN/VM; ventral medial substantia nigra. dlSN/DL; dorsal lateral substantia nigra. Scale bar 1mm.

Discussion

Parkinson's disease (PD) is characterized and defined neuropathologically by the loss of neurons in the substantia nigra pars compacta (SNpc) and the presence of Lewy bodies in that region as well as other brain areas. It has been estimated that motor symptoms appear in PD when at least 50% of nigral dopamine neurons and 70% of putaminal dopamine tissue content has been lost.[30,31] While the exact biochemical mechanism causing nigral cell loss in PD is not fully understood, proposed mechanisms include oxidative stress, mitochondrial dysfunction, inflammation, and protein misfoldings, e.g., the accumulation of alpha-synuclein into Lewy bodies.[32,33] Studies have shown a correlation between nigral neuronal loss and Lewy body load in some cortical areas of PD such as the olfactory bulb, but no correlations were found in other examined regions, including the SN.[34] LBs appear in various regions of the brain before the onset of motor symptoms, suggesting they may spread throughout the brain in a prion-like manner, causing pervasive neuronal dysfunction and cell death.[35,36] While it is not clear whether Lewy bodies are the primary cause of nigral cell loss in the SN or if they are a byproduct of other PD processes[36,37], some studies suggest there to be a "nigral neuronal reserve" within the substantia nigra, where the total number of pigmented neurons in a normally developed adult brain surpasses the minimum number of neurons needed for normal functioning, helping to explain how 50% of nigral dopamine neurons are lost prior to motor symptoms, and why some elderly individuals with non-nigral Lewy bodies do not always exhibit clinically relevant PD symptoms.[34]

While both volumetric analyses in MR and histology showed no difference in internal capsule volumes, MR volumetric data revealed a significant increase in putamen volumes of TD patients compared to healthy controls but no significant differences in posterior putamen volumes were observed in the histological analysis. Previous nonhuman primate research has shown the anterior and posterior striatal sections participate differently in the learning of sequential movements, as the learning of new sequences became deficient after GABA agonist injections in the anterior caudate and putamen, but not in the middle-posterior putamen.[38] As the middle-posterior putamen is well known to receive inputs from sensory-motor cortical areas, including the premotor and supplementary motor areas as well as the primary motor area[39,40] it seems likely that subsections of the putamen could be differentially effected in various movement disorders such as PD and PD motor subtypes. Still, striatal volume variation is challenging to separate from normal aging and PD dopaminergic cell loss, as negative associations between putamen volume and Hoehn and Yahr scales (that correlate with age) have been previously shown[41] and nigra-striatal neuron loss is approximately 60% by the time of PD symptom onset.[30] It is possible that the putamen is not differentially affected between PD motor subtypes as other brain regions and mechanisms may play greater roles in heterogeneous motor symptoms.

Oxidative stress is believed to play a major role in the mechanism of dopaminergic cell death in PD.[32] Iron is a redox-active transition metal critical to physiological processes in the nervous system, such as myelin synthesis, dopamine metabolism, and neurotransmitter regulation.[42] However, excess iron exacerbates oxidative stress mechanisms and can increase reactive oxygen species, leading to damage to DNA, RNA, proteins, and lipids.[43,44] Iron has also shown to be selectively elevated in the SN of PD patients while the degree of iron accumulation has shown to correlate with PD severity.[45-47] One study in a non-human primate model of PD demonstrated that the highest levels of SN iron accumulation correlated with the highest loss of DA neurons, the greatest oxidative stress in the SN, and the most severe PD-like motor deficits.[48]

Our findings suggest that iron accumulation in the ventral medial substantia nigra (vmSN) may play a role in the pathocircuitry of PD and may be associated with lower neuronal densities in specific motor subtypes. Qualitative results showed a visible and marked pattern of dark staining intensity in all samples within the vmSN compared to the dlSN. A previous study using high-pass filtered phase MRI to detect iron depositions showed SN phase shifts were positively correlated with UPDRS-III and bradykinesia-rigidity subscores but not with tremor subscores.[49] Here, nTD samples showed the highest iron depositions, albeit with the largest intersample variation, further showing iron accumulation may be stratified across disease motor subtypes and correlate with dopaminergic neurodegeneration. Important to note, iron concentration increases with age and is distributed differently across various brain areas[50,51] Varying progression rates and disease paths of PD may further influence iron-induced pathology, while iron pathology itself may be a secondary mechanism facilitating neurodegeneration rather than a primary cause.[52,53]

Limitations

To note, a sample size of our PD subtype group and health control group causes current analyses to have low power. Variability in cell density results in the SN compared to previous reviewed literature could be due to the stereological estimation method utilized, as a semi-quantitative cell counting technique that accounted for 10% of randomly selected frames from the entire SN was used, while a more scrutinous examination method within nigral subsections maybe be in closer cooperation with previous reported results. Due to large postmortem intervals and extended tissue fixation periods of the tissue, many immunohistochemical stainings showed to have large variability and inconsistencies across and between subjects, limiting the ability to quantify LBs and detail further biochemical mechanisms associated with our observed alterations. Therefore, more research is needed from larger cohorts of higher quality, for example, to inspect the relation between LBs and neuronal cell loss in substantia nigra subregions. Additionally, how other factors such as oxidative stress and inflammation contribute to nigral cell loss, LB formation, and volumetric differences in PD and PD subtypes should be explored in more depth.

Conclusion

This study contributes to growing investigations that bridge fundamental research of multimodal imaging of neurodegenerative tissue. Findings demonstrate the value of utilizing multimodal imaging to investigate anatomical changes in the brains of individuals who suffered from Parkinson's disease. By examining postmortem tissue with histo- and radiological imaging methods, results provide a unique opportunity to understand the underlying structural changes that contribute to the clinical manifestations of PD. The identification of potential motor subtype-specific differences highlights the importance of exploring the heterogeneity of PD and the need for personalized approaches to treatment. This study underscores the utility of *ex vivo* assessments in identifying specific motoric circuitry dysfunction in PD that could ultimately aid in the development of objective monitoring tools and the discovery of novel biomarkers for PD progression.

Acknowledgments: The funding source for this study is from Stichting Beheer Vermogen De Weijerhorst

References

1. Pringsheim, T., N. Jette, A. Frolkis, and T.D. Steeves, *The prevalence of Parkinson's disease: a systematic review and meta-analysis.* Mov Disord, 2014. **29**(13): p. 1583-90.
2. Kalia, L.V. and A.E. Lang, *Parkinson's disease.* Lancet, 2015. **386**(9996): p. 896-912.
3. Dauer, W. and S. Przedborski, *Parkinson's disease: mechanisms and models.* Neuron, 2003. **39**(6): p. 889-909.
4. Spillantini, M.G., M.L. Schmidt, V.M. Lee, et al., *Alpha-synuclein in Lewy bodies.* Nature, 1997. **388**(6645): p. 839-40.
5. Goetz, C.G., S. Fahn, P. Martinez-Martin, et al., *Movement Disorder Society-sponsored revision of the Unified Parkinson's Disease Rating Scale (MDS-UPDRS): Process, format, and clinimetric testing plan.* Mov Disord, 2007. **22**(1): p. 41-7.
6. Jankovic, J., M. McDermott, J. Carter, et al., *Variable expression of Parkinson's disease: a base-line analysis of the DATATOP cohort. The Parkinson Study Group.* Neurology, 1990. **40**(10): p. 1529-34.
7. He, N., K. Ghassaban, P. Huang, et al., *Imaging iron and neuromelanin simultaneously using a single 3D gradient echo magnetization transfer sequence: Combining neuromelanin, iron and the nigrosome-1 sign as complementary imaging biomarkers in early stage Parkinson's disease.* Neuroimage, 2021. **230**: p. 117810.
8. Rajput, A.H., A. Voll, M.L. Rajput, C.A. Robinson, and A. Rajput, *Course in Parkinson disease subtypes: A 39-year clinicopathologic study.* Neurology, 2009. **73**(3): p. 206-12.
9. van Rooden, S.M., W.J. Heiser, J.N. Kok, et al., *The identification of Parkinson's disease subtypes using cluster analysis: a systematic review.* Mov Disord, 2010. **25**(8): p. 969-78.
10. Xiang, Y., T. Gong, J. Wu, et al., *Subtypes evaluation of motor dysfunction in Parkinson's disease using neuromelanin-sensitive magnetic resonance imaging.* Neurosci Lett, 2017. **638**: p. 145-150.
11. Jellinger, K.A. and W. Paulus, *Clinico-pathological correlations in Parkinson's disease.* Clin Neurol Neurosurg, 1992. **94 Suppl**: p. S86-8.
12. Paulus, W. and K. Jellinger, *The neuropathologic basis of different clinical subgroups of Parkinson's disease.* J Neuropathol Exp Neurol, 1991. **50**(6): p. 743-55.
13. Boonstra, J.T., S. Michielse, Y. Temel, G. Hoogland, and A. Jahanshahi, *Neuroimaging Detectable Differences between Parkinson's Disease Motor Subtypes: A Systematic Review.* Mov Disord Clin Pract, 2021. **8**(2): p. 175-192.
14. Boonstra, J.T., H. McGurran, Y. Temel, and A. Jahanshahi, *Nigral neuropathology of Parkinson's motor subtypes coincide with circuitopathies: a scoping review.* Brain Struct Funct, 2022. **227**(7): p. 2231-2242.
15. Braak, H., K. Del Tredici, U. Rub, et al., *Staging of brain pathology related to sporadic Parkinson's disease.* Neurobiol Aging, 2003. **24**(2): p. 197-211.
16. Hornykiewicz, O., *Biochemical aspects of Parkinson's disease.* Neurology, 1998. **51**(2 Suppl 2): p. S2-9.
17. De Barros, A., G. Arribarat, J. Combis, P. Chaynes, and P. Peran, *Matching ex vivo MRI With Iron Histology: Pearls and Pitfalls.* Front Neuroanat, 2019. **13**: p. 68.
18. Bulk, M., W.M. Abdelmoula, R.J.A. Nabuurs, et al., *Postmortem MRI and histology demonstrate differential iron accumulation and cortical myelin organization in early- and late-onset Alzheimer's disease.* Neurobiol Aging, 2018. **62**: p. 231-242.
19. Trujillo, P., P.E. Summers, E. Ferrari, et al., *Contrast mechanisms associated with neuromelanin-MRI.* Magn Reson Med, 2017. **78**(5): p. 1790-1800.
20. Massey, L.A., M.A. Miranda, O. Al-Helli, et al., *9.4 T MR microscopy of the substantia nigra with pathological validation in controls and disease.* Neuroimage Clin, 2017. **13**: p. 154-163.
21. Williams, D.R. and I. Litvan, *Parkinsonian syndromes.* Continuum (Minneap Minn), 2013. **19**(5 Movement Disorders): p. 1189-212.
22. Gibb, W.R. and A.J. Lees, *The relevance of the Lewy body to the pathogenesis of idiopathic Parkinson's disease.* J Neurol Neurosurg Psychiatry, 1988. **51**(6): p. 745-52.
23. Meijer, F.J. and B. Goraj, *Brain MRI in Parkinson's disease.* Front Biosci (Elite Ed), 2014. **6**(2): p. 360-9.
24. Sengupta, S., A. Roebroeck, V.G. Kemper, et al., *A Specialized Multi-Transmit Head Coil for High Resolution fMRI of the Human Visual Cortex at 7T.* PLoS One, 2016. **11**(12): p. e0165418.

25. Alkemade, A., M.J. Mulder, J.M. Groot, et al., *The Amsterdam Ultra-high field adult lifespan database (AHEAD): A freely available multimodal 7 Tesla submillimeter magnetic resonance imaging database.* Neuroimage, 2020. **221**: p. 117200.
26. Pauli, W.M., A.N. Nili, and J.M. Tyszka, *A high-resolution probabilistic in vivo atlas of human subcortical brain nuclei.* Sci Data, 2018. **5**: p. 180063.
27. Mai, J., Majtanik, M., Paxinos, G., *Atlas of the Human Brain*. 4 ed. 2015: Academic Press.
28. Stiasny-Kolster, K., F. Sixel-Doring, C. Trenkwalder, et al., *Diagnostic value of the REM sleep behavior disorder screening questionnaire in Parkinson's disease.* Sleep Med, 2015. **16**(1): p. 186-9.
29. Jensen, E.B., & Gundersen, H. J. G., *Stereological estimation of surface area of arbitrary particles.* In Proceedings of the 7th International Congress for Stereology, 1991: p. 25-30.
30. Fearnley, J.M. and A.J. Lees, *Ageing and Parkinson's disease: substantia nigra regional selectivity.* Brain, 1991. **114 (Pt 5)**: p. 2283-301.
31. Kordower, J.H., C.W. Olanow, H.B. Dodiya, et al., *Disease duration and the integrity of the nigrostriatal system in Parkinson's disease.* Brain, 2013. **136**(Pt 8): p. 2419-31.
32. Dias, V., E. Junn, and M.M. Mouradian, *The role of oxidative stress in Parkinson's disease.* J Parkinsons Dis, 2013. **3**(4): p. 461-91.
33. Nicoletti, V., G. Palermo, E. Del Prete, M. Mancuso, and R. Ceravolo, *Understanding the Multiple Role of Mitochondria in Parkinson's Disease and Related Disorders: Lesson From Genetics and Protein-Interaction Network.* Front Cell Dev Biol, 2021. **9**: p. 636506.
34. Iacono, D., M. Geraci-Erck, M.L. Rabin, et al., *Parkinson disease and incidental Lewy body disease: Just a question of time?* Neurology, 2015. **85**(19): p. 1670-9.
35. Ma, J., J. Gao, J. Wang, and A. Xie, *Prion-Like Mechanisms in Parkinson's Disease.* Front Neurosci, 2019. **13**: p. 552.
36. Parkkinen, L., S.S. O'Sullivan, C. Collins, et al., *Disentangling the relationship between lewy bodies and nigral neuronal loss in Parkinson's disease.* J Parkinsons Dis, 2011. **1**(3): p. 277-86.
37. Power, J.H., O.L. Barnes, and F. Chegini, *Lewy Bodies and the Mechanisms of Neuronal Cell Death in Parkinson's Disease and Dementia with Lewy Bodies.* Brain Pathol, 2017. **27**(1): p. 3-12.
38. Miyachi, S., O. Hikosaka, K. Miyashita, Z. Karadi, and M.K. Rand, *Differential roles of monkey striatum in learning of sequential hand movement.* Exp Brain Res, 1997. **115**(1): p. 1-5.
39. Francois, C., G. Percheron, and J. Yelnik, *Localization of nigrostriatal, nigrothalamic and nigrotectal neurons in ventricular coordinates in macaques.* Neuroscience, 1984. **13**(1): p. 61-76.
40. Hoover, J.E. and P.L. Strick, *The organization of cerebellar and basal ganglia outputs to primary motor cortex as revealed by retrograde transneuronal transport of herpes simplex virus type 1.* J Neurosci, 1999. **19**(4): p. 1446-63.
41. Geng, D.Y., Y.X. Li, and C.S. Zee, *Magnetic resonance imaging-based volumetric analysis of basal ganglia nuclei and substantia nigra in patients with Parkinson's disease.* Neurosurgery, 2006. **58**(2): p. 256-62; discussion 256-62.
42. Ma, L., M. Gholam Azad, M. Dharmasivam, et al., *Parkinson's disease: Alterations in iron and redox biology as a key to unlock therapeutic strategies.* Redox Biol, 2021. **41**: p. 101896.
43. Pizzino, G., N. Irrera, M. Cucinotta, et al., *Oxidative Stress: Harms and Benefits for Human Health.* Oxid Med Cell Longev, 2017. **2017**: p. 8416763.
44. Sian-Hulsmann, J., S. Mandel, M.B. Youdim, and P. Riederer, *The relevance of iron in the pathogenesis of Parkinson's disease.* J Neurochem, 2011. **118**(6): p. 939-57.
45. Ayton, S. and P. Lei, *Nigral iron elevation is an invariable feature of Parkinson's disease and is a sufficient cause of neurodegeneration.* Biomed Res Int, 2014. **2014**: p. 581256.
46. Gorell, J.M., R.J. Ordidge, G.G. Brown, et al., *Increased iron-related MRI contrast in the substantia nigra in Parkinson's disease.* Neurology, 1995. **45**(6): p. 1138-43.
47. Liu, Z., H.C. Shen, T.H. Lian, et al., *Iron deposition in substantia nigra: abnormal iron metabolism, neuroinflammatory mechanism and clinical relevance.* Sci Rep, 2017. **7**(1): p. 14973.
48. Shi, L., C. Huang, Q. Luo, et al., *The Association of Iron and the Pathologies of Parkinson's Diseases in MPTP/MPP(+)-Induced Neuronal Degeneration in Non-human Primates and in Cell Culture.* Front Aging Neurosci, 2019. **11**: p. 215.

49. Martin-Bastida, A., N.P. Lao-Kaim, C. Loane, et al., *Motor associations of iron accumulation in deep grey matter nuclei in Parkinson's disease: a cross-sectional study of iron-related magnetic resonance imaging susceptibility.* Eur J Neurol, 2017. **24**(2): p. 357-365.
50. Sato, T., J.S. Shapiro, H.C. Chang, R.A. Miller, and H. Ardehali, *Aging is associated with increased brain iron through cortex-derived hepcidin expression.* Elife, 2022. **11**.
51. Ward, R.J., F.A. Zucca, J.H. Duyn, R.R. Crichton, and L. Zecca, *The role of iron in brain ageing and neurodegenerative disorders.* Lancet Neurol, 2014. **13**(10): p. 1045-60.
52. Ndayisaba, A., C. Kaindlstorfer, and G.K. Wenning, *Iron in Neurodegeneration - Cause or Consequence?* Front Neurosci, 2019. **13**: p. 180.
53. Riederer, P., C. Monoranu, S. Strobel, T. Iordache, and J. Sian-Hulsmann, *Iron as the concert master in the pathogenic orchestra playing in sporadic Parkinson's disease.* J Neural Transm (Vienna), 2021. **128**(10): p. 1577-1598.

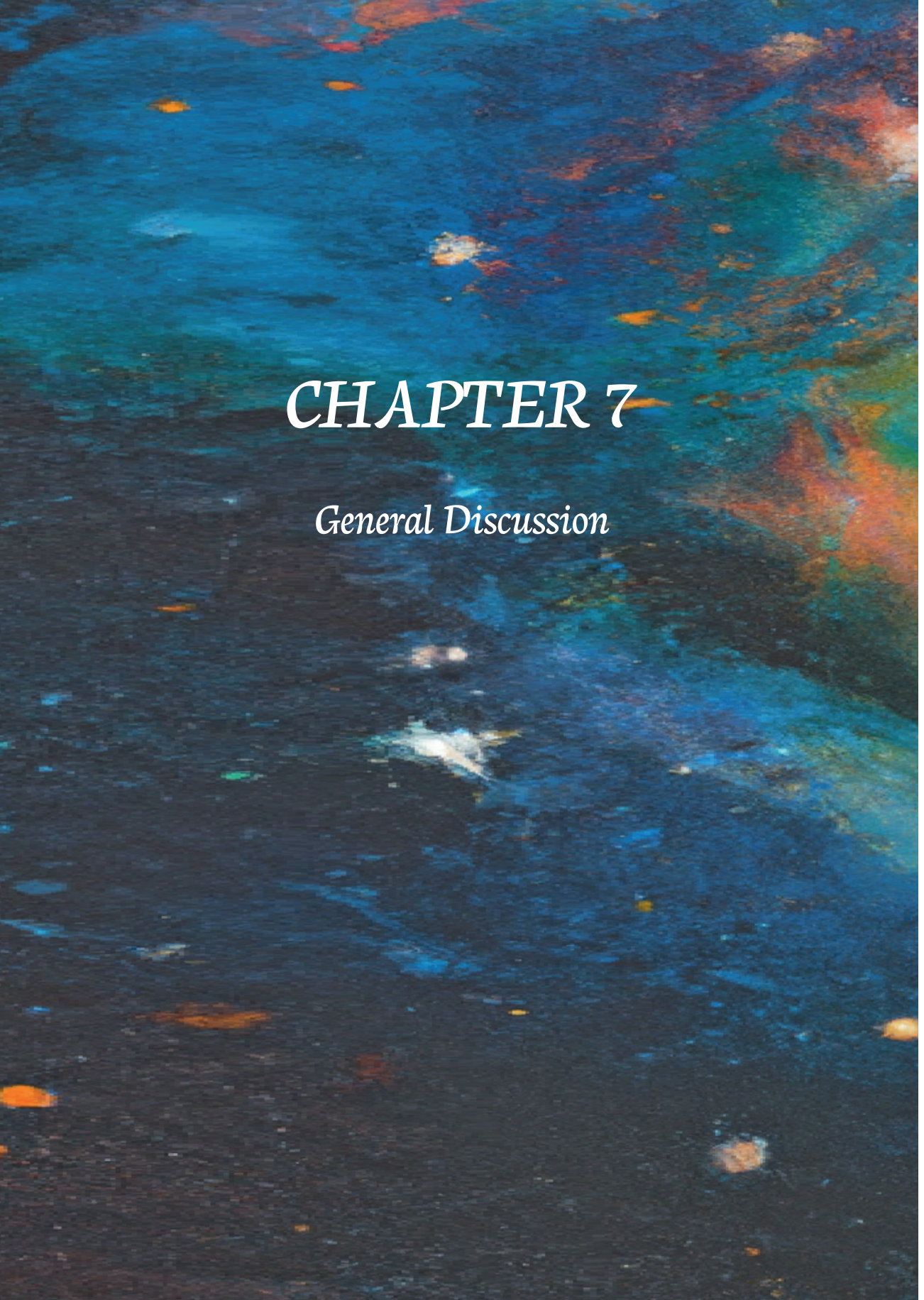

CHAPTER 7

General Discussion

Neuroimaging is a valuable tool in identifying neuronal alterations and predicting symptom manifestation in neurodegenerative diseases. Magnetic resonance imaging (MRI) can identify distinct patterns of neurodegeneration and neuroinflammation in Parkinson's disease (PD) patients and map biomarkers that correlate with clinical symptoms and disease progression. Diffusion imaging also has several advantages in the study of PD including its ability to detect subtle changes in the brain that may not be visible with other imaging techniques of lower resolution, and to map changes in the structure of specific regions of the brain, such as basal ganglia motor areas, to help track the progression of PD throughout the brain over time. Ultra-high field (UHF), or MRI of 7 Tesla and above, has rapidly become a popular technique in the field of neuroscience due to its ability to generate superior visualization of anatomic and functional aspects of the human brain.

Histological techniques have additionally provided valuable insights into the underlying pathology of PD. Through examination of post-mortem brain tissue, pathological features such as Lewy bodies, alpha synuclein aggregation, loss of dopaminergic neurons in the substantia nigra, iron accumulation, and other structural deficits work to unravel cellular mechanisms that contribute PD and distinguish circuitopathies between motor subtypes. Moreover, how these features differentially correlate with one another remains an active area of research. For example, the presence of Lewy bodies correlates with cell loss in the SN, as evidenced by numerous studies, although Lewy bodies are thought to represent a late stage in the disease process only after significant cell loss has occurred. Disentangling the relationship between these alterations, and a growing number of other degenerative biomarkers, could then prove crucial for a better understanding of the pathological mechanisms underlying PD subtypes.

Unravelling the motor circuitopathies in basal ganglia pathways in PD and PD subtypes is a formidable challenge. Pathways include the *direct* pathway (striatum-SNr/globus pallidus interna (GPi)-thalamus-cortex, responsible for motor excitation), the *indirect* pathway (striatum-globus pallidus externa (GPe)-subthalamic nucleus (STN)-SNr/GPi-thalamus-cortex, for motor inhibition), the *hyperdirect* pathway (STN-SNr/GPi-thalamus-cortex, as baseline motor inhibition), and the nigrostriatal projection (SNc-striatum, that is modulatory). The striatum is the main input for the SNr via the *direct* (striatum-SNr) and *indirect* (striatum-GPe-STN-SNr) pathways. Two classical functional hypotheses explaining pathophysiological circuitry underlying movement dysfunction in PD include the 'firing rate' model where dopamine depletion in the BG reduces excitation to striatal *direct* pathways that project to the GPi and reduces tonic inhibition to striatal *indirect* pathways that project to the GPe, and the 'firing pattern' model, suggesting oscillatory and/or synchronized firing patterns in the BG disables the processing and relaying of motor-related information leading to movement dysfunction. Although well thought out,

both models are limited in their ability to explain subtype manifestations, as pathological research does not definitively support the notion that tremor symptoms of PD are mainly caused by dysfunction of the *indirect* loop while bradykinesia is caused by dysfunction of the *direct* pathway.

Nambu et al. (2015) proposed a novel 'dynamic activity' model to reconcile the firing rate and firing pattern models, where signals from the direct pathway disinhibit thalamic neurons in a *center* thalamic area, *hyperdirect* and *indirect* pathways inhibit the *center* area, and *hyperdirect* and *direct* pathways inhibit the *surround* thalamic area. In this model, dopamine depletion is thought to reduce GPi inhibition via the *direct* pathway to the *center* area and facilitate GPi excitation via the *hyperdirect* and *indirect* pathways to the *center* and *surround* areas, leading to a reduction of thalamic and cortical disinhibition and subsequent akinesia. Furthermore, hyperkinetic disorders like tremors are then said to result from the combination of enhanced inhibition to the *center* area of the GPi via the *direct* pathway and reduced excitation via the *hyperdirect* and *indirect* pathways to the *center* and *surround* area causing uncontrolled thalamic and cortical disinhibition. Pathological data from both neuroimaging and histology support this model in how the GPi/SNr and it's subsections receives differential and competitive inputs from the *hyperdirect*, *direct*, and *indirect* pathways that modulate movement. Dissimilar neuropathological depositions in subpopulations of cells in the SN could further topographically underlie the functional variations in this model. Future subcortical and cortical stimulation studies are required to functionally map such striatum-derived inhibition and STN-derived excitation in the GPi to better characterize 'dynamic activity' alterations between PD motor subtypes. Future research should also aim to be complementary in this regard by taking into account various models of motor circuitry modulation, degenerative imaging, and fluctuating clinical presentations.

In recent years, there has been growing interest in combining information from MRI and histological sections of neuronal tissue to create a more comprehensive understanding of neuroanatomy and disease pathology. By identifying specific cellular and molecular mechanisms that contribute to the development and progression of PD, histological findings can be used to design more precise and targeted *in vivo* imaging techniques. For example, the identification of Lewy bodies and alpha-synuclein aggregation in specific brain regions *ex vivo* can lead to the development of more specific imaging protocols aimed at detecting these pathological features *in vivo*. Additionally, the use of histological techniques to identify patterns of neuropathology in motor subtypes of PD can provide a roadmap for designing multimodal imaging studies aimed at characterizing anatomical, functional, and molecular differences and varying subtype trajectories, and further work to identify new targets for therapeutic interventions, preventative strategies employed in early stages, or personalized tuning of late stage care.

However, the process of registering imaging modalities together can be quite challenging due to fundamental differences in contrast and resolution between techniques. MRI provides a non-invasive method for imaging the structure and function of the brain, but its spatial resolution is limited. In contrast, histological sections provide high-resolution images of neuronal tissue but require invasive procedures that can only be performed *ex vivo*. To combine information from these two modalities, researchers must use a process called coregistration that involves aligning the histological sections with the corresponding MRI scans. These processes can be challenging due to different contrasts, resolutions, and unique artifacts and distortions in each imaging modality. Some approaches to improve the registration processes use landmarks and modeling techniques to align and coregister images together. Landmarks are distinctive features in the images that can be used to establish correspondences between the different modalities, while the use of computer modeling techniques aids in the registration process. Despite these advances, there are still significant limitations to multimodal image registration; artifacts and background distortions can make it difficult to align images accurately, and there are often trade-offs between accuracy and speed in registration procedures. Overall, while the integration of MRI and histological sectioning holds great promise for advancing the understanding of neuroanatomy and disease pathology, continued efforts to improve coregistration processes are still necessary before researchers can realize the full potential of this approach.

The PD motor subtypes of TD and nTD have also shown to have substantial clinical variability over time, where after a 4-year follow-up in 325 PD patients, the proportion of recorded nTD patients was shown to have increased significantly, from 23.1% at baseline to 44.2%. Controversies then exist that TD and PIGD are not different PD subtypes but are instead different clinical PD stages with dissimilar disease progression features. Etiological PD models working to incorporate various motor and non-motor symptoms should also look towards including biomarkers such as blood, chemical, imaging, and metabolic markers, as groupings that are more multivariate may produce greater clinical applications and more stable subtyping. This will be aided by the utilization of large and open source data sets.

While MRI has proven to be a valuable tool in the assessment and diagnosis of PD, it too is not without its challenges. One of the main limitations of MRI in PD research is that it is an indirect measure of neural activity and structure. fMRI measures changes in blood flow, which may not accurately reflect the underlying neural activity and function. Furthermore, MRI is limited in its ability to assess the microscopic changes that occur in the brain in PD, such as the degeneration of individual neurons. Another challenge with MRI are technical limitations, such as image quality, scanner variability, and dissimilarity in image processing techniques used across research centers making concatenation of

studies difficult. The interpretation of MRI data can also be subject to bias and influenced by factors such as experience and training. Moreover, the use of MRI in PD research is limited by the availability of large, well-characterized datasets. While the size of MRI datasets in PD research has increased in recent years, there is still a need for larger, more diverse structural and functional datasets to advance our understanding of the role MRI can play in PD detection, monitoring, and treatment. Notwithstanding innate limitations, MRI remains indispensable in the assessment and diagnosis of PD, and has the potential to provide important insights into the neuronal basis of the disease. Further research is needed to address the limitations and challenges of using MRI in PD research and to understand how ultra-high fields (UFH) can be leveraged to advance our knowledge of neurodegenerative imaging.

Likewise, histological examinations are also not flawless; relying on the availability of high-quality post-mortem brain tissue can be challenging, limiting the sample size in studies. Changes in the brain structure that occur post-mortem, such as autolysis and degradation, can further compromise the quality of tissue specimen and lead to a misinterpretation of results. Moreover, histology only provides a snapshot of cellular and molecular changes that have occurred in the brain, characteristically being limited to a single point, thus failing to capture dynamic and progressive changes that occur in PD. Because histological examination is an invasive procedure requiring dissected brain tissue, it is unsuitable for longitudinal or repeated measurements tests or the real-time monitoring of disease progression. Despite these challenges, histology remains a vital tool in PD research, most notably when combined with neuroimaging. Improved dissection techniques and shorter postmortem intervals done to reduce degradation of the tissue will work to enhance future techniques and strengthen results.

This collective research embraces several methodological strengths worth highlighting. Firstly, we utilized a bespoke radio frequency coil during our UHF post-mortem imaging that granted us high-resolution images with exceptional signal-to-noise ratios. The use of UHF has been demonstrated to improve the visualization of microstructures in the brain and has shown to be particularly effective in detecting subtle changes in the nigrostriatal system of PD patients. Another significant strength is our large sample size when compared to many post-mortem imaging studies; a larger sample size increases the statistical power of a study thereby enhancing the ability to detect subtle differences and associations between variables. Lastly, the centralized (in-house) nature of the various routines employed in our research constitutes departmental strength. Centralizing numerous procedures, including tissue preparation, image acquisition, and histological analysis ensures consistency and minimizes variability between experiments. This approach enhances the reproducibility of future results and increases confidence in the accuracy of our findings

Combining information from MRI and histological sections of neuronal tissue can provide a more comprehensive understanding of the neuroanatomy of Parkinson's disease pathology. Advanced anatomical considerations can lead to the development of more specific imaging protocols aimed at detecting pathological features *in vivo*. Researchers and clinicians alike should be optimistic about the future of multimodal neurodegenerative neuroimaging; by developing more specific imaging protocols to detect pathological features in living patients, such work can lead to earlier and more accurate diagnoses and facilitate earlier intervention and personalized treatment plans. Ultimately, this approach has the potential to improve the lives of Parkinson's disease patients and their families by providing more effective and targeted therapies.

CHAPTER 8

Summary

The present thesis was aimed to investigate the neuroanatomical differences between Parkinson's disease (PD) tremor dominant (TD) and non-tremor dominant (nTD) motor subtypes. Findings suggest motor subtypes are associated with distinct neuroanatomical differences in the substantia nigra, the striatum, and in interconnections within. Furthermore, results provide support for the use of advanced MRI techniques and histological analysis in the exploration of PD etiologies. Here, a summary of the studies performed in this thesis is given.

Chapter 1 delivers a general overview of Parkinson's disease, the motor and non-motor symptoms, its prevalence within the human population, clinical diagnostic tools, possible causes and preventative factors, treatment options, the differing motor subtypes, and neurological imaging techniques including magnetic resonance imaging and histological analysis used to study the underlying mechanisms of action. Interdisciplinary research questions were formulated and the outline of subsequent chapters with the overall aims they address is laid out.

Chapter 2 provides a systematic review of previous neuroimaging studies showing diverse functional and structural alterations between TD-PD patients and those with nTD motor subtypes. Divergent pathophysiological, anatomical, and neurochemical mechanisms visible via various neuroimaging regimes across motor subtypes are discussed at length. To our knowledge, this review is the first to evaluate studies of diverse neuroimaging alterations between TD PD patients and those with nTD motor subtypes systemically. Data in this chapter persistently supports the notion that the subtype of TD is the more *benign* subtype as TD shows less negative alternations compared to nTD, while nTD show symptoms that are more aggressive, revealed by earlier and more rapid physical decline.

Main findings further point towards nTD patients having deficits within striato-thalamo-cortical (STC) circuitry and other thalamocortical projections related to cognitive and sensorimotor function, while TD patients show greater cerebello-thalamo-cortical (CTC) circuitry dysfunction. Furthermore, structural connectivity analyses display nTD having alterations of cortico–basal ganglia pathways while TD did not have such alterations, in line with the *"dimmer-switch model"* of PD resting tremor, where pathological activity in the STC from dopaminergic denervation of the GP triggers tremor-related responses in the CTC via the motor cortex where both circuits converge. In this model, the BG acts as a *light switch* triggering tremors on and off, while the CTC modulates the tremors intensity similar to a light dimmer. Results further show depletion of nigrostriatal dopamine and subsequent BG dysfunction alone is insufficient to characterize TD pathology fully. Cerebellular connections functionally and structurally associated with thalamus and pontine nuclei that have shown to synchronize with, mediate, and be directly related to tremor activity, further support the notion that a combination of STC and CTC circuitry

might be behind the generation of tremors in PD. Continued neuroimaging techniques are still required to isolate neural mechanisms underlying PD motor symptomologies. Such work will continue to aid in refining antemortem diagnoses and improve epidemiological and clinical-therapeutic trial designs.

In **Chapter 3**, the designing and implementation of a dedicated container for scanning postmortem brains in ultra-high field magnetic resonance imaging (UHF-MRI) scanners is presented. While postmortem imaging holds several challenges including altered T1 and T2 relaxation times as well as achieving optimized imaging contrasts at high resolution, it also grants advantages to *in vivo* measurements including longer scan times, less motion and physiological noise artifacts, and greater signal to noise ratios (SNR). During the development process, several considerations were made to optimize the container to be easy to use within MR facilities and engender high quality images with a low number of artefacts. The container proved to have the necessary qualifications needed for postmortem imaging including ease of transportation, vacuum sealing capabilities, and compatibility with previously designed sequences and procedures. Imaging procedures using a custom gradient echo (GRE) pulse sequence that utilize composite parallel excitation pulses with kT-points proved effective in acquiring high resolution T2* weighted data at 250 μm and diffusion weighted (DWI) data at 1 mm. Raw DWI scans had enough information to reconstruct structural white matter connections and grant us the ability to form a tractogram. Improvements to obtain even greater image quality including improved positioning of the tissue within the container and longer scanning times are mentioned, and the feasibility of this method not being limited by MRI magnet field strength is further discussed.

In **Chapter 4,** the findings of an ultra-high field diffusion imaging study on twelve post-mortem hemispheres (eight parkinsonian (four TD, four nTD) and four healthy controls) scanned with a specialized 9.4T human post-mortem brain radiofrequency coil are presented. Diffusion tensor analysis was performed for local scalar diffusion metrics and constrained spherical deconvolution (CSD) tractography was performed for global connectivity metrics. Previous studies investigating PD subtypes mainly employed lower field strengths (1.5-3T) *in vivo* while here we utilized 9.4T *ex vivo* imaging that granted us better resolution and allowed us to measure diffusion related discrepancies with refined spatial detail.

Our findings imply fundamental differences in neural mechanisms between motor subtypes in the latest stages of PD and support subtypes undergoing varied therapeutic approaches given their diverse etiologies. Results further support the notion that TD patients may show less negative alternations compared to nTD through neural reorganization. More specifically, our findings show the internal capsule may act as

a crossroads in networks involved in tremor symptoms while its diffusion variations may be a key pattern in the *fingerprint* of anatomical circuitopathy distinguishing PD motor subtypes. Several variations specific to PD motor subtypes found could also be quantifiable *in vivo* with clinical MR sequences and hold further translational value in detecting specific circuitopathy underlying PD motor subtype degeneration. Such a *fingerprint* would be multidisciplinary and encompass integrated anatomical, functional, and network influences, as well as clinical and chemical analyses to generate a more specified circuitopathy model for personalized information-based treatment. We hope future clinical tractography studies will elaborate on the role capsular fibers play during treatment selection and network analysis.

Chapter 5 presents a scoping review of previous literature comparing TD and nTD PD motor subtypes pathologically, using histological and immunohistochemical techniques. It is written with the aim to clarify observed pathology with underlying physiological circuitry theories. Results show an array of pathological examination techniques display significant differences between TD and nTD PD subtypes. In short, nTD PD patients show higher neuronal loss, gliosis, extraneuronal melanin deposits, and neuroaxonal dystrophy in multiple subregions of the substantia nigra (SN) related to the overactivity of the indirect motor loop, while TD patients show more severe cell loss specifically in medial SN subdivisions, and have damage in the retrorubral field A-8 that projects to the dorsolateral striatum and ventromedial thalamus in the direct motor loop.

Pathological studies show to be consistent with neuroimaging data and support contemporary mechanistic circuitry theories of PD motor symptom genesis. More specifically, pathological differences between PD subtypes in the SN support the '*dynamic activity*' model of PD symptom genesis; SN pathology may sustain the proposed center-surround topographical distribution of striatum-derived inhibition on the GPi/SNr that is correlated to motor disabilities. Such findings hold clinical implications in support of pathocircuitries and towards novel targets for treatment and interventions. Further multimodal neuroimaging and histological studies are still required to validate and expand upon these findings.

In **Chapter 6,** the findings of a histological study on the same twelve post-mortem hemispheres scanned in **Chapter 4** are presented and contrasted with the MRI data. Findings of this study demonstrate various histological metrics including cell density, volumetrics, and iron depositions are stratified across motor subtypes and may correlate with differential neurodegeneration. Results are mixed compared to MRI data most likely due to small sample sizes, large postmortem intervals, and extended tissue fixation periods of the tissue. The value of utilizing multimodal imaging to investigate anatomical changes in the brains of individuals who suffered from PD is further discussed. In short,

examining post-mortem tissue with histo- and radiological imaging methods provides a unique opportunity to understand the underlying structural changes that contribute to the clinical manifestations of PD and its motor subtypes.

In **Chapter 7**, a general discussion is given to provide an overview of the studies performed in this thesis, to reflect on the multimodal imaging methodologies used, and to provide a future perspective within the field.

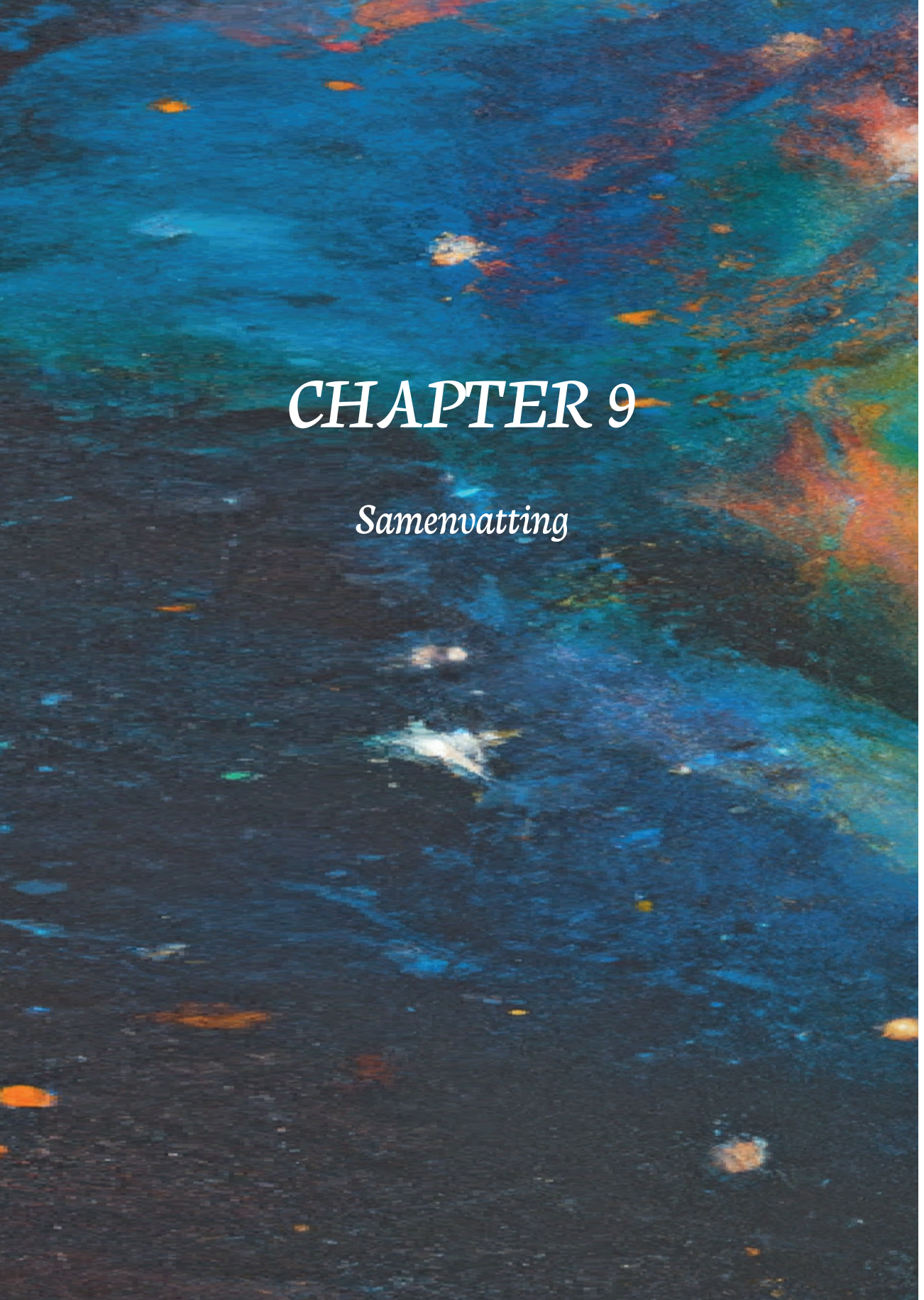

CHAPTER 9

Samenvatting

Dit proefschrift heeft tot doel de neuroanatomische verschillen tussen de motorische subtypes van de ziekte van Parkinson (PD), tremor dominant (TD) en niet-tremor dominant (nTD), te onderzoeken. De bevindingen suggereren dat motorische subtypes geassocieerd zijn met verschillende neuroanatomische verschillen in de substantia nigra, het striatum en in de onderlinge verbindingen daartussen. Bovendien bieden de resultaten steun voor het gebruik van geavanceerde MRI-technieken en histologische analyse bij het onderzoek naar de etiologie van PD. Hier wordt een samenvatting gegeven van de in dit proefschrift uitgevoerde studies.

Hoofdstuk 1 geeft een algemeen overzicht over de ziekte van Parkinson, de motorische en niet-motorische symptomen, de prevalentie binnen de menselijke bevolking, klinische diagnostische instrumenten, mogelijke oorzaken en preventieve factoren, behandelingsmogelijkheden, de verschillende motorische subtypes, en neurologische beeldvormingstechnieken, waaronder magnetische resonantiebeeldvorming en histologische analyse, die worden gebruikt om de onderliggende werkingsmechanismen te bestuderen. Er zijn interdisciplinaire onderzoeksvragen geformuleerd en de opzet van de daaropvolgende hoofdstukken met de algemene doelstellingen die zij beogen is uiteengezet.

Hoofdstuk 2 geeft een systematisch overzicht van eerdere neuroimaging studies die diverse functionele en structurele verschillen laten zien tussen TD-PD patiënten en patiënten met nTD motorische subtypes. Uiteenlopende pathofysiologische, anatomische en neurochemische mechanismen die zichtbaar zijn met verschillende neuroimaging methoden in de motorische subtypes worden uitvoerig besproken. Voor zover ons bekend, is dit overzicht het eerste dat studies van uiteenlopende neuroimaging verschillen tussen TD PD patiënten en patiënten met nTD motorische subtypes systematisch evalueert. De gegevens in dit hoofdstuk blijven de opvatting ondersteunen dat het subtype TD het meer goedaardige subtype is, aangezien TD minder negatieve alternaties vertoont dan nTD, terwijl nTD symptomen vertonen die agressiever zijn, wat blijkt uit een vroegere en snellere lichamelijke achteruitgang.

De belangrijkste bevindingen wijzen er verder op dat nTD-patiënten beperkingen hebben binnen de striato-thalamo-corticale (STC) circuits en andere thalamocorticale projecties die verband houden met cognitieve en sensomotorische functies, terwijl TD-patiënten een grotere cerebello-thalamo-corticale (CTC) disfunctie vertonen. Verder blijkt uit structurele connectiviteitsanalyses dat nTD veranderingen hebben in de cortico-basale ganglia paden, terwijl TD dergelijke veranderingen niet hebben, in overeenstemming met het "dimmer-switch model" van PD-tremor in rust, waarbij pathologische activiteit in de STC door dopaminerge denervatie van de globus pallidus (GP) tremor-gerelateerde reacties in de CTC uitlokt via de motorische cortex waar beide circuits samenkomen. In dit model werkt de basale ganglia (BG) als een lichtschakelaar die tremor in- en uitschakelt, terwijl

de CTC de intensiteit van de tremor moduleert als een lichtdimmer. De resultaten tonen verder aan dat de uitputting van nigrostriatale dopamine en de daaruit voortvloeiende disfunctie van de BG alleen onvoldoende is om de pathologie van TD volledig te karakteriseren. Cerebellaire verbindingen die functioneel en structureel verbonden zijn met kernen van de thalamus en de pontine en waarvan is aangetoond dat ze synchroniseren met, mediëren bij en rechtstreeks verband houden met tremoractiviteit, ondersteunen verder het idee dat een combinatie van STC- en CTC-circuits ten grondslag ligt aan het ontstaan van tremor bij PD. Om de neurale mechanismen die ten grondslag liggen aan de motorische symptomen van PD te isoleren zijn nog meer neurobeeldvormende technieken nodig. Dergelijk werk zal blijven bijdragen tot het verfijnen van antemortem diagnoses en het verbeteren van epidemiologische en klinisch-therapeutische proefopzetten.

In **hoofdstuk 3** wordt het ontwerp en de implementatie van een speciale container voor het scannen van postmortale hersenen in UHF-MRI-scanners gepresenteerd. Hoewel postmortale beeldvorming een aantal uitdagingen inhoudt, waaronder gewijzigde T1- en T2-relaxatietijden en het bereiken van optimale beeldvormingscontrasten bij hoge resolutie, biedt het ook voordelen ten opzichte van in vivo metingen, waaronder langere scantijden, minder bewegingsartefacten en fysiologische ruis, en een grotere signaal-ruis-verhouding (SNR). Tijdens het ontwikkelingsproces zijn verschillende overwegingen gemaakt om de container te optimaliseren zodat hij gemakkelijk te gebruiken is binnen MR-faciliteiten en beelden van hoge kwaliteit oplevert met een laag aantal artefacten. De container bleek de nodige voordelen te hebben voor postmortale beeldvorming, waaronder transportgemak, vacuümafsluiting en compatibiliteit met eerder ontworpen sequenties en procedures. Beeldvormingsprocedures met een aangepaste gradiënt-echo (GRE) pulssequentie die gebruik maakt van samengestelde parallelle excitatiepulsen bleken effectief in het verkrijgen van hoge resolutie T2* gewogen beelden op 250 µm en diffusie gewogen (DWI) gegevens op 1 mm. De ruwe DWI-scans bevatten voldoende informatie om structurele verbindingen in de witte stof te reconstrueren en ons in staat te stellen een tractogram te vormen. Verbeteringen om een nog betere beeldkwaliteit te verkrijgen, waaronder een betere positionering van het weefsel in de container en langere scantijden, worden genoemd, en de haalbaarheid van deze methode die niet wordt beperkt door de sterkte van het MRI-magneetveld wordt verder besproken.

In **hoofdstuk 4** worden de bevindingen gepresenteerd van een ultra-hoogveld diffusie MRI beeldvormend onderzoek op twaalf postmortale hemisferen (acht parkinsonpatienten (vier TD, vier nTD) en vier gezonde controles) gescand met een gespecialiseerde 9,4T menselijke postmortale hersenspoel. Diffusie tensor analyse werd uitgevoerd voor lokale diffusie maten en zogenaamde constrained spherical deconvolution (CSD) tractografie werd uitgevoerd voor globale connectiviteit maten. Eerdere studies naar PD-subtypen maakten voornamelijk gebruik van lagere veldsterktes (1,5-3T) in vivo, terwijl wij hier

gebruik maakten van 9,4T ex vivo beeldvorming die ons een betere resolutie gaf en ons in staat stelde diffusie gerelateerde discrepanties te meten met verfijnd ruimtelijk detail.

Onze bevindingen wijzen op fundamentele verschillen in neurale mechanismen tussen motorische subtypes in de laatste stadia van PD en ondersteunen subtypes die verschillende therapeutische benaderingen vragen gezien hun uiteenlopende etiologie. De resultaten ondersteunen verder de notie dat TD patiënten minder negatieve veranderingen kunnen vertonen in vergelijking met nTD door neurale reorganisatie. Meer specifiek tonen onze bevindingen aan dat het interne kapsel kan fungeren als een kruispunt in netwerken die betrokken zijn bij tremorsymptomen, terwijl de diffusievariaties ervan een belangrijk patroon kunnen zijn in de vingerafdruk van anatomische circuit pathologie (circuitopathie) die motorische PD-subtypes onderscheidt. Verschillende variaties die specifiek zijn voor motorische PD-subtypen zouden ook in vivo kunnen worden gekwantificeerd met klinische MR-sequenties en hebben verdere translationele waarde bij het opsporen van specifieke circuitopathie die ten grondslag ligt aan degeneratie van het motorische PD-subtype. Een dergelijke biomarker zou multidisciplinair zijn en geïntegreerde anatomische, functionele en netwerkinvloeden omvatten, alsmede klinische en chemische analyses om een meer gespecificeerd circuitopathiemodel te genereren voor gepersonaliseerde, op informatie gebaseerde behandeling. Wij hopen dat toekomstige klinische tractografie studies dieper zullen ingaan op de rol die capsulaire vezels spelen bij behandelingsselectie en netwerkanalyse.

Hoofdstuk 5 geeft een overzicht van eerdere literatuur waarin de motorische subtypen TD en nTD PD pathologisch worden vergeleken, met behulp van histologische en immunohistochemische technieken. Het is geschreven met het doel de waargenomen pathologie te verduidelijken met onderliggende fysiologische circuittheorieën. De resultaten wijzen op een reeks pathologische onderzoekstechnieken die significante verschillen laten zien tussen TD en nTD PD subtypes. Kortom, nTD PD patiënten vertonen meer neuronaal verlies, gliose, extraneuronale melanine afzettingen, en neuroaxonale dystrofie in meerdere subregio's van de substantia nigra (SN) gerelateerd aan de overactiviteit van de indirecte motorische lus, terwijl TD patiënten ernstiger celverlies vertonen specifiek in mediale SN subdivisies, en schade hebben in het retrorubrale veld A-8 dat projecteert naar het dorsolaterale striatum en ventromediale thalamus in de directe motorische lus.

Pathologische studies blijken consistent te zijn met neuroimaging gegevens en ondersteunen hedendaagse mechanistische circuittheorieën over het ontstaan van motorische symptomen in PD. In meer detail, ondersteunen pathologische verschillen tussen PD subtypes in de SN het 'dynamische activiteit' model van het ontstaan van PD symptomen; SN pathologie kan de voorgestelde centrum-surround topografische distributie van striatum-afgeleide inhibitie op de globus pallidus pars interna/substantia nigra pars reticulata

ondersteunen die gecorreleerd is met motorische handicaps. Dergelijke bevindingen hebben klinische implicaties ter ondersteuning van pathologische circuits en wijzen naar nieuwe richtingen voor behandeling en interventies. Verdere multimodale neuroimaging en histologische studies zijn nog nodig om deze bevindingen te valideren en uit te breiden.

In **hoofdstuk 6** worden de bevindingen van een histologisch onderzoek op dezelfde twaalf postmortale hemisferen die in **hoofdstuk 4** zijn gescand, gepresenteerd en gecontrasteerd met de MRI-gegevens. De bevindingen van dit onderzoek tonen aan dat verschillende histologische metrieken, waaronder celdichtheid, volumetrie en ijzerafzettingen, gelaagd zijn over de motorische subtypen en kunnen correleren met differentiële neurodegeneratie. De resultaten zijn gemengd in vergelijking met MRI-gegevens, waarschijnlijk door de kleine steekproefgrootte, de lange postmortale intervallen en de langere fixatieperiode van het weefsel. De waarde van het gebruik van multimodale beeldvorming om anatomische veranderingen te onderzoeken in de hersenen van personen die aan PD leden, wordt verder besproken. Kortom, het onderzoek van postmortaal weefsel met histologische en radiologische beeldvormingsmethoden biedt een unieke gelegenheid om inzicht te krijgen in de onderliggende structurele veranderingen die bijdragen tot de klinische manifestaties van PD en de motorische subtypes daarvan.

In **hoofdstuk 7** wordt een algemene discussie gegeven om een overzicht te geven van de in dit proefschrift uitgevoerde studies, om te reflecteren over de gebruikte multimodale beeldvormingsmethoden en om een toekomstperspectief te bieden binnen het vakgebied.

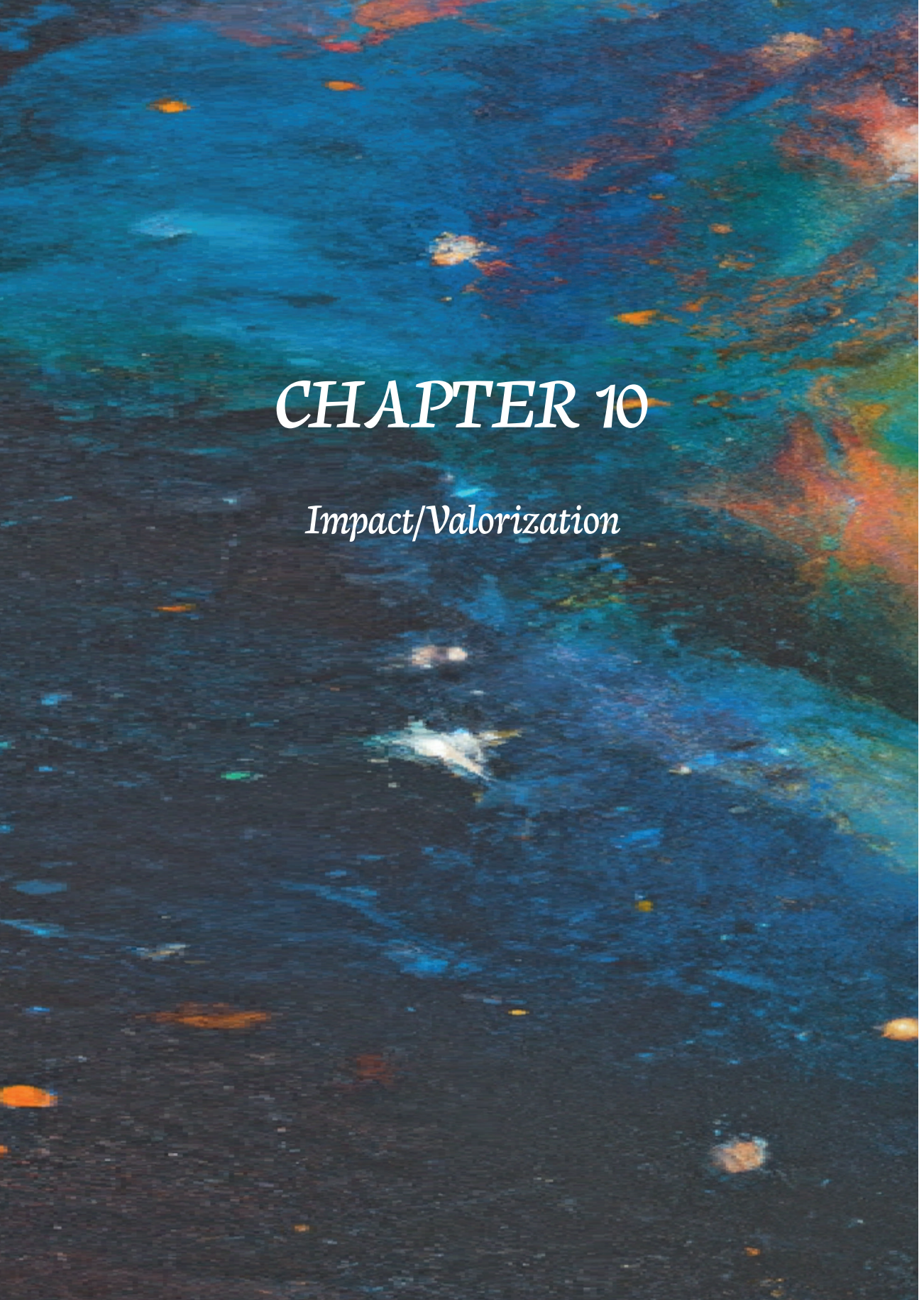

CHAPTER 10

Impact/Valorization

Parkinson's disease (PD) is a progressive and complex neurodegenerative disorder. PD patients show highly heterogeneous clinical characteristics and can be categorized into diverse motor subtypes based on clinical symptom presentation. Variable presentations of symptoms suggest divergent pathophysiological, neuroanatomical, and neurochemical mechanisms during disease progression. Moreover, patients with non-tremor dominant (nTD) symptoms display more aggressive alternations compared to TD revealed by earlier and more rapid physical decline, and report lower overall quality of life scores. The success and efficiency of a variety of available Parkinsonian treatment options ranging from pharmacological to neurosurgical also differ between subtypes. Therefore, generating a more comprehensive understanding of the neuroanatomical mechanisms underlying various motor subtypes in PD can then work towards creating more tailored treatments for subtypes, improve monitoring abilities as symptoms progress, and possibly even identify the disease at an earlier asymptomatic stage.

Deep brain stimulation (DBS) surgery is an invasive and effective treatment option for PD patients. However, the nuclei targeted with the neurostimulator during DBS surgery have neighboring small structures that can be difficult to differentiate using conventional MRI techniques. UHF-MRI then offers a promising solution to this problem by providing higher spatial resolution and greater contrast-to-noise ratios (CNR), thus improving the targeting of deep brain nuclei by offering better visual differentiating between neuronal structures adjacent to one another. This can enable clinicians to target the affected areas more precisely during surgery and improve therapeutic outcomes for patients. UHF imaging can additionally aid in parcellating interconnected neuronal clusters leading to a more comprehensive understanding of the neuroanatomy of PD and PD motor subtype pathology and progression. The use of UHF imaging techniques in combination with DBS surgery for PD, therefore, has the potential to revolutionize the field and lead to better outcomes for patients.

Ex vivo MRI of large neuronal tissue can be a valuable tool for improving *in vivo* MRI of PD patients. *Ex vivo* MRI obtains higher-resolution images of the brain with greater detail and accuracy than *in vivo* MRI allows as it can be performed with longer imaging times and without the limitations imposed by motion artifacts or physiological noise. More accurate maps of brain anatomy, such as the size, shape, and variation of different brain regions, as well as more detailed maps of brain connectivity involving distributed white matter tracts, grants researchers and clinicians the ability to better identify and map structural changes that have occurred in those who suffered with PD. By comparing *in vivo* scans with the detail *ex vivo* MRI scans permit, neuroscientists can identify new biomarkers specific to PD to be used to improve the accuracy of *in vivo* MRI biomarkers in the diagnosis and progression tracking of living PD patients. Alongside detailed clinical histories, *ex vivo* MRI can provide a more accurate and comprehensive assessment of the changes that occur

in the disease over time by comparing images of brain tissue from individuals with PD at different stages of the disease and those with various motor and non-motor subtypes. Advanced MR processing and analysis techniques, once and currently reserved for *ex vivo* research purposes, can be further used to inform and improve *in vivo* MRI sequences and ultimately develop better diagnostic and monitoring tools for PD.

In our department there is currently a longitudinal, observational, ultra-high field MRI study in PD patients entitled 'TRACK-PD' with the aim to make important contributions and improvements to the current diagnostic process in PD. The research will take four years and involve three test days where participants will undergo memory tests, fill in questionnaires, wear motion sensors, and have brain scans. More specifically, the project aims to 1) identify distinctive MRI characteristics in PD patients and to create a diagnostic tool based on these differences, to 2) correlate MRI characteristics to clinical phenotype, genetics, and progression of symptoms, and to 3) detect future imaging biomarkers for disease progression that could be valuable for the evaluation of new therapies. TRACK-PD is part two of a tripartite work package in combination with the results of this thesis (part one) to better understand PD and to develop new biomarkers for disease progression to aid in future therapy development. Eventually, these combined projects may lead to better predictive models for individual PD patients and push the field closer to more personalized medicine.

The clinical variability for the PD motor subtypes TD and nTD is substantial, particularly for the postural instability and gait difficulty (PIGD) subtype. It has been suggested that TD and PIGD are not different PD subtypes but rather different clinical stages with dissimilar disease progression features. Therefore, moving forward, conventional PD motor subtyping may not have proficient clinical applicability. Multivariate groupings that incorporate various motor and non-motor symptoms as well as other biomarkers may produce greater clinical applications and prove more stable over time. However, it is still unknown exactly why certain subpopulations of cells in particular nuclei undergo different degeneration patterns within each PD subtype, what initiates these divergences, whether they are a cause or a consequence of other co-occurring pathogenic mechanisms, and how they may be best targeted for treatment. To address these issues, multidisciplinary and translational approaches are necessary. Combining the expertise of neurologists, neuroscientists, radiologists, and other medical specialists, as is done here, will lead to a better understanding of PD and its various subtypes. Translational research that bridges the gap between fundamental science and clinical application is crucial for identifying and developing effective therapies that target the underlying mechanisms within each PD motor subtype. Furthermore, non-motor symptoms such as sleep disorders, gastrointestinal dysfunction, and cognitive impairments are common in PD and significantly affect patients' quality of life. Therefore, a more comprehensive approach

that incorporates both motor and non-motor symptoms is necessary to provide care that is more effective for all PD patients.

In this thesis, advanced multimodal neuroimaging techniques have been developed to study anatomical variation in PD motor subtypes and have opened up new avenues of neurodegenerative research to shed light on underlying mechanisms. While fine-tuning imaging parameters and the coregistration of images is a challenging task, cutting-edge technologies in both MR and histology have been developed to address these issues. The enormous amounts of data generated by these techniques pose a challenge for storage and analysis, but new methods for handling these large datasets are being developed, and will one day prove indispensable for proper patient care. In addition to various structural data, the future inclusion of functional data, behavioral phenotypes, and biochemical analyses will provide a more comprehensive understanding of the disease along with its dynamic motor and non-motor subtypes. As the field of neurodegenerative imaging continues to progress, we have hope these advancing techniques will lead to the development of more effective diagnostic and treatment strategies, and one day, ultimately rid the world of Parkinson's disease.

CHAPTER 11

Curriculum Vitae

Jackson Tyler Boonstra was born March 3rd, 1994 in Cambridge, Massachusetts. He graduated from Arlington High School (2012) receiving varsity letters in track and cross country and completing Psychology and English honors courses. He attended Fitchburg State University joining leadership roles in the Psychology Club and the Psychological Science Curriculum Committee. There, he obtained a Bachelor's of Science (2016) in Psychological Science, *cum laude,* with a minor in biology focusing on cognitive sciences. Following graduation he was accepted into de Universiteit van Amsterdam (The University of Amsterdam) for a Research Master's program in Brain and Cognitive Sciences. In his first internship in the Psychology Department under the supervision of dr. J. (Janna) Cousijn of the Faculty of Social and Behavioural Science, he researched magnetic resonance imaging and cannabis dependency. His following literature thesis focused on temporary cannabinoid use for patients with PTSD under the supervision of Prof dr. HGJM (Eric) Vermetten MD, researcher at the Military Mental Health Service of the Dutch Ministry of Defense, and under the co-supervision of dr. H.J. (Harm) Krugers, the program director of his research master. During his second internship he worked for Het Nederlands Herseninstituut (The Netherlands Institute for Neuroscience (KNAW)) under the director Prof dr. Dick Ferdinand Swaab MD, founder of the Nederlandse Hersenbank (The Dutch Brain Bank). There he studied histological and sexual dimorphisms in Alzheimer's disease on postmortem neuronal tissue. Upon completion, he was hired temporarily to continue the project. After graduating his Master's degree (2018) under the cognitive neuroscience track, he obtained a PhD candidacy position at Maastricht University in the Department of Neurosurgery supervised by prof dr. Yasin Temel MD, and dr. Ali Jahanshahianvar. His project focused on investigating magnetic resonance imaging and immunohistochemical markers within postmortem hemispheres of Parkinson's disease motor subtypes. Utilizing the available 9.4 Tesla MRI at the Maastricht Health Campus, and conducting subsequent histological analyses in the Faculty of Health, Medicine and Life Sciences, he incorporated multimodal imaging techniques to better understand the microstructure of disease related neuronal areas. During his candidacy, he was a member of the International Parkinson and Movement Disorder Society alongside being webmaster and social media coordinator for the Deep Brain Stimulation Society. He supervised technical students, presented at international conferences, and sat on the PhD representative committee of the School for Mental Health and Neuroscience. He defended his PhD on June 26th, 2023.

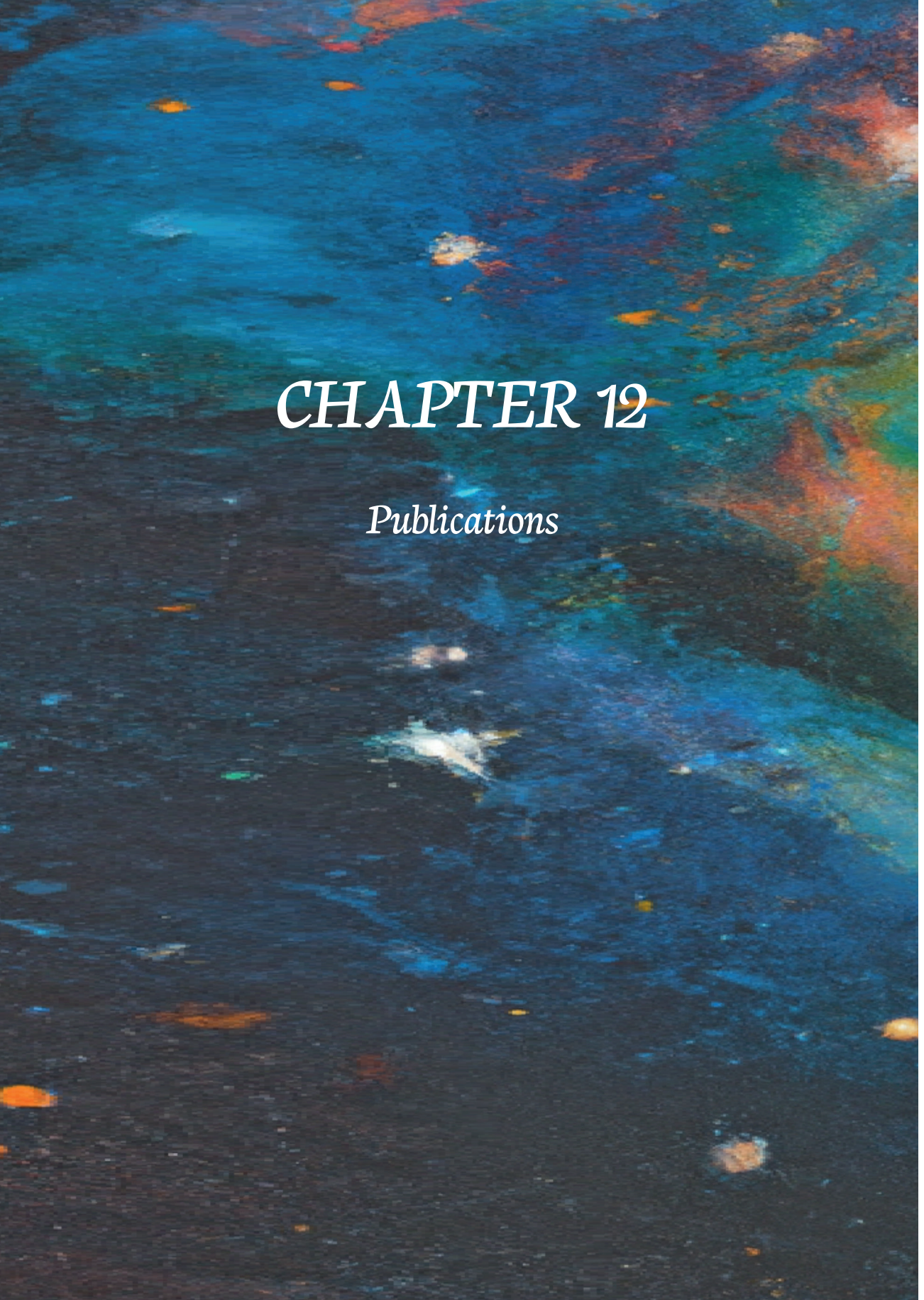

CHAPTER 12

Publications

First Author

Boonstra JT, Michielse S, Temel Y, Hoogland G, Jahanshahi A. Neuroimaging detectable differences between Parkinson's disease motor subtypes: a systematic review. *Movement disorders clinical practice 8 (2), 175-192, 2021.*

Boonstra JT, Michielse S, Roebroeck A, Temel Y, Jahanshahi A. Dedicated container for postmortem human brain ultra-high field magnetic resonance imaging. *Neuroimage 235, 118010, 2021.*

Boonstra JT, McGurran H, Temel Y, Jahanshahi A. Nigral neuropathology of Parkinson's motor subtypes coincide with circuitopathies: a scoping review. *Brain Structure and Function 227 (7), 2231-2242, 2022.*

Co-Author

Bao AM, Hu YT, Chen XL, Huang SH, **Boonstra J**, McGurran H, Swaab D. Early growth response-1 stimulates acetylcholinesterase during the course of Alzheimer's disease. *IBRO Reports 6, S490-S491, 2019.*

Roet M, **Boonstra J**, Sahin E, Mulders AEP, Leentjens AFG, Jahanshahi A. Deep brain stimulation for treatment-resistant depression: Towards a more personalized treatment approach. *Journal of Clinical Medicine 9 (9), 2729, 2020.*

Liu H, Temel Y, **Boonstra J**, Hescham S. The effect of fornix deep brain stimulation in brain diseases. *Cellular and Molecular Life Sciences 77, 3279-3291, 2020.*

Hu YT, **Boonstra J**, McGurran H, Stormmesand J, Sluiter A, Balesar R, Verwer R, Swaab D, Bao A. Sex differences in the neuropathological hallmarks of Alzheimer's disease: focus on cognitively intact elderly individuals. *Neuropathology and Applied Neurobiology 47 (7), 958-966, 2021.*

Son G, Jahanshahi A, Yoo SJ, **Boonstra JT**, Hopkins DA, Steinbusch HWM, Moon C. Olfactory neuropathology in Alzheimer's disease: A sign of ongoing neurodegeneration. *BMB reports 54 (6), 295, 2021.*

Alosaimi F, **Boonstra JT**, Tan S, Temel Y, Jahanshahi A. The role of neurotransmitter systems in mediating deep brain stimulation effects in Parkinson's disease. *Frontiers in Neuroscience 16, 2022.*

Jahanshahi A, **Boonstra J**, Alosaimi F, Ozsoy O, Michielse S, Temel Y. Hidden brain atrophy in ultra-high-field MR images in a transgenic rat model of Huntington's disease. *Brain Disorders, 2022.*

In-progress:

Boonstra JT, Michielse S, Temel Y, Jahanshahi A*, Roebroeck A*. Ultrahigh field MRI of Parkinsonian post-mortem human brains. *Under review.*

Boonstra JT, Temel Y, Alosaimi F, Roebroeck A, Jahanshahi A. Neuropathological imaging aspects of Parkinson's disease motor subtypes. *In preparation.*

*These authors contributed equally

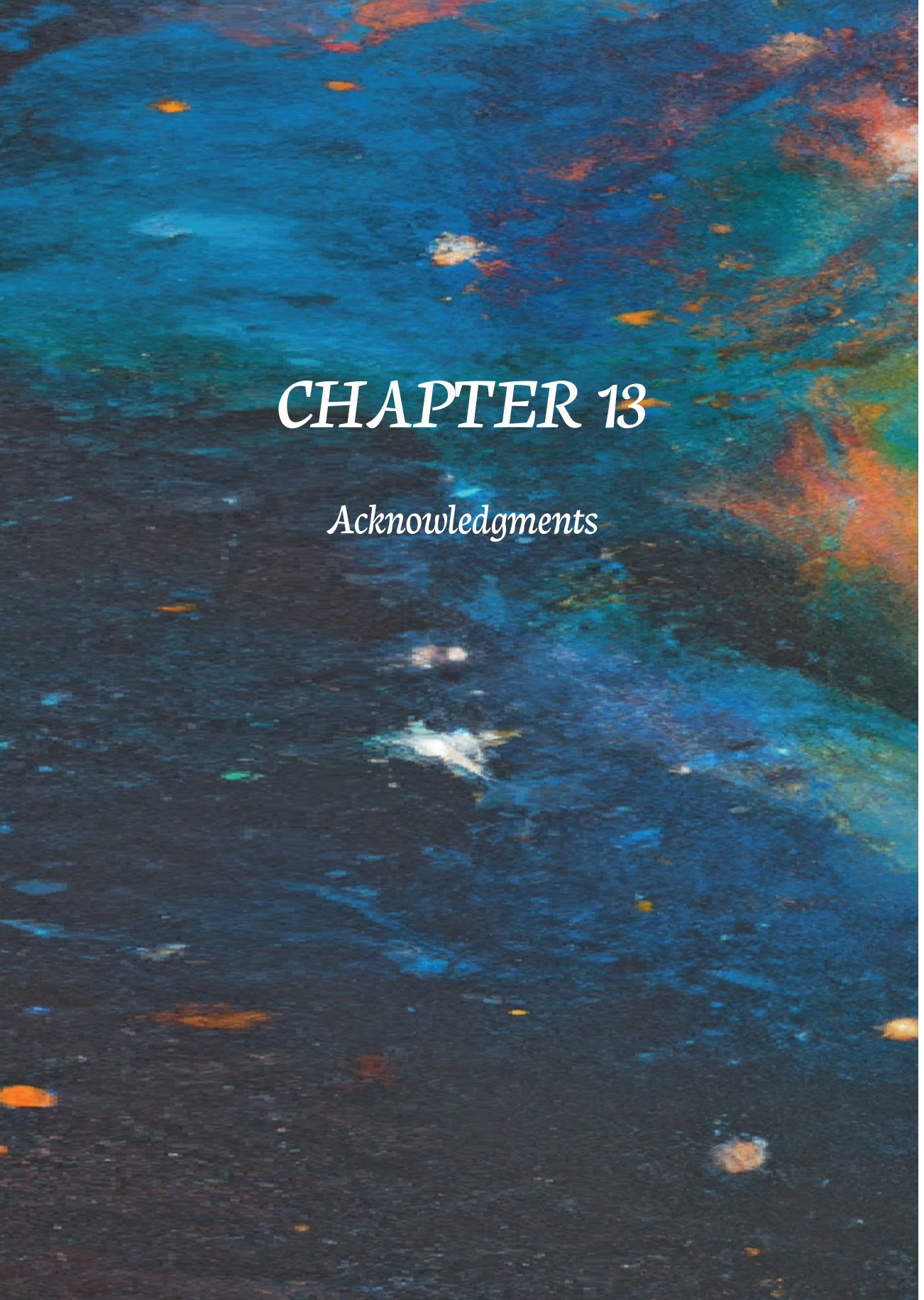

CHAPTER 13

Acknowledgments

To my supervisor team,

My first and largest thank you goes to **Ali**, for you were the perfect supervisor. I often don't use the word perfect, but you hit the mark. You trusted me, guided me, and believed in my scientific spirit. I always felt and still feel that I can talk to you about any challenge and we will work it out together. I hope our professional and personal friendship continues for many years to come.

To **Yasin**, a mentor one can only dream of having. You've taught so many things in the last four and a half years, from academic pros to managerial insights. I am humbled to have been under your wing for so long. Thank you for teaching me all that you have.

To **Alard**, I am forever grateful. This project would not have flown so high had it not been for your expertise and discernment in design and execution. Thank you for our pragmatic and productive one-on-ones and positivity all throughout.

To my paranymphs,

Daan, words cannot express how thankful and happy I am to have shared an office with you for all these years. From the off-topic chats we would have to the gossip we'd share, every conversation and occurrence was positive, friendly, joyful, and sincere. You made me look forward to coming to work. I wish nothing but the best and greatest life and happiness for you and your family forever and ever.

To **Berkhan**, my newest best friend. While we have only known each other for a few months, every interaction has made me smile. We have shared laughs, stories, drinks, and secrets with each other as if we were lifelong friends. I cherish our friendship deeply. Thank you for everything.

To my research group,

Faisal, my closest coworker. I will never forget the long hours in the lab together, that didn't feel like long hours because we just talked so naturally about life. I learned so much from you, about science, religion, and family. Thank you for being such so cool.

To **Faris**, thank you for welcoming me into your office, your life, and your work. Since meeting you I have respected your work ethic and friendly nature. I hope our paths cross again in the future.

To **Govert**, I thank you for your support and wisdom during my time here. I always found it cool you'd have the lights off in your office, radio on, hammering out work. I am very happy we have a publication together and will miss you sincerely when I am gone.

To the rest of my 5 star group, **Christian**, **Sarah, Mark, Linda, Stijn, Pieter, Kim, Liu, Jana, Danielle, Anouk, Amée, Dani, Felix, David,** thank you all for being such wonderful colleagues and making my scientific work that much more powerful.

To my friends back home,

Aaron Breen; Master Breen, Ruler of the Skies, Emperor of the Unknown. After all these years, thank you for still being friends with me, and for the comment *"You are one of the smartest people I know but you dress like a homeless person."* that lives rent free in my head. You're continuous support, detailed (yet unfounded) critiques, and full-hearted friendship throughout my life has given me hope, strength, and wisdom through many obstacles. I promise to always be there for you, as you have been for me, as we continue to support one another into a prosperous yet mysterious future. You are also better at guitar than me and always will be, but I am still older.

Eli, thank you for your lifelong friendship, boundless creativity, and pertinacious spirit. You have taught me many valuable life lessons I still live by and with. I have enjoyed being your friend every single day of my life and I hope that remains forever.

To Alex **Verspyck,** my homie. Every second with you is pure joy. From gaming to driving to vibing to going out to shopping to eating and drinking and talking, you're a true true friend. Thank you for being who you are. Penguin hug.

To my brother **Alexander** and his wife **Elizabeth**, thank you for being a perfect couple, wonderful people, and such great siblings towards me. To my niece **Kennedy,** I am going to spoil you rotten when you are older.

To **Alec**, thank you for being there for me through thick and thin. Regardless if I'm across the pond or back home, we will travel odd lands together. Please keep making music, no matter what.

To my parents, thank you both for loving me, supporting me, and pushing me into college; I've clearly learned to love it.

To my partner,

Valentina, thank you for being such a wonderful confidant, friend, scholar, and partner to me. I would not have survived the last year of my PhD without you. I love you dearly, and I look forward to all our future endeavors together.

To the party room,

To **Philippos**, my funniest coworker. Thank you for putting up with my shit. You really made the office more than just a work place. Your office became a haven where spirits would be lifted and bottle caps would fly. Your sense of humor and willingness to embrace pranks, jokes, and stunts was one of the main reasons I enjoyed coming to work every day. Thank you for everything.

To **Katherine**, although you are not funny at all, I respect all of your efforts with fervor. In all honesty, your ability to put up with all our jokes over the years speaks towards your comedic expertise. Thank you for letting me procrastinate in your office with you, and for inviting me on your Neuroethics podcast - that was a treat. I wish the best for your blooming career and wonderful family.

To **Rick**, here is a GitHub link to an R script that prompts chatGPT to thank you for all the help you have provided me. You cultivated my research analytic skills and explored the possibilities of software with me in unforgettable ways. Moreover, you are a great friend, excellent drinking buddy, and an amazing human/genius.

To **Chris & Hailey**, I love you both an unbelievable amount. Thank you being unbelievably good friends. Reminiscing about America kept me from getting too homesick, and our countless nights out together were always amazing. The barbeques and drunken cycles home are also unforgettable to me. **Chris**, it was an honor being your paranymph. Thank you for that privilege, and for overall being such an amazing friend.

Renzo, from the bottom of my heart, thank you for continuously encouraging me to be a better scientist and keeping a positive mindset towards both work and life. You are both a gentlemen and a scholar. I promise to join you in the city center for Carnival next year.

Igor, you are one of the nicest guys I know, and I always wanted you to be at every meeting, lunch break, conference, and party. There are few people who can discuss such *next-level* conversations the way you can. Your intelligence and wit never ceased to amaze me, no matter what life threw at you. Never stop being you, and always remember to 'Turn on, tune in, and drop out'.

Mathilde, thank you for your kindness, honesty, friendship, and delightful sense of humor. Although short lived I appreciate the times we've spent together and the positive ambiance you brought with you everywhere, helmet and all. It's been a pleasure getting to know you.

Valentine, I wanted to extend my gratitude for the good laughs, enjoyable card games, and thoughtful jokes we've shared. You like the rest of the party room brought a lot of happiness to my work life. Thank you for being part of creating such memorable times.

To those ahead of me,

Christian, thank you for being such a down to earth friend with me for such a long time. Your passion and entrepreneurial drive has inspired me in many regards. I can be quite obnoxious at times, but you put up with it because you, more than most, understand that banter, knowledge, and ambition leads people to some wild ideas. Thank you for your endless hospitality inside and outside the lab, and for sharing such a strong friendship with me.

Glen, Thank you for every conversation we had, be it politics, the economy, cryptocurrency, sports, but especially good movies. *"I'm the guy who does his job. You must be the other guy!"* Quoting Bostonian films with you in the lunchroom gave me chuckles that would last for days. It delights me that you and **Perla** have made such a wonderful home for yourself. I will miss you sincerely.

Ellis, thank you for being such a kind friend and an honest person. I'm so happy you got your postdoc position that you so rightfully deserve. Keeping fighting the good fights. I wish all the best for you, your career, and your future.

Dean, lowkey you might be one of the smartest coworkers I've ever had, while in the same breath also the most friendly and charismatic person to hang with. I love how you tickle your friends just to get a ruse out of them. Please keep making funny photos of everyone and being the life of so many parties.
Sven, thank you for your guidance and shared passion for tissue dissection. I always enjoyed talking to you in the lab, be it about work or European vs American culture. I hope that your academic success continues and our roads keep crossing.
Fred, thank you for being not only a mentor but also a great colleague. Your guidance and support has been invaluable to me. I appreciate your participation on my reading committee and for taking the time to attend my defense online. I look forward to the day we can hang out together in Boston.

To the technicians,
To **Helen**, a genius technician. The quality and timely outcome of my project is due solely from your distinguished expertise. Thank you for teaching me all that you have.
Denise, thank you for your friendliness and scientific rigor. I still find it adorable how much your daughter looks like you.
Wouter, thank you for your patience and expertise towards my work in and outside of the lab.
Sandra, I thank you for all of the wonderful and nuanced discussions we would have, laboratory related and otherwise.

To others in my department,
Dear **Maarten,** thank you for reading every single page of my thesis before checking for your thank you. Here it is. Please reread chapter 4. Also you're cool. Stay cool.
To **Sarah, Nycke, Gunter, Ghazi, David, Manon, Clara, Roman, Ana, Aryo, Jeroen, Sylvana, Bethany, Laurence, Rachelle, Thomas, Martin, Maxime,** and **Maghed,** I express my heartfelt gratitude to each and every one of you for your professional and personal support over the past 4.5 years. It has been an incredible journey, and you have all made it easier for me.

To my office mates,
Caterina, you deserve a special thank you. Our office friendship grew over the years into something so lovely, I have missed it since the day you left. You were someone I could talk about anything to, vibe with, gossip and chat; just the best type of distress conversations one wishes to have with someone they trust. Thank you for being such an understanding friend and honest person.
To **Michelle,** I see such a prosperous future for you, like those who sat in that seat before you. Even thought I was not in your group or in your office for that long, thank you for being so down to earth and relatable.

To **Pilar, Mario, Qian, Simon, Houan, Brit, Nikita, Tanya, Peng, Anja, Beatrice, Shenghua, Marina, Peter,** Thank you for allowing me to sit in your office all these years, despite not being part of your research group. I blocked the doorway, distracting your students, and procrastinated with Daan countless times, but we all learned from one another and made so many new friends. I'm grateful to have been part of your team in this way.

To support staff,
Tim, thank you for being such a personable division leader that I could talk to about anything.
Paul Verjans, thank you for your engineering genius.
Andreas Herrler, thank you for your guidence, expertise, and wisdom.

In Loving Memory Of
Carleddie Clinton of South Austin Texas
April 8, 1993 ~ April 23, 2023